# Optimization and Application of Broadband Fiber Raman Amplifiers


**Li Zhaohui**

**School of Electrical & Electronic Engineering**

A thesis submitted to the Nanyang Technological University
in fulfillment of the requirement for the degree of
Doctor of Philosophy

**2006**

# Acknowledgement

I would like to thank many people for their help in completing this thesis, but my foremost and earnest appreciation goes to my supervisor, Associate Professor Lu Chao, for his professional guidance, invaluable assistance and kind encouragement throughout my graduate studies as well as his constructive comments on this thesis.

I want to express my special thanks for Dr. Wen Yang Jing and Associate Professor Cheng Tee Hiang for their great help on my research work and good suggestion on my thesis and future career. I would also like to express my sincere appreciation to Associate Professor Ampalavanapillai Nirmalathas of Melbourne University, Professor Lu Fuyun of Nankai University and Professor Wu Chongqing of Beijing Jiao Tong University for their helpful guidance and discussion. I wish to thank Dr. Li Zhihong, Dr. Dong Yi, Dr. Zhao Chunliu, Dr. Chen Jian, Dr. Dong Xinyong, Dr. Ding Lei and Dr. Wang Yixin for their kind guidance, great help and fruitful discussion on my research work.

Special thanks go to the staff and students in Institute for Infocomm Research, Singapore, including Dr. Zhou Xiaoqun, Dr. Hao Jianzhong, Mr. Ng Jun Hong, Ms. Xie Bing, Mr. Wang Xiaoyan, Mr. Lou Junjun, Mr. Xu Zhaowen, Mr. Su Lei and Mr. Wang Ying.

At last, this thesis is dedicated to my parents, my sisters and my wife for their love and support.

# Summary

Fiber *Raman* amplifier (FRA) was first demonstrated by *Stolen* and *Ippen* in the early 1970's. From the mid- to late- 1990s, with technological advance in some important fields, such as new types of fiber with high *Raman* gain coefficient, new *Raman* pump lasers with high output power and some all fiber components, there has been revived interest in distributed *Raman* amplifier (DRA). Since then, DRA has been studied extensively due to its fundamental advantages compared with the lumped amplifier, such as *Erbium* doped fiber amplifier (EDFA). First, *Raman* gain can be obtained in all kinds of fiber and hence it is easier to upgrade the existing transmission line from the terminal ends. DRA can also improve the noise performance and reduce the penalty from fiber nonlinear effects in transmission system, allowing for longer amplifier spans, higher bit rates and smaller channel spacing. In addition, since stimulated *Raman* scattering (SRS) is a non-resonant effect, *Raman* gain is available over the entire low attenuation region of optical fiber ranging from approximately 1.3$\mu m$ to 1.6$\mu m$.

This thesis first discusses the gain characteristics, noise, polarization and nonlinear impairments of DRA and then reviews some recent progresses and new applications of DRA in detail. Many issues associated with the practical applications of DRA are identified. In order to solve these issues, several simplified optimization algorithms and novel schemes for the optimization and application of DRA are proposed. The specific contributions are summarized as followings:

A geometry compensation technique (GCT) is proposed to optimize the broadband flat gain spectrum of a multi-wavelength backward pumped DRA. Utilizing the geometrical slope compensation technique, gain flattening design of a broadband DRA can be simplified significantly. This method can also enable the dynamic gain control of *Raman* amplifiers.

In order to improve the accuracy of GCT and increase the convergence speed of the genetic algorithm (GA), a hybrid optimization algorithm based on GCT and GA is proposed in this thesis. This model selects the pump wavelengths using GCT and pump path integrals using GA respectively. In this way, two-dimensional random searches in GA can be reduced to one-dimensional random search, leading to increased convergence speed. In addition, the accuracy of the GCT can be improved significantly.

The effect of a piece of highly nonlinear photonic crystal fiber (PCF) on the noise characteristics of DRA is studied for the first time in this thesis. The experimental results demonstrate that the optical signal to noise ratio (OSNR) of the distributed backward-pumped *Raman* amplifier will be improved when a piece of highly nonlinear PCF is inserted at the beginning of the amplification span.

Based on dual order stimulated *Raman* scattering (SRS) of a single 1395nm *Raman* fiber laser (RFL) in 75km single mode fiber (SMF) and its corresponding dispersion compensation fiber (DCF) module, hybrid *Raman*/EDFA for L-band amplification is realized. By comparing the performance of gain and noise in four types of hybrid amplifier with different

span configurations, it is found that the distribution of the secondary L-band amplification obtained from *Erbium* doped fiber (EDF) along the span has a influence on the performance of hybrid amplifier. Gain and noise performance of hybrid amplifier can be improved by optimizing the position of EDF.

A novel technique for polarization dependent gain (PDG) suppression using a polarization scrambler (PS) is proposed and demonstrated in this thesis. Investigations on PDG due to signal-to-signal *Raman* interaction (SSRI) among 40-wavelength division multiplexed (WDM) signal channels are carried out experimentally to evaluate the system performance after incorporating a PS in the WDM communication system.

This thesis also proposes some new applications of DRA, such as *Raman* assisted Radio over fiber (RoF) network, *Raman* assisted fiber optical parametric oscillator (FOPO) and *Raman* assisted broadband light source. In the case of *Raman* assisted RoF network, the impairment induced by stimulated *Brillouin* scattering (SBS) effect and noise characteristics of WDM fiber radio network assisted by DRA or EDFA are first investigated.

For the case of *Raman* enhanced nonlinear effect, the influence of *Raman* amplification on the output characteristics of FOPO is investigated in detail.

At the end of this thesis, a polarization insensitive high power broadband source is demonstrated based on the combined effects of dual-order SRS, parametric process in highly nonlinear fiber and *Erbium* doped super-fluorescent.

# Contents

# List of Figures

# List of Tables

# List of Acronyms

| | |
|---|---|
| $A_{eff}$ | Effective Mode Field Area |
| AGC | Automatic Gain Control |
| AOM | Acousto-Optic Modulator |
| ASE | Amplified Spontaneous Emission |
| AWG | Arrayed Waveguide Grating |
| BER | Bit Error Ratio |
| BPSK | Binary Phase Shift Keying |
| BS | Base Station |
| CO | Central Office |
| CSR | Crosstalk to Sub-carrier Ratio |
| CW | Continuous Wave |
| DC | Direct Current |
| DCF | Dispersion Compensating Fiber |
| DE-MZM | Dual-Electrode *Mach-Zehnder* Modulator |
| DEMUX | De-Multiplexer |
| DGD | Differential Group Delay |
| DMF | Dispersion Managed Fiber |
| DOP | Degree of Polarization |
| DPSK | Differential Phase Shift Keying |
| DRA | Distributed *Raman* Amplifier |
| DRBS | Double *Rayleigh* Backscattering |
| EDF | *Erbium* Doped Fiber |
| EDFA | *Erbium* Doped Fiber Amplifier |
| ENF | Effective Noise Figure |
| FBG | Fiber *Bragg* Grating |
| FOPO | Fiber OPO |
| FOSRS | First Order SRS |
| FRA | Fiber *Raman* Amplifier |
| FSK | Frequency Shift Keying |
| FWM | Four Wave Mixing |
| GA | Genetic Algorithm |
| GCT | Geometry Compensation Technique |
| GS-EDFA | Gain-shifted EDFA |
| HNDSF | Highly Nonlinear Dispersion Shifted Fiber |
| HNLF | Highly Nonlinear Fiber |
| ISO | Isolator |
| IF | Intermediate Frequency |
| IFWM | Intra-Channel Four Wave Mixing |
| IXPM | Intra-Channel Cross Phase Modulation |

| | |
|---|---|
| LD | Laser Diode |
| LO | Local Oscillator |
| MPI | Multiple Path Interference |
| MUX | Multiplexer |
| NF | Noise Figure |
| NZDSF | Non-Zero Dispersion Shift Fiber |
| OA | Optical Amplifier |
| OOK | On-off Keying |
| OSA | Optical Spectrum Analyzer |
| $OSNR_{ASE}$ | OSNR of ASE |
| $OSNR_{DRBS}$ | OSNR of DRBS |
| OPO | Optical Parametric Oscillator |
| OSNR | Optical Signal to Noise Ratio |
| OSSB | Optical Single Sideband |
| OTDR | Optical Time Domain Reflect Meter |
| OXC | Optical Cross Connect |
| RFL | *Raman* Fiber Laser |
| RIN | Relative Intensity Noise |
| RN | Remote Node |
| RoF | Radio over Fiber |
| PA | Polarization Analyzer |
| PBC | Polarization Beam Combiner |
| PC | Polarization Controller |
| PCF | Photonic Crystal Fiber |
| PD | Photo Detector |
| PDG | Polarization Dependent Gain |
| PDL | Polarization Dependent Loss |
| PID | Proportional Integral Derivative |
| PLL | Phase Locked Loop |
| PMD | Polarization Mode Dispersion |
| PPRI | Pump-to-Pump *Raman* Interaction |
| PRBS | Pseudo-Random Bit Sequence |
| PS | Polarization Scrambler |
| PSRI | Pump-to-Signal *Raman* Interaction |
| RPC | *Raman* Pump Combiner |
| SA | Simulated Annealing |
| SBS | Stimulated *Brillouin* Scattering |
| SFDR | Spur Free Dynamic Range |
| SHB | Spectral Hole Burning |
| SMF | Single Mode Fiber |
| SNR | Signal to Noise Ratio |
| SOP | State of Polarization |
| SOSRS | Second Order SRS |

| | |
|---|---|
| SRS | Stimulated *Raman* Scattering |
| SSRI | Signal-to-Signal *Raman* Interaction |
| TDFA | Thulium Doped Fiber Amplifier |
| TDM | Time-Division Multiplexing |
| WDM | Wavelength Division Multiplexed |
| XGM | Cross Gain Modulation |
| XPM | Cross Phase Modulation |
| ZDW | Zero Dispersion Wavelength |

# Chapter 1

# Introduction

## 1.1 Motivation

### 1.1.1 Bandwidth Demand in Optical Communication System

Over the last few years, there has been an increasing data-driven bandwidth demand for high capacity fiber optic transmission systems ranging from short to ultra-long haul systems. This has led to a rapid development of new types of fiber, all-fiber components, amplification schemes, modulation formats and detection techniques [1, 2].

Recently, many new types of fiber with high transmission performance have appeared, such as non-zero dispersion shift fiber (NZDSF), photonic crystal fiber (PCF), high *Raman* gain coefficient fiber and low loss fiber [1]. In addition, the availability of all-fiber components to replace bulk optics has led to the revolution in optical communication system. For example, fiber *Bragg* gratings (FBG), special couplers and wavelength division multiplexers (WDM) have made splicing easier in all-fiber communication system [1]. In most of the current fiber communication systems, on-off keying (OOK) is the dominant modulation format, in which the intensity of optical carrier is modulated by data

into two levels. At the receiver end, the OOK signal is incident directly on a photo-detector, which converts light into electric signal through the photoelectric effect. During the 1980s to 1990s, alternative modulation and detection techniques were studied intensively in order to improve the receiver sensitivity of OOK with direct detection. New techniques pay attention to the modulation of phase or frequency of optical carrier, such as differential phase shift keying (DPSK) and frequency shift keying (FSK). New detection techniques including homodyne and heterodyne detection were explored to improve the sensitivity of the receiving system. However, the works in these directions have stopped in the early 90's due to the invention of low cost *Erbium* doped fiber amplifier (EDFA). Since then, EDFA has been the driving force in high capacity optical communication system. In recent years, the quest for higher performance optical communication system has driven researcher to re-look at some alternative optical amplifiers. One of the most important ones is distributed *Raman* amplifier (DRA) [3].

DRA can improve the noise performance and reduce the nonlinear penalty compared with conventional lumped amplifier, such as EDFA, it has been applied extensively in long-haul, high-speed optical communication systems with substantially improved system performance comparing with conventional system [1, 2, 4].

### 1.1.2 Advantages of Fiber *Raman* Amplifier

Compared with the conventional optical amplifiers, fiber *Raman* amplifier (FRA) has the following advantages: First, stimulated *Raman* scattering (SRS)

effect exists in all kinds of fiber and hence it is easier and more cost-effective to upgrade the communication system from the terminal ends. The second advantage is that the gain spectrum provided by *Raman* amplifier can be tailored by adjusting the pump wavelengths. As a result, multi-wavelength *Raman* pumps can be used to broaden the amplification bandwidth [1]. Third, SRS is a non-resonant effect, which means that *Raman* gain is available over the entire low attenuation region of the fiber ranging from approximately $1.3\mu m$ to $1.6\mu m$.

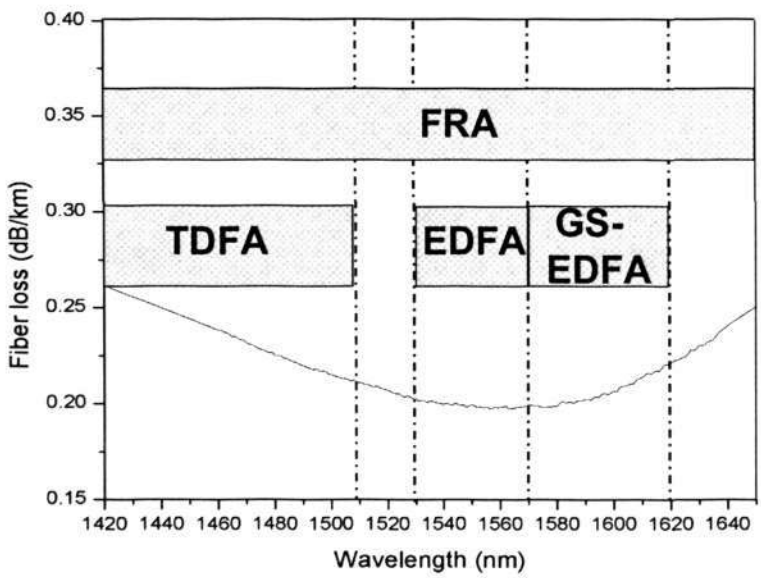


*Figure 1-1 Gain bandwidth available for TDFA, EDFA, GS-EDFA and FRA*

As shown in Figure 1-1, several communication bands co-exist within the low attenuation region of single mode fiber (SMF). Optical amplifiers based on rare-earth ions can only provide a limited gain bandwidth. For example, *Thulium* doped fiber amplifier (TDFA) operates in the S-band, which stretches from roughly 1480 to 1525nm, EDFA operates in the C-band, which stretches from 1530 to 1565nm and gain-shifted EDFA (GS-EDFA) operates in the L-

band, which stretches from about 1565 to 1625nm. FRA gain can cover C-band, L-band and even S-band. Generally, discrete *Raman* amplifiers are utilized to open up new communication windows for wavelength multiplexing such as at 1300nm, 1400nm, or short wavelength S-band [1, 4].

The fourth advantage is that *Raman* amplification does not depend on the relative direction of the pump and wavelength division multiplexed (WDM) signal channels, thus allowing many kinds of pumping configurations, such as forward pumping scheme, backward pumping scheme and bi-directional pumping scheme, as illustrated in Figure 1-2 [1, 2, 4].

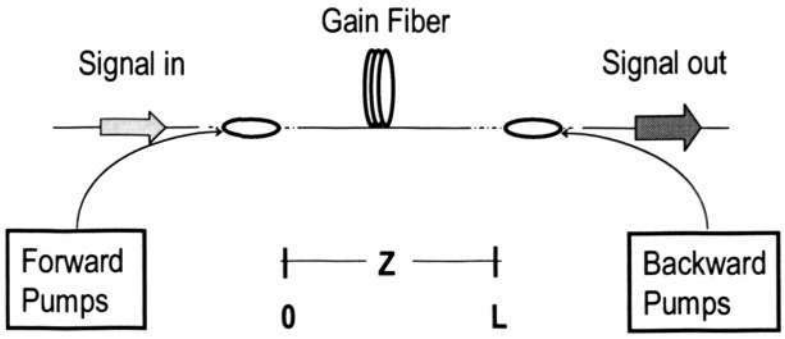


*Figure 1-2 Raman pumping configurations*

Compared with the lumped optical amplifiers, such as discrete *Raman* amplifier or EDFA, DRA has many advantages, which enables the use of DRA in many long-haul and ultra-long-haul transmission system [1]. The key advantage is that DRA can optimize the signal power distribution along the transmission span. Using a DRA to improve the optical signal to noise ratio (OSNR) and reduce the nonlinear penalty is illustrated in Figure 1-3. In this figure, the signal power distribution is plotted versus distance for a periodically amplified system.

The saw-tooth like curves correspond to lumped amplification, while the dotted curves correspond to the use of DRA. It can be found from Figure 1-3 that there is an upper limit and a low limit in terms of signal power distribution for amplification. If the signal enters the fiber span beyond the high power limitation, it suffers from higher nonlinear effect. If the signal enters the low power region, higher noise degradation will be induced for the next amplifier. Consequently, the OSNR remains higher with the use of the DRA. For lumped amplification, the power at the amplifier span input side is within the high power limit region and power at the amplifier span output side is within the low power limit region, which leads to increased nonlinear penalty and degraded OSNR. However, DRA can reduce the overall excursion that the signal experiences, which is shown in Figure 1-3. When using DRA, the signal power at the input and output sides can be outside of two power limit regions, which can reduce nonlinear penalty and improve OSNR simultaneously [1, 2, 4].

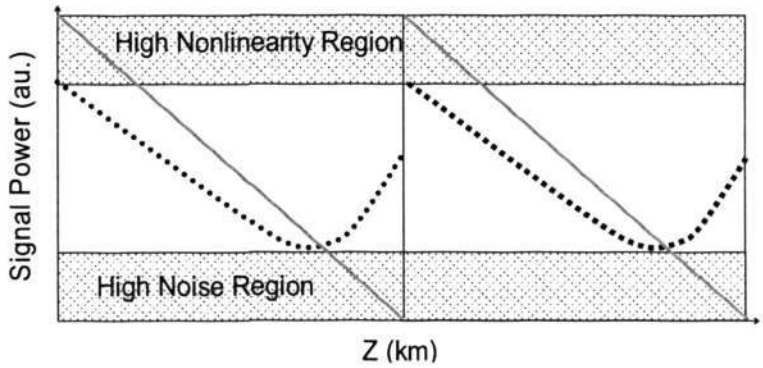


*Figure 1-3 Comparison of signal power distribution along amplification span in lumped and distributed amplifier. Solid line: lumped amplifier; Dotted line: distributed amplifier*

### 1.1.3 Challenges in Applications of Fiber *Raman* Amplifier

Besides the advantages of DRA, there are also a number of challenges preventing *Raman* amplifier from becoming the dominant means of optical

amplification in optical communication system. The first one is the relatively poor pumping efficiency of FRA compared with that of EDFA. As a result, FRA requires much higher pumping power than that required by EDFA. The second disadvantage is due to the fast response of FRA, which degrades the system performance due to relative intensity noise (RIN) transferring from *Raman* pumps to signal channels [5-7]. The third disadvantage is that normal *Raman* amplifier implementation suffers from polarization dependent gain (PDG). Studies on the impact of PDG and polarization dependent loss (PDL) in long-haul optical amplified systems have shown that bit error ratio (BER) fluctuations are a strong function of the combined effects of PDG and PDL [8-15]. In addition, double *Rayleigh* backscattering (DRBS) noise is also an important challenge for DRA. Both gain and noise flattened DRA design using multiple wavelength *Raman* pump lasers is another challenge. Although much research has been done, a simple while effective design methodology is yet to be found. All these issues need to be addressed in order to improve the performance of DRA based systems.

### 1.1.4 New Applications of Fiber *Raman* Amplifier

In addition to application in long haul distributed transmission systems, FRA has also found applications in new areas recently. These include *Raman* assisted all optical signal processing, remote sensor systems and radio over fiber (RoF) systems.

Wavelength conversion is recognized as an important function in future optical networks employing WDM and optical cross connect (OXC). Four-wave

mixing (FWM) or cross phase modulation (XPM) are important nonlinear effects in optical fibers that have potential applications in high speed wavelength conversion as well as all-optical signal processing. However, low conversion efficiency and a relatively narrow parametric bandwidth limit their usefulness. In order to overcome these limitations, there have been many studies on the use of combined nonlinear effects, such as parametric amplification, *Raman* amplification and FWM. The influence of *Raman* amplification on the conversion efficiency, parametric bandwidth and polarization insensitive characteristics of FWM and XPM has been studied extensively recently [16-32].

It is known that the sensitivity of fiber sensor is limited by the attenuation of probe signal. Recently, *Raman* amplification assisted remote fiber sensors are being used to extend the span range and increase the sensitivity of the sensor. There are two types of configurations, one is utilizing a continuous wave (CW) *Raman* pump to provide distributed *Raman* gain for the probe signal and backscattered signal along the span link directly; another is using *Raman* pump lasers to remotely pump a piece of *Erbium* doped fiber (EDF) located down the sensing fiber. In the second scheme, *Raman* pump provides the *Raman* amplification for both the probing signal and backscattered signal. In addition, the remaining pump power is also used to remotely pump a piece of EDF located within the span link and hence provides secondary amplification [33-35].

## 1.2 Objectives

Although FRA has been studied extensively, many research issues still need to be addressed. The objectives of the study in this thesis are to identify these problems and to find suitable solutions. In particular, the research study aims to address the following issues:

1. Investigation on the gain flattening optimization algorithms of DRA

1.1) To study fast and simple optimization algorithms based on the geometrical characteristic of SRS spectrum.

1.2) To study the performance of hybrid optimization algorithm based on geometry compensation technique (GCT) and genetic algorithm (GA).

2. Suppression of impairments induced by DRA

2.1) To investigate the effect of inserting a piece of PCF on the noise performance of DRA.

2.2) To investigate the effect of inserting a piece of remote EDF pumped by dual-order SRS on the noise performance of DRA.

2.3) To study the influence of signal to signal *Raman* interaction (SSRI) on the PDG and also investigate the effects of fiber polarization mode dispersion (PMD) and *Raman* gain coefficient of different gain fibers on PDG.

3. Exploration of new applications of DRA

3.1) To investigate the gain and noise performance in the downlink and uplink of RoF network under the assistance of DRA and study the effect of DRA on the nonlinear degradation of RoF network.

3.2) To investigate the characteristics and features of fiber optical parametric oscillator (FOPO) assisted by *Raman* amplification.

3.3) To generate high power broadband light source based on hybrid effects of dual-order SRS, parametric process and super-fluorescent.

## 1.3 Major Contributions

The major contributions of the thesis are listed as followings:

This thesis first proposes an effective GCT to optimize the broadband gain spectrum of *Raman* amplifier. Through linearly approximating a given *Raman* gain profile into several asymptotic segments, gain flattening design of DRA can be achieved through simple geometrical slope compensation using gain spectra from different pump lasers. This method greatly simplifies the design procedures and enables real time control of *Raman* amplifiers in optical communication systems.

In order to improve the accuracy of GCT and increase the convergence speed of GA, a hybrid optimization algorithm based on GCT and GA is proposed in this thesis. This model optimizes the pump wavelengths using GCT and pump path integrals using GA respectively. In this way, two dimensional random searches in GA can be reduced to one dimensional random search.

This thesis also studies the effect of a piece of highly nonlinear PCF on the noise characteristics of a backward pumped DRA. The PCF has a high *Raman* gain coefficient and a high *Rayleigh* scattering coefficient. When an optical signal passes through 100m highly nonlinear PCF followed by 25km SMF, the optical signal noise ratio (OSNR) of the ASE and the DRBS are improved simultaneously.

Based on dual-order SRS of a single 1395nm RFL in 75km SMF and its corresponding DCF, a hybrid *Raman*/EDFA for L-band amplification is studied in this thesis. It is found that the distribution of the secondary L-band amplification obtained from the EDF along the span link has a great influence on the performance of the hybrid amplifier. Both the gain and noise performance of the hybrid amplifier can be improved greatly by optimizing the position of the EDF. Moreover, flat gain bandwidth can be extended from L-band to C+L band by recycling the residual first order SRS (FOSRS) to pump a piece of EDF with optimal length.

A novel PDG suppression technique is proposed based on a wavelength dependent polarization scrambler (PS). Investigations on PDG due to SSRI among 40 WDM channels are carried out experimentally to evaluate the system performance after incorporating a PS in the system.

This thesis investigates the power limitation induced by SBS effect and noise characteristics of WDM fiber-radio network assisted by DRA or EDFA. Experimental results indicate that forward pumped DRA can increase the link

optical output power limited by SBS effect in downstream transmission and backward pumped DRA can improve signal to noise ratio (SNR) in upstream transmission, which is verified by transmission experiments using binary phase shift keying (BPSK) format. Moreover, experimental results show that DRA does not introduce additional impairment from inter-channel crosstalk due to XPM and degradation in spur free dynamic range (SFDR) [36-46].

Assisted by SRS, a continuous-wave pumped, all-fiber optical parametric oscillator around 1523nm is investigated in this thesis. Furthermore, a depolarized broadband source of about 20nm (1570nm ~1640nm) based on combined effects of SRS and parametric effect is obtained [47-52].

At the end of this thesis, a novel technique is proposed by applying a single 1395nm RFL to generate a depolarized broadband source. This broadband source is based on the second order SRS, parametric FWM in 3km highly nonlinear dispersion shift fiber (HNDSF) and *Erbium*-doped super-fluorescent by recycling the residual FOSRS to pump 10m EDF. A broadband spectrum from 1520nm to 1620nm with stable output powers more than 200mW is achieved as pump power reaches 1.3W [53-56].

## 1.4 Organization

This thesis is organized into six chapters.

In Chapter 1, a brief introduction is given to present the motivation, objectives and major contributions by the author in this thesis.

In Chapter 2, the fundamental concepts, background knowledge of the FRA are first discussed and then the recent progresses in this area are reviewed.

In Chapter 3, several optimization algorithms are proposed to obtain broadband flat multi-wavelength backward pumped DRA. A simple GCT is first proposed to optimize a multi-wavelength backward pumped DRA based on the geometric characteristics of *Raman* gain profile. Then a hybrid optimization algorithm based on the GCT and GA is proposed, which can overcome the disadvantages in both GCT and GA.

Chapter 4 first discusses noise sources in DRA and then proposes some solutions to suppress these impairments in the *Raman* amplified system.

- Experimentally study the effect of a piece of nonlinear PCF on the noise characteristics of a backward pumped DRA.

- Utilizing dual-order SRS to pump a piece of remote EDF located down the fiber span to improve the noise and gain performances.

- Using a PS to reduce PDG effectively while keeping the PMD value of the transmission system at low level simultaneously.

Chapter 5 first introduces the application of DRA to improve the performance of WDM fiber-radio network without introducing additional impairment from inter-channel crosstalk due to XPM and degradation of SFDR. Then a *Raman*

assisted polarization insensitive FOPO is developed and investigated. In addition, a depolarized broadband light source ranging from 1570nm to 1640nm with high output power and flat spectrum is generated simultaneously due to the combined action of the second order SRS (SOSRS) and parametric process. At the end of this chapter, a broadband light source based on SOSRS, parametric FWM in 3km highly nonlinear dispersion shift fiber together with *Erbium*-doped super-fluorescent is presented.

Finally, Chapter 6 summarizes the work in this thesis with some conclusions and gives plans for further research in the area.

# Chapter 2

# Fiber *Raman* Amplifier and its Characteristics

## 2.1 Introduction

Fiber *Raman* amplifier (FRA) was first demonstrated by *Stolen* and *Ippen* in the early 1970's [57]. However, since high power and low cost pump laser diode (LD) was not available at that time, throughout the 1970s and the first half of the 1980s, FRA remained primarily laboratory curiosities [2]. By the early part of 2000s, there has been a fast explosive development of optical fiber communication driven by the demand on data bandwidth [58, 59]. In conjunction with the maturity of high power *Raman* pump sources [60-64], distributed *Raman* amplifier (DRA) has demonstrated some superior performance over conventional optical amplifiers, such as *Erbium* doped fiber amplifier (EDFA). It can improve the noise performance and reduce the nonlinear penalty in fiber communication systems, allowing for longer

amplifier spans. As a result, many long haul or ultra-long-haul fiber optic transmission systems have chosen DRA [1, 31, 65-74]. Lumped or discrete *Raman* amplifiers are primarily used to increase the capacity of the optical networks by opening up new wavelength windows for wavelength division multiplexed (WDM) communication, which cannot be achieved by using rare earth doped fiber amplifiers [75-77]. However, there still exist many issues associated with FRA for its practical application. The objectives of this chapter are to identify these issues [1, 4].

The contents of this chapter are shown as follows. The basic principle of FRA and the definition of gain and noise figure of FRA are introduced in section 2.2. Then several types of pumping schemes of DRA are discussed in section 2.3, including multi-wavelength backward pumped broadband flat DRA, time division multiplexing (TDM) pumping scheme and higher order *Raman* amplification. Section 2.4 discusses the gain characteristics of FRA, including new optimization algorithms of multi-wavelength backward pumped broadband flat DRA, *Raman* gain characteristics in different types of gain fibers, gain saturation characteristics of DRA, transient effect in saturated *Raman* amplifier together with its gain control and gain tilt due to signal to signal *Raman* interaction (SSRI). Noise sources in DRA are discussed in section 2.5, which include amplified spontaneous emission (ASE), double *Rayleigh* backscattering (DRBS), relative intensity noise (RIN) and impairments induced by polarization dependent gain (PDG) or non-degenerated four wave mixing (FWM) between pump and signal channels. Section 2.6 reviews new applications based on *Raman* amplification, such as *Raman* assisted FWM, *Raman* assisted parametric

amplifier, *Raman* assisted cross phase mixing (XPM) and remote fiber sensor system.

## 2.2 Basic Principle of Fiber *Raman* Amplifier

### 2.2.1 Physical Model of Stimulated *Raman* Scattering

The basic physical process of FRA is stimulated *Raman* scattering (SRS) interaction between pump and signal waves, as shown in Figure 2-1. In this process, pump photon first transfers to a virtual upper energy state, then gives up energy to create a new photon at signal wavelength, plus some residual energy, which is absorbed by phonons (vibration energy) [57, 78]. As a result, signal lights are amplified. SRS process occurs when the high power pump and signal waves are launched into fiber in counter-direction or co-direction.

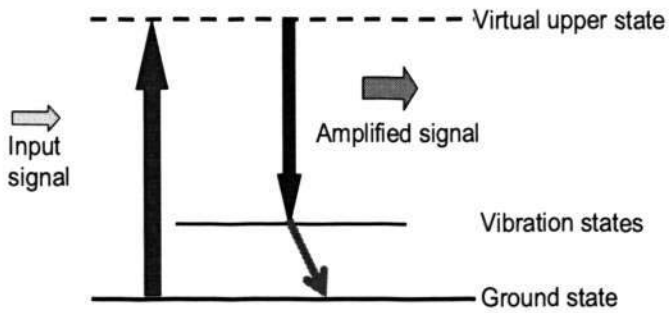


*Figure 2-1 Physical process of stimulated Raman scattering*

### 2.2.2 Mathematical Model of a Fiber *Raman* Amplifier

In steady state, wave propagation in a multi-wavelength pumped *Raman* amplifier can be described by a set of coupled nonlinear Equations (2-1) and (2-2). It takes into account the following physical effects: spontaneous *Raman* emission and its temperature dependent characteristics, DRBS noise, *Raman* interaction between a number of pump and signal waves in either direction,

pump-to-pump, signal-to-signal *Raman* interactions and wavelength-dependent linear attenuation experienced by all the pump and signal waves [78-80].

$$
\begin{aligned}
\frac{}{} &= - \quad + \nu \quad \nu \\
&+ \int_{>\nu} \frac{}{} \nu-\zeta \quad \zeta + \quad \zeta \quad \nu \ \zeta \\
&+ \int_{>\nu} \nu \frac{}{} \nu-\zeta \quad \zeta + \quad \zeta \quad + \frac{}{\zeta-\nu\ /\ -} \ \zeta \\
&- \int_{<\nu} \frac{}{} \nu-\zeta \quad \zeta + \quad \zeta \quad \nu \ \zeta \\
&+ \int_{<\nu} \nu \frac{}{} \nu-\zeta \quad \zeta + \quad \zeta \quad + \frac{}{\zeta-\nu\ /\ -} \ \zeta
\end{aligned}
$$

ERROR: syntaxerror
OFFENDING COMMAND: ‘ ¤ • ]]?b— O \? ? Z’ *Œ 0 N AF q¥ § 60 = 8 vł

pump-to-pump, signal-to-signal *Raman* interactions and wavelength-dependent linear attenuation experienced by all the pump and signal waves [78-80].

$$\begin{aligned}\frac{dP_f(z,\nu)}{dz} &= -\alpha(\nu)P_f(z,\nu)+\gamma(\nu)P_b(z,\nu)\\ &+\int_{>\nu}\frac{g_r}{A_{eff}}(\nu-\zeta)[P_f(z,\zeta)+P_b(z,\zeta)]P_f(z,\nu)d\zeta\\ &+\int_{>\nu}2h\nu\frac{g_r}{A_{eff}}(\nu-\zeta)[P_f(z,\zeta)+P_b(z,\zeta)][1+\frac{1}{e^{h(\zeta-\nu)/kT}-1}]d\zeta\\ &-\int_{<\nu}\frac{g_r}{A_{eff}}(\nu-\zeta)[P_f(z,\zeta)+P_b(z,\zeta)]P_f(z,\nu)d\zeta\\ &+\int_{<\nu}2h\nu\frac{g_r}{A_{eff}}(\nu-\zeta)[P_f(z,\zeta)+P_b(z,\zeta)][1+\frac{1}{e^{h(\zeta-\nu)/kT}-1}]d\zeta\end{aligned} \tag{2-1}$$

$$\begin{aligned}\frac{dP_b(z,\nu)}{dz} &= -\alpha(\nu)P_b(z,\nu)+\gamma(\nu)P_f(z,\nu)\\ &+\int_{>\nu}\frac{g_r}{A_{eff}}(\nu-\zeta)[P_f(z,\zeta)+P_b(z,\zeta)]P_b(z,\nu)d\zeta\\ &+\int_{>\nu}2h\nu\frac{g_r}{A_{eff}}(\nu-\zeta)[P_f(z,\zeta)+P_b(z,\zeta)][1+\frac{1}{e^{h(\zeta-\nu)/kT}-1}]d\zeta\\ &-\int_{<\nu}\frac{g_r}{A_{eff}}(\nu-\zeta)[P_f(z,\zeta)+P_b(z,\zeta)]P_b(z,\nu)d\zeta\\ &+\int_{<\nu}2h\nu\frac{g_r}{A_{eff}}(\nu-\zeta)[P_f(z,\zeta)+P_b(z,\zeta)][1+\frac{1}{e^{h(\zeta-\nu)/kT}-1}]d\zeta\end{aligned} \tag{2-2}$$

In both equations, $P_f(z,\nu)$ and $P_b(z,\nu)$ are the power distribution of forward and backward propagating frequency $\nu$ at distance $z$ along the fiber link respectively; $\alpha(\nu)$, $A_{eff}$ and $\gamma(\nu)$ are fiber attenuation, fiber effective area and *Rayleigh* backscattering coefficient, respectively; $g_r(\Delta\nu)$ is the *Raman* gain coefficient between two waves separated by frequency $\Delta\nu$; $h$ is the *Planck*'s constant; $k$ is the *Boltzman*'s constant; $T$ is temperature of the fiber.

If the spontaneous *Raman* scattering and *Rayleigh* backscattering are ignored, which have little influence on the gain spectrum of a *Raman* amplifier, wave

propagation model for *Raman* amplifier can be simplified as the following Equations (2-3) [81, 82].

$$\pm \frac{dP_k}{dz} = -\alpha_k P_k + \sum_{j=1}^{k-1} \frac{g(\nu_j,\nu_k)}{K_{eff} A_{eff}} P_j P_k - \sum_{j=k+1}^{m+n} \frac{\nu_k}{\nu_j} \frac{g(\nu_k,\nu_j)}{K_{eff} A_{eff}} P_j P_k \quad (2\text{-}3)$$

where the frequencies are numerated in decreasing order ( $\nu_i > \nu_j$ *for* $i < j$ ), indexes $k = 1, 2 \ldots n$ correspond to the backward propagating pump waves (the minus sign on the left hand) and indexes $k = n+1, n+2 \ldots n+m$ correspond to the forward propagating signal waves (plus sign on the left hand side). Here, the values $P_i$ , $\nu_i$ and $\alpha_i$ describe the power, frequency and fiber attenuation coefficient for the $i^{th}$ wave ( $i = 1, 2 \ldots n+m$ ) respectively. $K_{eff}$ accounts for polarization dependent characteristics between the pump and signal since the *Raman* gain is polarization dependent, which is between 1 and 2.

After some mathematical manipulations to the Equations (2-3), the gain model of the signal channel in *dB* can be described as linear superposition of the gain spectra with respective weighting factors, as given in Equation (2-4).

$$G\_dB = KK \times (-\alpha \times L + \sum_{j=n+1}^{n+m} g(\nu_j,\nu_k) \times I_j + \sum_{j=1}^{n} g(\nu_j,\nu_k) \times I_j)$$

$$KK = 10 \times \log(e);\ k = n+1, n+2 \ldots n+m \quad (2\text{-}4)$$

$$I_j = \int_0^L P_j(z) dz \quad (2\text{-}5)$$

In this equation, $I_j$ corresponds to the path integral, which is defined as the integration of the power distribution of a given *Raman* pump laser or a signal wave along the span link, as shown in Equation (2-5). $k = n+1, n+2 \ldots n+m$ represent WDM signal waves, $j = 1, 2 \ldots n$ represent *Raman* pump lasers. $\alpha$ and $L$ represent wavelength dependent loss in fiber and the length of *Raman* gain fiber respectively. $e$ is the base of the natural system of logarithms. The first term represents the effect of linear attenuation of signal waves, the second term represents SSRI and the third term represents pump to signal *Raman* interaction (PSRI).

### 2.2.3 Definition of Gain Characteristics in *Raman* Amplifier

Generally, on-off gain and net gain are used to describe the *Raman* amplification characteristics of FRA. On-off gain is defined as the increase of output signal power when the *Raman* pumps are turned on, which is shown in Equation (2-6).

$$G_{ON-OFF} = \frac{P_{s\_pump\_ON}(L)}{P_{s\_pump\_OFF}(L)} \tag{2-6}$$

where $P_{s\_pump\_ON}(L)$ and $P_{s\_pump\_OFF}(L)$ correspond to the output signal power as *Raman* pumps are turned on or off respectively.

Similarly, net gain is defined as the increase of output signal power when the *Raman* pump lasers are turned on compared with the input signal power, which is shown in Equation (2-7).

$$G_{net} = \frac{P_s(L)}{P_s(0)} \tag{2-7}$$

where $P_s(L)$ corresponds to the output signal power as *Raman* pumps are turned on and $P_s(0)$ is the input signal power.

### 2.2.4 Definition of Noise Performance in *Raman* Amplifier

Quantitative analysis of degradation of system performance induced by noise sources is an important issue for optical amplifier. Here, noise figure ($NF$) is chosen to quantify the influence of noise sources of FRA on the optical communication system. The definition of $NF$ is shown in Equation (2-8).

$$NF = \frac{SNR_{in}}{SNR_{out}} \tag{2-8}$$

where $SNR_{in}$ and $SNR_{out}$ are the signal to noise ratio ($SNR$) of the input and output electrical signal respectively.

For a *Raman* amplified system, where the signal-spontaneous beat noise is the dominant noise source, $NF$ can be approximated as Equation (2-9).

$$NF \approx \frac{2P_A^+(L)}{h\nu B_{ref} G_{net}} + \frac{1}{G_{net}} \tag{2-9}$$

where $P_A^+(L)$ is the ASE power in one polarization component in bandwidth $B_{ref}$, $h$ is *Planck*'s constant, $\nu$ is the frequency of the signal wave and $G_{net}$ is the net gain of FRA in signal wave. The first term in Equation (2-9) corresponds to the noise coming from ASE and the second term accounts for shot noise [4].

In the case of cascaded FRA, overall degradation of communication system induced by noise can be defined as $NF_{overall}$ in Equation (2-10), where $NF_i$ and $G_i$ are the $NF$ and net gain for the $i^{th}$ amplifier in the cascaded FRA amplified communication system [4].

$$NF_{overall} = NF_1 + \frac{NF_2 - 1}{G_1} + \frac{NF_3 - 1}{G_1 G_2} + \ldots\ldots \qquad (2\text{-}10)$$

In order to make comparison of the noise performance between lumped and distributed amplifiers, $NF_{eff}$ is introduced and defined in Equation (2-11), where $L_{dB}$ is the passive span loss [4].

$$NF_{eff}(dB) = NF - L_{dB} \qquad (2\text{-}11)$$

Since DRBS noise is an important issue for DRA and the system performance will be degraded greatly due to DRBS. In order to consider the influence of DRBS and ASE noise together, a total $NF$ is defined in Equation (2-12) [4].

$$NF_{total} \approx NF_{sig-span} + NF_{shot} + NF_{DRBS}$$
$$\approx \frac{2P_A^+(L)}{h\nu B_{ref} G_{net}} + \frac{1}{G_{net}} + \frac{\left(\frac{5}{9}\right)P_{DRBS}}{h\nu\sqrt{\frac{B_e^2 + B_o^2}{2}}G_{net}} \quad (2\text{-}12)$$

The first term $NF_{sig-span}$ in this equation corresponds to noise from signal-spontaneous beating, the second term $NF_{shot}$ represents the shot noise and the third term $NF_{DRBS}$ accounts for DRBS noise induced multiple path interference (MPI). $P_{DRBS}$ is the double backscattered power, $B_o$ and $B_e$ are the signal bandwidth and electrical filter bandwidth respectively.

## 2.3 Pumping Schemes of Fiber *Raman* Amplifier

### 2.3.1 Multi-wavelength Pumped Broadband FRA

Since the SRS spectrum of a single *Raman* pump is extremely broad and thus flat *Raman* gain bandwidth can be extended by adding new *Raman* pump lasers. Multi-wavelength *Raman* pumps had been used to demonstrate broadband *Raman* amplifiers with bandwidth more than 100nm covering C+L-band and gain ripple less than 0.5dB. Figure 2-2 shows the schematic of a commercial *Raman* pump module using three high-power LDs with different wavelengths to obtain a C+L-band *Raman* gain spectrum. The wavelengths of *Raman* pump are 1427nm, 1457nm and 1495nm respectively. In order to eliminate the polarization dependence of the *Raman* gain, each *Raman* pump has two polarization-multiplexed LDs using polarization beam combiner (PBC) and each LD is stabilized by using an external FBG to achieve a stable output.

Three *Raman* pump lasers with different wavelengths are then combined together using two *Raman* pump combiner (RPC) [2, 83].

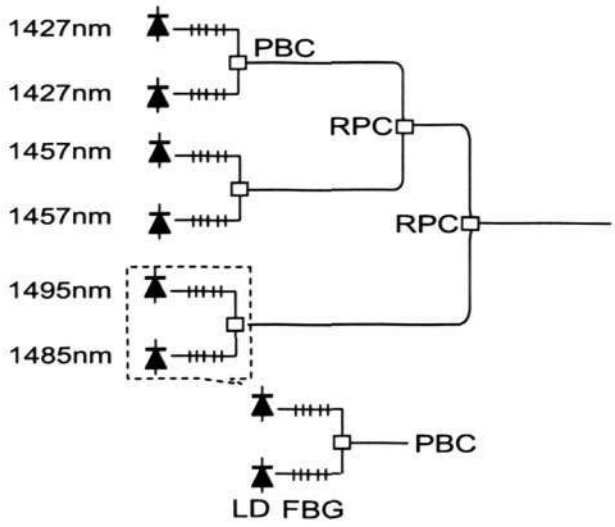


*Figure 2-2 Schematic diagram of three wavelength high power pump LDs*

Although multi-wavelength *Raman* pumps can provide broadband and flat gain spectrum, several detrimental effects limit the system performance even in case of backward pumped DRA. First, due to pump to pump *Raman* interactions, *Raman* pump lasers at short wavelength will transfer energy to those at long wavelength band [78]. As a result, *Raman* pumps must be designed to concentrate most power at short wavelengths in order to maximize the gain whilst maintaining a flat gain spectrum. Second, since short wavelength *Raman* pumps will give most gain near the beginning of the fiber link, while long wavelength *Raman* pumps will drain much energy from short wavelength *Raman* pumps and hence provide higher *Raman* gain at the end of fiber span. As a result, noise performance at long wavelength band will be better than that at short wavelength band. That means the noise performance is not the same for all WDM signal channels although exhibiting the same gain value [84, 85]. In

addition, pump-to-pump FWM will degrade the performance of DRA amplified communication systems as the fiber zero dispersion wavelength (ZDW) located among the pump bands [86-91].

### 2.3.2 High-order *Raman* Amplifier

Recently, high-order *Raman* pumping scheme has been utilized to optimize the signal power distribution along the fiber span and hence improve the noise performance. In a conventional second-order *Raman* amplifier, two *Raman* pumps are required, the first order *Raman* pump has higher power, while the second order *Raman* pump has relatively low power. First order *Raman* pump with high output power is used to amplify second order *Raman* pump with relative low power and then the amplified second order *Raman* pump is used to realize the second order amplification of signal waves. In this way, second-order DRA can move the gain of signal waves further toward the end of span link. As a result, noise performance of the second order *Raman* amplifier can be improved [92, 93]. In addition, some experiments have shown that the second order *Raman* pumping scheme can be used to reduce the *NF* tilt inherent to the broadband WDM communication system using DRA [94].

Although noise performance can be improved by using high order DRA, other impairments, such as MPI noise due to DRBS, RIN and nonlinear effects will become significant due to the high-order *Raman* amplification. Experimental results indicate that the RIN transferring function in the second-order DRA is nearly 15dB higher than that in the first-order DRA [95, 96].

### 2.3.3 Time-division Multiplexing Pumping Scheme

TDM pumping technology is utilized to eliminate SRS interactions among various pump wavelengths. In this scheme, *Raman* pumps with different wavelengths are temporally separated or one tunable single-wavelength pump laser is swept over a wavelength path. In this way, pump-to-pump FWM and the energy transferring among the *Raman* pumps can be eliminated. As a result, the power arrangement of different *Raman* pump lasers will become more reasonable and the degradation of the noise performance at short wavelength region can be suppressed [97]. The main problem associated with TDM pumping scheme is that the peak power of individual pump laser must be increased in order to achieve the same *Raman* gain. However, since the SRS interaction between *Raman* pumps with small wavelength separation is not strong as that between *Raman* pumps far away from each other, TDM pumping technology can be utilized only between *Raman* pump lasers with large wavelength separation and hence can reduce the requirement for peak power of *Raman* pumps [98].

However, since the amplitude modulations of *Raman* pumps can be easily transferred to the signal channels due to cross gain modulation (XGM) in forward pumped DRA. As a result, the modulation information overlaid onto the signal channels will degrade the performance of the transmission system since it causes some distortion to the original data signals. In addition, even for a backward pumped DRA, low frequency modulation of *Raman* pumps will give rise to DRBS and ASE noise, which also degrades the transmission quality of signals greatly. Consequently, although the TDM pumping scheme can

eliminate the nonlinear interactions among *Raman* pumps, the additional complexity and new introduced noise prevent this scheme from practical application in transmission system [99-103].

### 2.3.4 Hybrid *Raman*/EDFA Pumping Scheme

Although DRA has played a key role in improving the noise performance and extending the transmission span, relatively low pumping efficiency due to small *Raman* gain coefficient of transmission fibers and a significant amount of wasted pump power, has limited its practical application in transmission systems. In order to reduce the waste of *Raman* pump and consequently to increase overall power conversion efficiency, the unused residual *Raman* pump is recycled by using a pump reflector [104] or employing new fibers with high *Raman* gain coefficient [105]. Hybrid *Raman*/EDFA is reported in [106] to improve the power conversion efficiency, where the residual pump power after dispersion compensation fiber (DCF) is recycled for secondary signal amplification in a segment of *Erbium* doped fiber (EDF) following the DCF. In addition, hybrid *Raman*/EDFA and *Raman*/TDFA can also be used to extend the gain bandwidth [107, 108].

Compared with common first-order *Raman* amplifications, second-order *Raman* amplifications can improve the noise performance further [92]. However, a relatively low pumping efficiency of the second-order *Raman* scattering and a significant amount of wasted first-order pump power are also issues need to be addressed before their practical application in transmission systems [88-92]. In Chapter 4 of this thesis, a *Raman*/EDFA hybrid amplifier based on dual-order

SRS of a single-pump is discussed in detail, which can increase the pumping efficiency and improve the noise performance of a transmission system.

## 2.4 Gain Characteristics of a *Raman* Amplifier

### 2.4.1 *Raman* Gain Characteristics in Different Gain Fibers

*Raman* amplification can be realized in all kinds of fiber. However, *Raman* gain coefficients measured are not the same for different fibers and are determined by many parameters. The magnitude of the SRS profile is determined by effective mode-field area ($A_{eff}$) at signal or pump wavelength, while the shape of SRS profile is determined by respective fractions of $GeO_2$ and *Silica*. Because the $A_{eff}$ of DCF, dispersion shift fiber (DSF) and single mode fiber (SMF) are different, the amplitudes of SRS profile of these fibers are not the same. However, due to the same fraction of $GeO_2$ and *Silica* in these three kinds of fiber, their normalized SRS profiles are almost the same. Recently, several kinds of new fiber have been developed, such as highly nonlinear fiber (HNLF) and photonic crystal fiber (PCF), which have much higher *Raman* gain coefficient than that of conventional fibers. The large *Raman* gain coefficient of HNLF is due to the small effective area and higher $GeO_2$ doping concentration [2]. While the large *Raman* gain coefficient of PCF is also influenced by its special waveguide structure. The waveguide structure of one kind of highly nonlinear PCF is shown in Figure 2-3, the hybrid core region comprising a germanium-doped center element ( $n$ =1.487) surrounded by three fluorine-doped regions ( $n$ =1.440) is embedded in a standard triangular air/silica cladding structure. The diameter of the doped elements equals the pitch ( $\Lambda$ =1.5 $\mu m$ ).

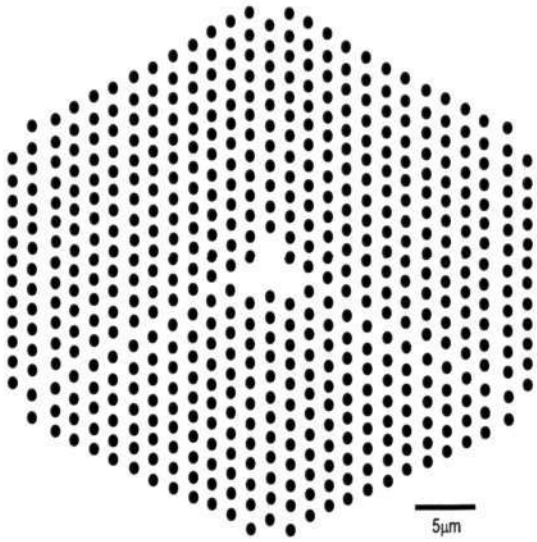


*Figure 2-3 Transverse structure of the highly nonlinear photonic crystal fiber*

Generally, the $A_{eff}$ of DCF, HNLF, SMF, DSF, and PCF are $15\mu m^2$, $55\mu m^2$, $80\mu m^2$, $10\mu m^2$ and $6\mu m^2$ respectively, and their corresponding loss coefficients at pump and signal wavelength are shown in Table 2-1.

| | DCF | HNLF | SMF | DSF | PCF |
|---|---|---|---|---|---|
| *Loss@1550 (dB/km)* | 0.49 | 0.7 | 0.22 | 0.21 | 9 |
| *Loss@1450 (dB/km)* | 0.69 | 0.85 | 0.25 | 0.25 | 9 |
| $A_{eff}(\mu m^2)$ | 15 | 10 | 80 | 55 | 6 |

*Table 2-1 Parameters of five types of fibers*

### 2.4.2 Gain Saturation Effect in Fiber *Raman* Amplifier

Gain saturation effect in FRA is characterized by the decreasing of gain when increasing the total launched optical signal power [109]. Although the gain saturation effect of *Raman* amplifier system is much smaller than that of EDFA

system [110], signal power fluctuation will be caused by add/drop channels due to gain saturation effect in FRA system. In addition, gain saturation effect of FRA is wavelength dependent, therefore *Raman* gain spectrum over a wideband signal channels will become tilted due to gain saturation effect [110].

### 2.4.3 Gain Transient Effect in Fiber *Raman* Amplifier

In modern optical telecommunication systems, channel add/drop events and accidental cable cuts will induce sudden fluctuations in the overall launched signal power into an optical amplifier. Such kind of power fluctuation of the launched optical signals has been observed to induce gain transient effects in EDFA amplified communication system [111]. As a result, gain excursions of the surviving channels have to be controlled within a small range in order not to affect the quality of communication system. There have been many proposed schemes to realize the gain control in EDFA amplified system.

Recently, gain transient effect has also been observed in saturated *Raman* amplifier [109, 112, 113]. The reason is that the strong power of the signal leading edge at the end of *Raman* amplifier depletes the injected pump and hence the residual part of the signal pulse cannot obtain the same gain as high as that in the signal pulse leading edge.

In order to assure the quality of the transmission system utilizing DRA, gain excursion of the surviving channels induced by adding/dropping signal channels must be controlled. Many control schemes have been proposed.

1) One of the gain control schemes is utilizing optical gain clamping technique, which can suppress the gain variation from 20dBm to 2.7dBm [114, 115]. However, this control technology requires an optical feedback loop to sustain a clamping laser to suppress the transient effect of the signal channel, which is not practical for long-haul DRA.

2) In order to find an effective gain clamping scheme for DRA, hybrid amplifier, which consists of short length EDFA and long haul DRA [116-118], is adopted to control the gain transient effect in DRA. Experimental results indicate that controlling the gain transient effect in the hybrid EDFA/DRA system can be realized by only controlling the gain transient effect of EDFA.

3) Another kind of gain control scheme is realized based on electrical control method completely, which is effective for both the discrete *Raman* amplifier and DRA. Transient gain control can be achieved through utilizing algorithm of the proportional-integral-derivative (PID) [119].

### 2.4.4 *Raman* Gain Tilt in a Broadband DRA

*Raman* gain tilt is also an important issue that should be considered in broadband DRA design for WDM communication system. The origin of gain tilt is mainly due to the SSRI among wideband WDM signal channels. Because the overall *Raman* gain spectrum in cascaded DRA will become dramatically tilted due to the accumulation of degradation from individual span, some

particular signal channels will suffer excessive penalties induced by nonlinear impairment or noise degradation [12, 78, 120-122].

In order to suppress the dynamic degradation in particular signal channels due to gain tilt in cascaded DRAs, many schemes have been proposed to control this effect.

1) One scheme is utilizing hybrid EDFA/DRA to limit the accumulation of gain tilt in long-haul WDM communication system [121].

2) It has been known that gain saturation effect will also lead to *Raman* gain tilt. However, gain tilt induced by gain saturation effect behaves in an opposite manner to that caused by SSRI in DRA. Therefore, gain saturation effect can be utilized to suppress the gain tilt induced by SSRI effect, maintaining flat *Raman* gain spectrum over wideband WDM signal channels [122].

## 2.5 Noise Impairments of a *Raman* Amplifier

In addition to the advantage of broadband flat gain spectrum provided by DRA, good noise performance is also an important aspect of DRA. A number of noise sources exist in DRA, which will be described briefly here. In Chapter 3 and Chapter 4 of this thesis, some novel schemes are proposed and discussed to optimize the gain and noise performance of DRA theoretically and experimentally in detail.

### 2.5.1 Noise from Amplified Spontaneous Emission

The most important noise source appeared in DRA is ASE noise. The level of ASE noise can be assumed to be relatively low and it does not deplete the power of pump and signal waves, as a result, ASE power is purely additive for each channel and the modeling of ASE noise can be described as Equation (2-13).

$$\frac{dP_{ASE,k}}{dz} = -\alpha_k P_{ASE,k} + \sum_{\substack{j=1 \\ j\neq k}}^{n+m} g(\nu_j,\nu_k) \times P_j \times (P_{ASE,k} + h\nu_k \Delta\nu F_{phon}(\nu_j,\nu_k)) \quad (2\text{-}13)$$

$$N_{phon} = \left(\exp\left(h|\nu_j - \nu_k|\right)/KT - 1\right)^{-1} \quad (2\text{-}14)$$

where $P_{ASE,k}$ is used to represent the forward propagating ASE power in the $k^{th}$ signal channel with bandwidth $\Delta\nu$ and the parameter $F_{phon}(\nu_j,\nu_k)$ in the spontaneous *Raman* scattering term is related to the number of optical photons $N_{phon}$, which is defined in Equation (2-14) [82, 88].

During the past few years, many schemes have been proposed to improve the performance of DRA by minimizing the ASE noise.

1) First one, DRA combining forward and backward pumping configuration can achieve better noise performance [69, 123].

2) Another proposed scheme utilizes effective-area managed fiber, such as dispersion-managed fiber (DMF) within the span link to distribute the

*Raman* gain more evenly along the fiber link [69]. In this way, noise performance can also be improved.

3) Other proposed schemes include the use of the second- or higher order DRA, which can extend the *Raman* gain further to the span end. In this way, signal power distribution along the span link can be made more evenly and hence the noise performance can be improved [92-94].

### 2.5.2 Relative Intensity Noise Transferred from Pump to Signal

Since SRS is a fast effect, which occurs in about sub-picosecond time scale. Therefore, power fluctuations in *Raman* pump lasers will be transferred to signal waves as one kind of noise. This phenomenon can be described in frequency domain as a transferring function of RIN from pump to signal waves, as shown in Equation (2-15).

$$RIN_S(f) = H(f) RIN_P(f) \tag{2-15}$$

For a given FRA, the transferring function $H(f)$ depends on the pumping direction, pump and signal wavelength and on-off *Raman* gain. In addition, some characteristics of *Raman* gain fiber, such as fiber length, pump loss coefficient, dispersion and dispersion slope will also influence the RIN transferring efficiency [6, 117, 124, 125].

There have been many schemes to reduce the impairment of RIN noise on the performance of communication system. The direct way is to lower the RIN

noise inherent to *Raman* pump lasers [126, 127]. RIN transfer suppression in the second order forward pumped DRA can be realized by intensity modulating the seed pump laser to counteract the RIN noise of the first order *Raman* pump laser. This technique enables the use of *Raman* fiber laser (RFL) in forward pumped scheme [128, 129].

### 2.5.3 Double *Rayleigh* Back-Scattering Noise in DRA

*Rayleigh* scattering is another important noise source for DRA in addition to ASE noise and RIN. Generally, *Rayleigh* scattering in conventional fibers arises from the light interaction with a material having uneven density. Fluctuation of the material density and composition occurring during the fiber manufacture process creates random in-homogeneities that result in refractive index variations.

Different from the conventional lumped optical amplifier, the original low level of *Rayleigh* scattering signal will be enhanced in DRA. That is because the backscattered signal will be amplified twice by distributed amplification when it passes through the reflection sites. Figure 2-4 illustrates the generation and accumulation process of DRBS noise in single span DRA with length $L$ [123, 130-133].

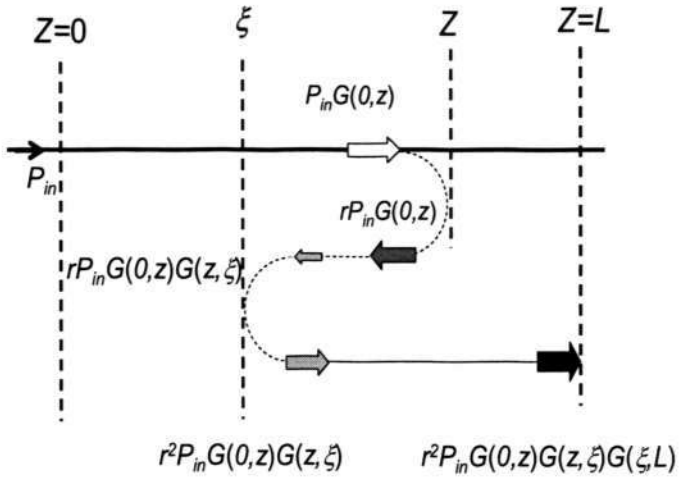


*Figure 2-4 Schematic of the accumulation of small-signal model for DRBS noise*

### 2.5.4 OSNR Tilt over Wideband WDM Signal Channels

Recently, multi-wavelength *Raman* pumps have been used to demonstrate a DRA with flat gain bandwidth exceeding 90nm. However, for such a broadband communication system, SSRI will induce power to be transferred from short wavelength channels to the long wavelength ones. As a result, the short wavelength signal channels experience additional loss. In addition, SRS interaction among *Raman* pumps will transfer power from short wavelength *Raman* pumps to the long wavelength *Raman* pumps. Therefore, for a backward pumped DRA, short wavelength *Raman* pumps will give most gain near the output of the fiber link where their pump power is large, while the long wavelength *Raman* pumps will drain much energy from the short wavelength *Raman* pumps and will be able to penetrate further into the fiber link, providing higher *Raman* gain towards the input end in long wavelength signal channels. As a result, the noise performance at long wavelength band will be better than that at short wavelength band. That means although a flat *Raman* gain spectrum over broadband WDM signal channels is achieved, noise figure is not the same

among all the signal channels. This will degrade the system performance since the system limitations are mainly determined by the noise performance in the worst signal channel [85].

Recently, several optimizing schemes have been proposed to flatten the noise performance over wideband WDM signal channels in DRA:

1) Since optical amplification prior to transmission loss can generally suppress the subsequent ASE noise, forward pumped DRA has better noise performance than backward pumped one, therefore moving some shortest wavelength *Raman* pump lasers as forward pump lasers can compensate the tilt of optical signal to noise ratio (OSNR) [84].

2) Since TDM pumping scheme can remove the SRS interaction among *Raman* pump lasers, the degradation of noise performance in short wavelength region can be mitigated to some extend by using TDM pumping scheme [99].

3) Some experiments have indicated that second-order DRA can be utilized to flatten noise performance over wideband WDM signal channels [62].

### 2.5.5 Polarization Dependent Gain Characteristics in DRA

SRS process is polarization dependent. The *Raman* gain between co-polarized waves is almost one order of magnitude higher than that between orthogonal polarized waves near the peak amplitude of SRS profile [4]. As a result, random

amplitude fluctuations due to PDG can occur if the relative polarization states of pump or signal waves vary randomly [4]. Studies on the impact of PDG and polarization dependent loss (PDL) in long-haul DRA have shown that bit error ratio (BER) fluctuations are a strong function of the combined effects of PDG and PDL [11].

Polarization induced penalty exists in both pump-to-pump *Raman* interaction (PPRI) and PSRI. In order to reduce such kind of impairment induced by the polarization effect of *Raman* pumps, there are two techniques to generate the polarization independent pump sources. One scheme is utilizing PBC to multiplex two independent polarized pump LDs with the same wavelength. Another scheme is using fiber Lyot depolarizers to depolarize the pump LDs with large spectral line-width [15].

PDG caused by PSRI or PPRI has been well resolved by depolarizing the *Raman* pump LDs [15]. However, not much research has been carried out on the mitigation of PDG caused by SSRI. Because SRS interaction also exists among WDM signal channels, it is suggested theoretically that PDG is also a function of the relative polarization orientation among signal channels. However, the practical impairment of PDG produced in real *Raman* amplified communication system is not as large as that analyzed. That is because the correlation between the states of polarization (SOP) of the signal waves is lost within a few kilo-meters fiber due to polarization mode dispersion (PMD) effect, which implies that in the communication system with high PMD, PDG due to

SSRI can be suppressed effectively [14]. However, for a real communication system, low accumulated PMD is desirable.

In Chapter 4 of this thesis, a simple scheme to reduce the PDG caused by SSRI for a low PMD communication system is proposed and discussed in detail.

### 2.5.6 Pump-to-Signal Four-Wave Mixing in FRA

Efficient FWM can also occur between pump and signal waves if they co-propagate in a fiber with zero dispersion wavelength located between the pump and signal waves. Therefore, such pump-signal FWM can be an issue when co-pumping is used. [86]. The new FWM products will have a spectrum that closely resembles the longitudinal mode structure of the *Raman* pumps. The high-power (about 250mW) pump LD has multiple FP wavelengths centered around 1453nm, which is stabilized by an external FBG. Figure 2-5 shows the multi-longitudinal mode spectrum of the pump FP LD, where the near longitudinal modes are represented by $f_{p'}$ and $f_p$. The longitudinal mode spacing of pumps $\Delta f = f_{p'} - f_p$ is about 30GHz.

When a 250mW *Raman* pump laser co-propagates with a 1mW 1529.6-nm DFB laser in 50-km NZDSF, the additional side lobes will appear around the central wavelength of DFB laser in the output optical spectrum. This is because the zero-dispersion wavelength of the NZDSF is 1497nm, which is located between the pump and signal waves. The reproduction of the FP structure from the pump to signal waves due to FWM can not be observed in SMF, DSF and DCF with zero-dispersion wavelengths at 1310, 1547 and 1710nm respectively.

As shown in Figure 2-6, the generated FWM signals around the signal waves $f_{sn} = f_s \pm n \times 30GHz\,(n = 1, 2, 3.....)$ correspond exactly to the FWM components arising from the central pump frequency $f_p$ and its longitudinal side-modes $f_{pn} = f_p \pm n \times 30GHz\ \ (n = 1, 2, 3.....)$.

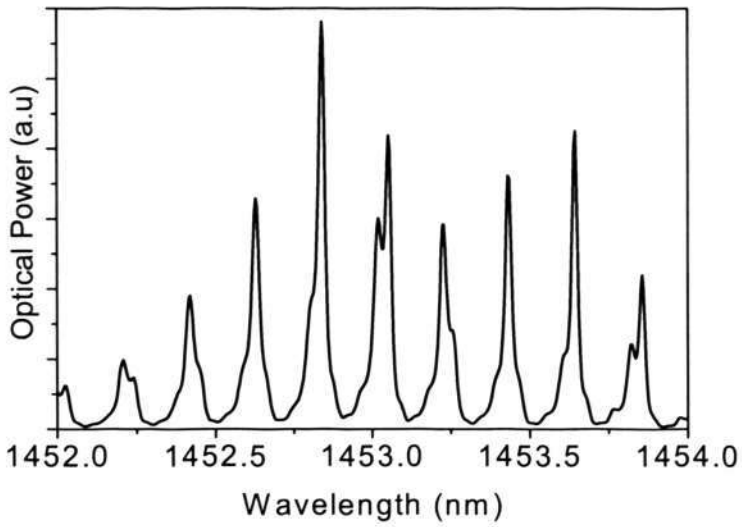


*Figure 2-5 Multi-longitudinal mode spectrum of pump FP LDs*

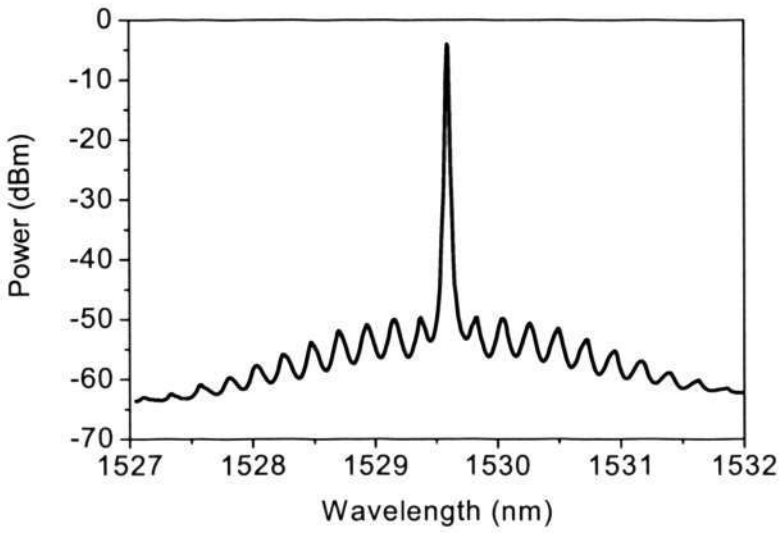


*Figure 2-6 Pump-to-signal four wave mixing*

There have been many reports on pump-to-signal FWM in DRA [91], where efforts are mostly made to reduce the FWM interactions. One of effective solutions is introducing a suitable amount of dispersion just before the pump module to avoid the pump-to-signal FWM [91].

## 2.6 New Applications of Fiber *Raman* Amplifier

### 2.6.1 *Raman* Assisted Four-Wave Mixing

Wavelength conversion is recognized as an important function in future optical networks employing WDM and optical cross connect (OXC) [16]. FWM is one of the important nonlinear effects in optical fibers that have potential applications in high speed wavelength conversion as well as all-optical signal processing. However, low conversion efficiency and a relatively narrow parametric bandwidth limits its applications. To address these limitations, there have been many studies on the combination of multiple nonlinear effects, such as parametric amplification, *Raman* amplification and FWM reported and analysed. Early theoretical and experimental studies reveal that *Raman* assisted FWM typically leads to the improvement of conversion efficiency and parametric bandwidth of systems. It is found that the conversion efficiency of FWM under the assistance of *Raman* amplification can be improved by up to 30dB, and parametric bandwidth can be extended to more than 30nm, as compared to that with no *Raman* assistance [17-19].

### 2.6.2 *Raman* Assisted Cross Phase Modulation

It has been demonstrated by many experiments that *Raman* amplification in HNLF can enhance the parametric amplification and wavelength conversation

based on FWM. Recently, experimental results indicate that XPM based wavelength conversions can also be enhanced under the assistance of *Raman* amplification. The most important parameters that influence the conversion efficiency of XPM are the nonlinear coefficient, chromatic dispersion of the fiber, the effective fiber length ($L_{eff}$) and the *Raman* pump power. Since the nonlinear coefficient and chromatic dispersion are the characteristics inherent to gain fiber and the fixed input power of pump waves is assumed for comparison, the only parameter influenced by *Raman* amplification is the effective fiber length.

When there is no assistance from *Raman* amplification, $L_{eff}$ is only determined by the loss of the fiber, which is defined by Equation (2-16), where $P_p$ and $\alpha_p$ are the *Raman* pump power and the attenuation of fiber at pump wavelength respectively.

$$\begin{aligned} L_{eff}^{noRA} &= \left(1 / P_p(0)\right)\int_0^L P_p(z)dz \\ &= \left(1 - e^{-\alpha_p L}\right)/\alpha_p \end{aligned} \tag{2-16}$$

When considering the *Raman* assistance, the $L_{eff}$ can be modified as Equation (2-17), where $g_R$ is the *Raman* gain coefficient and $A_{eff}$ is the effective mode-field area.

$$L_{eff}^{RA} = \int_0^L \exp\left[g_R \frac{P_p}{A_{eff}} \frac{e^{-\alpha_p L}\left(e^{\alpha_p z} - 1\right)}{\alpha_p} - \alpha_p z\right] dz \tag{2-17}$$

By comparing the $L_{eff}$ in two cases, it can be found that the $L_{eff}$ can be increased under the assistance of *Raman* amplification. As a result, *Raman* amplification can be used to significantly enhance the XPM effect and increase the conversion efficiency [30-32].

### 2.6.3 Remote Sensor Assisted by DRA

Fiber sensor is limited by the attenuation of the probe signal, which will degrade the sensitivity of the fiber sensor greatly. Recently, *Raman* amplification assisted remote fiber sensors are being used to extend the span range and improve the sensitivity of the sensor. There are two schemes: one is utilizing a continuous wave (CW) *Raman* pump to provide distributed *Raman* gain for the probe signal along the span link directly. Another scheme is utilizing the residual *Raman* pump power to pump a remotely located EDF and hence provides secondary amplification in addition to distributed *Raman* gain along the sensing fiber provided by *Raman* pump [33-35].

## 2.7 Conclusions

This chapter first discusses the basic principle of FRA and then introduces several simplified gain and noise modeling of FRA. After reviewing the origination of SRS and the amplification characteristics of DRA compared with EDFA, several types of classical pumping schemes of FRA are introduced and their corresponding advantages and disadvantages are discussed respectively. Then gain characteristics associated with FRA are discussed, such as gain tilt due to SSRI, *Raman* gain saturation characteristics and transient gain effect. In addition, noise sources in FRA are discussed in detail and noise suppression

schemes for these noise sources are also reviewed in detail. At the end of this chapter, some new applications of FRA are introduced, such as *Raman* assisted FWM and XPM in communication network and *Raman* assisted remote fiber sensor system.

# Chapter 3

# Optimization of Broadband Gain Spectrum of DRA

## 3.1 Introduction

Because distributed *Raman* amplifier (DRA) has distinctive flexibility in amplification bandwidth, substantial attention has been paid to the design of multi-wavelength backward pumped DRA with ultra-wide and ultra-flat *Raman* gain spectrum [1, 4]. Optimization of wavelength and power of each *Raman* pump laser to achieve a flat *Raman* gain spectrum over wideband WDM signal channels is an important issue in DRA design. However, due to pump-to-pump *Raman* interaction (PPRI) and pump-to-signal *Raman* interaction (PSRI), a set of coupled nonlinear equations are required to model the *Raman* amplification process, as shown in section 2.2.2 [78]. No simple relationship between *Raman* gain and pump power of multi-wavelength *Raman* pumps can be found unless

major simplifications are adopted. However, these simplifications will compromise the accuracy of the optimized results [134].

Although no simple relationship between *Raman* gain and pump power of multi-wavelength pump lasers can be found, it is shown that the logarithmic *Raman* gain expressed in *dB* can be given as linear superposition of pump path integrals (integration of pump power distribution of a given pump wavelength along the fiber), as shown in Equation (2-4) [81, 82]. As a result, fast optimization algorithm can be realized by finding the pump wavelengths and pump path integrals first, before an iterative algorithm is used to obtain the pump power.

Recently, several novel optimization algorithms have been proposed to achieve a broadband *Raman* gain spectrum. For example, genetic algorithm (GA) is used to find the pump wavelengths and pump path integrals [81, 82]. This approach allows the DRA design to be achieved more effectively, however, its convergence speed is very slow due to the fact that two dimensional random searches (pump wavelength and pump path integrals) employed in GA. Another kind of hybrid GA is proposed based on the clustering fitness sharing and elite replacement. However, since its optimization parameters are still dependent on the pump wavelengths and pump powers, large numbers of iterations are required to solve coupled nonlinear equations in this optimization algorithm. Simulated annealing (SA) is also adopted to find the pump wavelength and pump power directly [135]. Again, because of the limitation inherent to SA, the optimized results may converge to local optimal results. Because all of above

optimization algorithms begin their optimization process with random search for the optimized parameters from the initial seeds, time consuming iterations are normally required. Recently, a new single-layer feed forward neural network is employed to optimize the pump powers [136]. This method is fast however the pump wavelength optimization cannot be included.

In order to remove the iterative nature arising from the optimization algorithms, such as GA and SA, this thesis proposes a geometry compensation technique (GCT) based on the geometry characteristics of *Raman* gain profile [137]. In this model, through approximating a given *Raman* gain profile and fiber loss profile using several asymptotic lines, flat gain spectrum design is converted to a simple geometry equalization problem and it is also possible to separate the compensation of gain curve profiles (involving the determination of the pump wavelengths and pump path integrals) from the calculation of pump power values. This method greatly simplifies the design procedure and enables fast amplifier performance optimization to be carried out. However, it is difficult to rely on GCT alone to reduce the ripple of broadband gain spectrum to be less than 0.8dB. In addition, the complexity of this scheme will increase when signal-to-signal *Raman* interaction (SSRI) and wavelength dependent loss spectrum of the fiber are considered.

In order to solve the trade-off associated with the optimization speed and optimization accuracy in GCT, this thesis also proposes a novel hybrid optimization algorithm based on the GCT and GA. This model realizes the optimization of the pump wavelengths using GCT and pump path integrals

using GA respectively. In this way, two-dimensional random searches in GA can be reduced to one-dimensional random search. In addition, more reasonable pump power arrangement can be achieved using this kind of hybrid optimization algorithm.

This chapter is organized as follows. A simple technique to optimize a multi-wavelength backward pumped DRA based on the geometry characteristics of *Raman* gain profile is proposed in section 3.2. In section 3.3, a novel hybrid optimization algorithm based on the combination of GA and GCT is proposed to improve the optimization performance of GCT and GA further. This model obtains the optimal wavelength and pump path integrals by using GCT and GA respectively.

## 3.2 Optimization Using Geometry Compensation Technique

### 3.2.1 Background

GA has been utilized to find the optimal pump wavelengths and pump path integrals along the fiber link before iterative algorithm is applied to determine the required pump powers. This approach allows the *Raman* amplifier to be designed accurately. However, its convergence can be very slow due to the complexity of GA. In this section, a simple optimization algorithm is proposed to optimize a multi-wavelength backward-pumped DRA based on the geometry characteristics of the *Raman* gain profile. This technique approximates the *Raman* gain profile using several straight lines and utilizes slope compensation

technique to achieve flat and wideband gain profile. Good simulation results are obtained.

### 3.2.2 Theoretical Model and Design Procedure

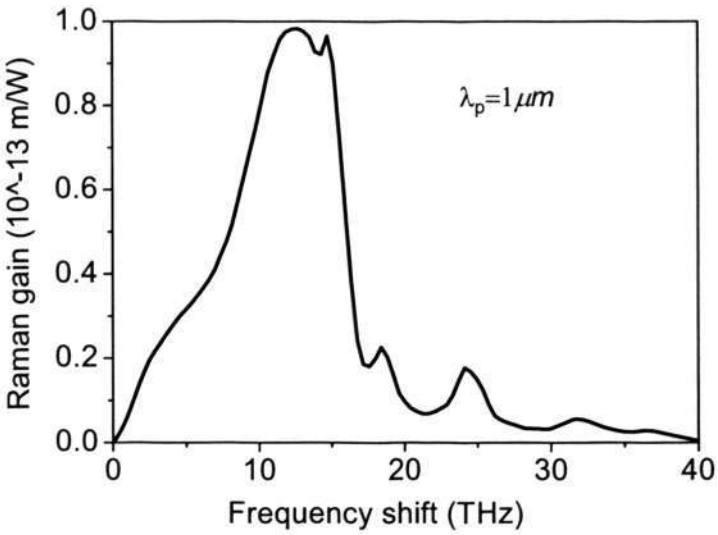


*Figure 3-1 Raman gain coefficient of single mode fiber*

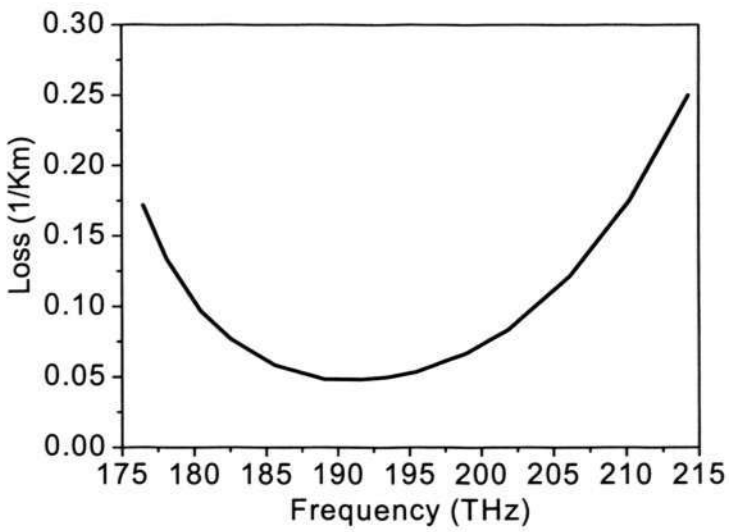


*Figure 3-2 Loss profile of single mode fiber*

Generally, *Raman* gain fiber used for DRA is single mode fiber (SMF). Typical *Raman* gain spectrum of a silica fiber at pump wavelength $\lambda_0 = 1\mu m$ and loss profile of SMF used in the optimization algorithm are given in the Figure 3-1 and Figure 3-2.

As shown in Equation (2-4), the logarithmic net *Raman* gain of the $kth$ signal wave in dB can be described as a linear superposition of the gain spectra of individual pump wavelengths with respective weighting factors given by the corresponding pump path integrals.

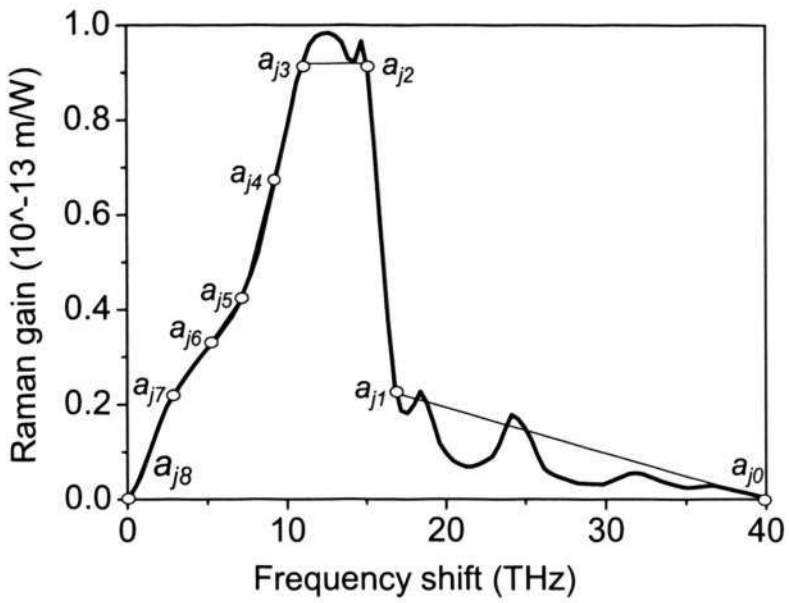


*Figure 3-3 Asymptotic linear approximation of a typical Raman gain spectrum $g_R(\Delta\nu)$ of a silica fiber at pump wavelength $\lambda_0 = 1\mu m$*

In the proposed design approach, the *Raman* gain profile of a given pump wavelength $j$ is described using multi-segment straight lines $a_{j0}a_{j1}a_{j2}a_{j3}a_{j4}a_{j5}a_{j6}a_{j7}a_{j8}$, as shown in Figure 3-3. For simplicity, frequency

rather than wavelength is used for the gain spectrum representation. For *Silica* fiber, the frequency intervals are $a_{j1}a_{j2} = a_{j3}a_{j4} = a_{j4}a_{j5} = a_{j5}a_{j6} = a_{j6}a_{j7} = a_{j7}a_{j8}$=1.7$THz$ and $a_{j2}a_{j3}$=3.4$THz$ respectively.

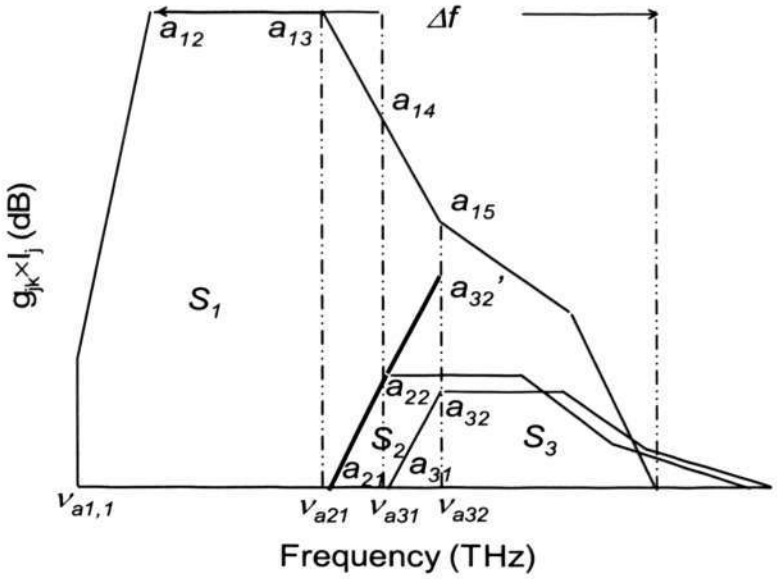


*Figure 3-4 Schematic diagram of the geometric compensation scheme ($i = 2, 3, 4$), with wavelength independent loss considered. $S_1$, $S_2$ and $S_3$ show the partial gain spectral; $\Delta f$ shows the target amplification band; $\nu_{a11}$, $\nu_{a21}$, $\nu_{a31}$ and $\nu_{a32}$ are related to frequency allocation of gain spectra from individual pumps.*

In Figure 3-4, $S_1$ is used to represent the gain spectrum of the longest wavelength pump, while $S_2$, $S_3$, $S_4$ … and $S_n$ are used to represent the gain spectra of the other pump wavelengths. Typically the pump path integral of the longest wavelength pump laser $S_1$ is much larger than those from the other pump wavelengths due to strong pump-to-pump *Raman* interactions (PPRI). As a result, the contribution of $a_{j0}a_{j1}$ can be ignored and hence the gain spectra of all the other pump wavelengths are represented with $a_{j1}a_{j2}a_{j3}a_{j4}a_{j5}a_{j6}a_{j7}a_{j8}$ ($j = 2, 3 \ldots n$). Since the portion of gain spectrum of $a_{12}a_{13}$ can be considered flat, it is possible to equalize the rest of the gain spectrum of $S_1$ using contributions

from the $a_{j1}a_{j2}(j=2,3...n)$ portion of the gain spectra of all the other pump lasers to achieve a flat gain spectrum. The range of the gain spectrum to be equalized will decide the number of pump wavelengths required.

A C-band DRA with three pump wavelengths is used as an example and the pump laser with the longest wavelength is assumed to be $S_1$ and the two other pumps are $S_2$ and $S_3$, which is indicated in Figure 3-4. The loss of the fiber is considered to be wavelength independent at first. The flat gain profile can be achieved for the signal channels over a frequency region $\Delta f$ in the gain profile corresponding to the pump laser with the longest wavelength. After the gain bandwidth region for the amplifier has been decided, the frequency of the longest wavelength pump laser is decided accordingly. Then $a_{j1}a_{j2}(j=2,3)$ in the gain profile of the two other pump lasers are used to compensate a portion of the gain profile of $S_1$ to obtain a flat gain spectrum. To compensate the slope of $a_{13}a_{14}$ in $S_1$ with the slope of $a_{21}a_{22}$ in $S_2$, the frequency of point $a_{21}$ should be equal to that of point $a_{13}$, thus the frequency of the second pump laser should be shifted 5.1*Thz* (about 37.5nm) from that of the longest wavelenghth pump laser. The pump path integral $I_2$ of $S_2$ should be such that the slope of $a_{21}a_{22}$ is the same as the slope of $a_{13}a_{14}$ but with opposite sign. Similarly to compensate $a_{14}a_{15}$ using $a_{31}a_{32}$ of $S_3$, the frequency of point $a_{31}$ should be equal to that of point $a_{22}$. Thus the frequency of the third pump laser should be shifted 1.7*Thz* (about 12.75nm) from the frequency of $S_2$. The pump integral $I_3$ of $S_3$ should be such that the slope of $a_{31}a_{32}$ is the same as the slope of $a_{14}a_{15}$ but with opposite sign. When wider amplifier bandwidth is required, more

pump wavelengths can be utilized to compensate the other part of $S_1$ in the same way. The frequencies of all the pump lasers can be determined accordingly. From the above discussions, the following Equation (3-1) can be obtained for $n \le 4$.

$$I_1 = \frac{G/(10\log(e)) + \alpha \times L}{g(\nu_{a_{1,2}})}$$

$$I_j = I_1 \times \frac{(g(\nu_{a_{1,j+1}}) - g(\nu_{a_{1,j+2}}))}{\nu_{a_{1,j+1}} - \nu_{a_{1,j+2}}} \times \frac{\nu_{a_{j,1}} - \nu_{a_{j,2}}}{g(\nu_{a_{j,1}}) - g(\nu_{a_{j,2}})}$$

$$j = 2 \ldots n \qquad (3\text{-}1)$$

For $n > 4$, the contribution to the slope of $S_1$ from $S_2$ to $S_{j-1}$ should also be considered. Here $G$ is the targeted *Raman* net gain in *dB*, $I_1$ is the pump path integral of $S_1$ and $I_j$ is pump path integral of $S_j$, $\nu_{a_{ij}}$ is the frequency corresponding to point $a_{ij}$ and $g(\nu_{a_{ij}})$ is the *Raman* gain coefficient at frequency $\nu_{a_{ij}}$.

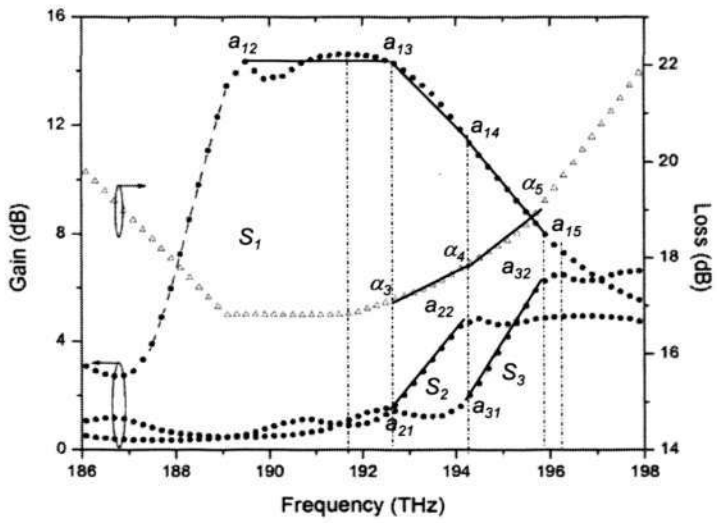


*Figure 3-5 Schematic diagram of the geometric compensation scheme ($i = 2, 3, 4$), with wavelength dependent loss considered. Triangle: wavelength dependent loss of the fiber; Circle: individual gain spectral*

In the above discussion, loss profile of fiber is assumed wavelength independent. However, it is not the case in a practical system. To consider wavelength dependent loss, the loss spectrum of fiber over the same wavelength range as $S_1$ is also represented by multi-segment lines $\alpha_3\alpha_4\alpha_5$ with $1.7THz$ per segment, as shown in Figure 3-5, where the solid lines highlight the parts in the geometrical compensation model. New model is used to modify the slope of $S_1$ and hence Equation (3-1) can be modified as Equation (3-2):

$$I_j = \frac{I_1\left(g\left(\nu_{a_{1,j+1}}\right)-g\left(\nu_{a_{1,j=2}}\right)\right)-\left(\alpha\left(\nu_{a_{1,j+1}}\right)-\alpha\left(\nu_{a_{1,j+2}}\right)\right)}{\nu_{a_{1,j+1}}-\nu_{a_{1,j+2}}} \times \frac{\nu_{a_{j,1}}-\nu_{a_{j,2}}}{g\left(\nu_{a_{j,1}}\right)-g\left(\nu_{a_{j,2}}\right)}$$

$$j = 2 \ldots n \left(n \le 4\right) \tag{3-2}$$

Where $\alpha\left(\nu_{a_{ij}}\right)$ is the loss at frequency $\nu_{a_{ij}}$. This will enable the required pump path integrals to be obtained, taking into account the wavelength dependant loss. It can be seen from Figure 3-5 that the dotted lines ignored are the origin of gain ripple. Due to the nonlinear interaction, i.e. PSRI, PPRI and etc, the pump powers cannot be derived directly from the pump path integrals. An iterative method can be used to obtain the pump powers from the coupled nonlinear *Raman* propagation equations [81]. Typically a few iterations will enable the required pump powers to be obtained. Here, *Raman* gain tilt due to SSRI is not considered since it is related to transmission system parameters. However, it is reasonable to ignore such kind of effect in obtaining the inter-channel *Raman* interaction slope for a given input signal condition without amplification and then use it to rectify the slope of $S_1$. In this way the effect of the inter-channel *Raman* interaction slope can also be equalized in the *Raman* amplifier design.

More divisions for straight-line approximation of a gain profile can result in lower ripple and calculation error. However, this in turn requires more pump lasers. In practical implementation that may not be cost-effective and the design procedure tends to be more complex and inefficient when compared with GA.

### 3.2.3 Numerical Example and Discussions

The proposed technique is applied to optimize a C-band *Raman* amplifier design as an example. The amplifier is backward pumped by three pump wavelengths with 80km SMF and 0dB targeted net gain. It is designed for DWDM system with 40 channels from 1530nm to 1565nm with input signal power at 1mW/ch. Wavelength dependent loss spectrum of the fiber is considered in the design.

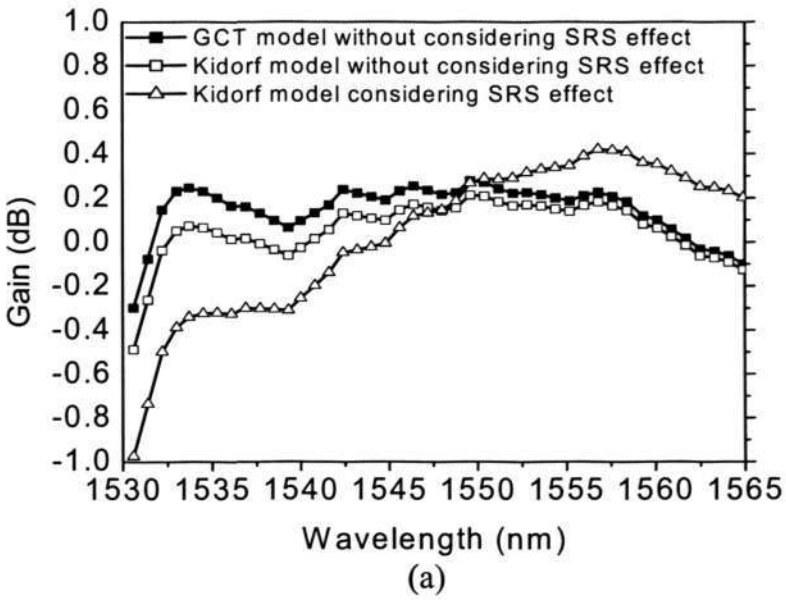

(a)

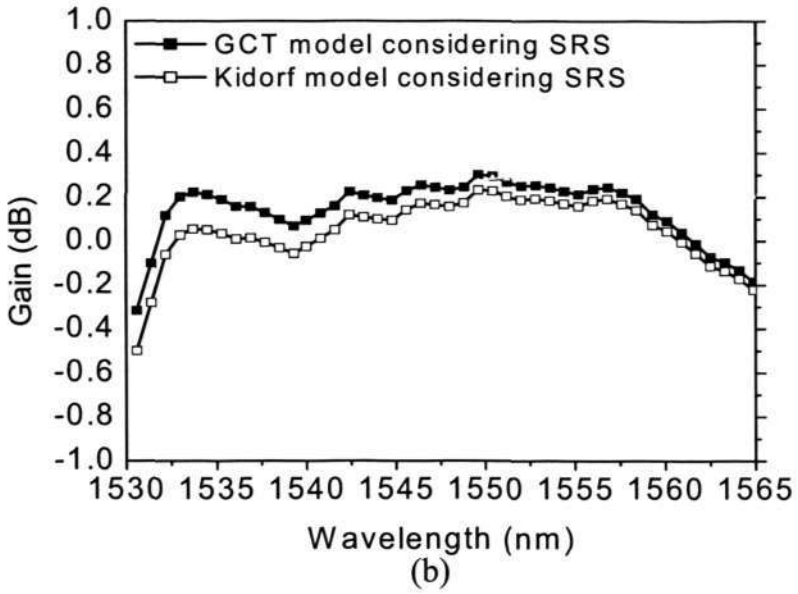


*Figure 3-6 Example of a C-band Raman amplifier design (a) without considering inter-channel Raman interaction; (b) with inter-channel Raman interaction included*

After applying the design procedure discussed above, the resultant theoretical gain curve is given in Figure 3-6 (a). Obviously a flat gain spectrum with ripple less than 1dB can be obtained. The gain ripple is mainly at the two sides of the gain spectrum. If more pump wavelengths are used for compensation, better flatness can be obtained. In this design, the wavelengths of the pump lasers are 1422.5nm, 1434nm and 1469nm, while the corresponding pump powers are 654mW, 349mW and 275mW respectively. A complete numerical model given by *Kidorf* is used to verify the simulation result which considers the amplified spontaneous emission (ASE) power and *Rayleigh* backscattering but not inter-channel *Raman* interaction among signal channels [78]. The result is shown in the same figure. Apart from a slight difference in net gain, good agreement with theoretical design result is achieved. The very small difference observed is as expected since in the design procedure the effects of *Rayleigh* scattering and ASE were not considered. When considering inter-channel *Raman* interaction

among signals in the *Kidorf* model, the net gain spectrum will tilt noticeably as shown in Figure 3-6 (a). This can be rectified by considering the effect of inter-channel *Raman* interaction in the amplifier design. Here the slope of inter-channel *Raman* interaction with the given input signal condition is obtained first and is then used to modify the slope of $S_1$ in the design process before the compensation procedure is carried out. After the amplification condition is established, the newly obtained inter-channel *Raman* interaction value is then used to modify the slope of $S_1$ before a new compensation procedure is carried out. Very little iteration is required since the *Raman* tilt hardly changes after the signal distribution in the presence of the *Raman* pump is more or less established. The obtained new result is plotted in Figure 3-6 (b). The modified pump powers are 682mW, 370mW and 254mW respectively. Clearly, this allows flat net gain spectrum to be achieved even if inter-channel *Raman* interaction is taken into consideration.

## 3.3 Optimization of DRA using Hybrid Optimization Algorithm

### 3.3.1 Background

In section 3.2, in order to remove the iterative nature of GA, a novel optimization algorithm has been proposed based on the geometry characteristics of *Raman* gain profile [137]. However, it is difficult to rely on this scheme alone to reduce the ripple of broadband gain spectrum to be less than 0.8dB in the simulation example of last section. In addition, GCT will become complex

when SSRI interaction and wavelength dependent loss of the fiber needs to be considered.

In order to increase the optimization efficiency and improve the optimization accuracy in the design of DRA, a novel hybrid optimization algorithm based on GCT and GA is proposed in this section. In the hybrid optimization algorithm, optimized pump wavelengths are obtained using GCT, while the optimized pump path integrals are obtained using GA. As a result, two dimensional random searches in GA can be simplified to one dimensional random search for optimized pump path integrals since the pump wavelengths have been optimized using GCT without any iteration of random search and optimization accuracy of GCT can be improved greatly by GA simultaneously. In addition, more reasonable pump power arrangement can be obtained utilizing this hybrid optimization scheme than those obtained using GA.

### 3.3.2 Theoretical Model and Design Approach

Figure 3-7 shows the flow chart of hybrid optimization algorithm based on GA and GCT.

In step A, *Raman* pump wavelengths are first determined by using GCT according to the desired *Raman* gain bandwidth. This step is very fast without iteration in GCT if ignoring the wavelength dependence loss of fiber and SSRI.

In step B, pump wavelengths obtained from GCT can be adopted directly as the known parameters for GA and only need to search for the corresponding pump

path integral of each pump laser using GA. In this way, two dimensional random search of GA can be reduced to one dimensional random search.

Step C shows how to compensate the gain tilt effect induced by SSRI using GA. SSRI can be compensated by iterating GA, which starts with the signal power integrals computed in the absence of any pump laser and updates them using the new values by iterating GA each time. Only few of these iterations are required because the *Raman* tilt hardly changes after the signal power distribution in the presence of *Raman* pump is more or less established [81, 82].

In step D, using the same approach as proposed in [81], pump powers can be derived from the pump path integrals by using an iterative method to solve the coupled nonlinear *Raman* propagation equations.

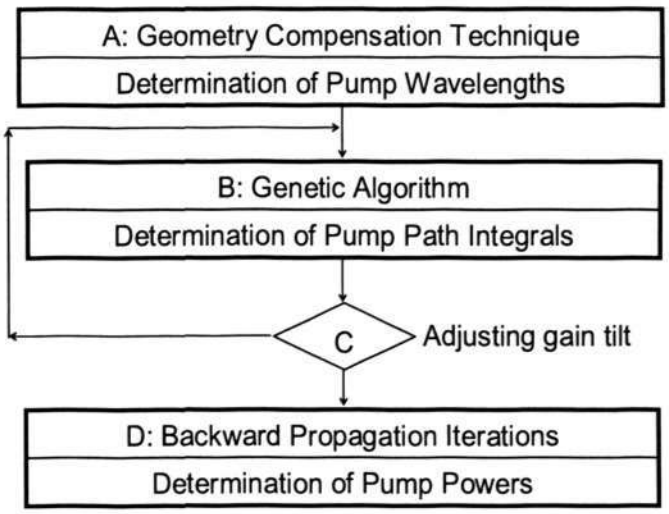


*Figure 3-7 Flow chart of hybrid optimization algorithm based on GA & GCT*

### 3.3.3 Numerical Example and Discussions

In this section, hybrid optimization algorithm based on GA and GCT is applied to optimize a C-band DRA. The DRA is backward pumped by three *Raman* pump lasers in 80km SMF to achieve 0*dB* targeted net gain. It is designed for DWDM system with 40 signal channels from 1530nm to 1565nm with input signal level at 0dBm per channel. Following the flow chart of hybrid optimization algorithm, pump path integrals and pump wavelengths are first obtained using GCT. In order to simplify the GCT, wavelength dependent loss of *Raman* gain fiber and SSRI are not considered in this step. The optimized *Raman* gain spectrum obtained by using GCT is shown in Figure 3-8.

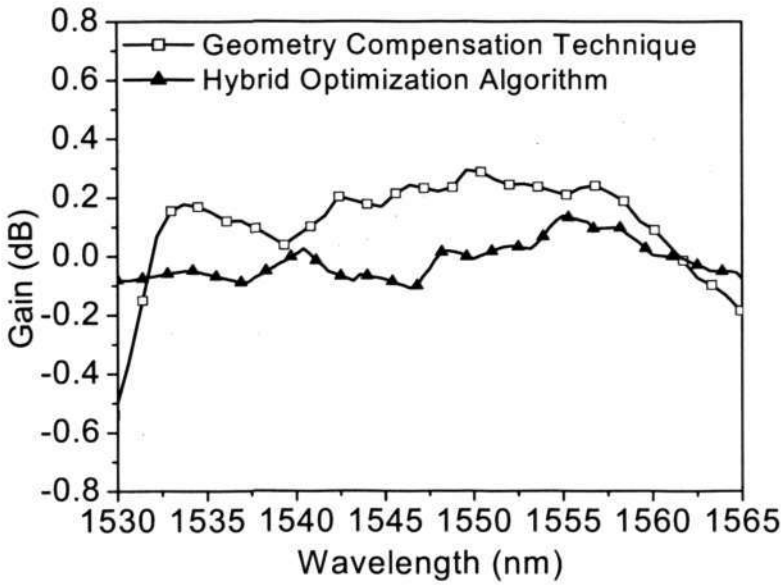


*Figure 3-8 Raman gain spectra using GCT and hybrid optimization algorithm*

Optimization result indicates that it is difficult to rely on GCT alone to achieve a broadband *Raman* gain spectrum with gain ripple less than 0.8*dB*. The pump wavelengths and pump path integrals obtained by GCT are shown in Table 3-1. In order to obtain the flatter *Raman* gain spectrum, further optimization of

*Raman* pump integrals is necessary. Then the *Raman* pump wavelengths obtained from GCT are used as the initial parameters of GA, while the pump path integrals obtained from GCT are optimized by using GA further. In this step, both wavelength dependent loss spectrum of the *Raman* gain fiber and SSRI will be considered. As shown in Figure 3-8, a flatter *Raman* gain spectrum with maximal ripple less than 0.2dB can be achieved based on the hybrid optimization algorithm. The final optimized results obtained by hybrid optimization algorithm are shown in Table 3-1. It is found that the pump path integrals in GA only need a little adjustment compared with those obtained by using GCT.

| Pump wavelength (nm) | 1422.5 | 1434 | 1469 |
|---|---|---|---|
| Pump path integral using GCT (km.mW) | 2218 | 1666 | 5033 |
| Pump integral using hybrid algorithm (km.mW) | 2477 | 1839 | 4902 |

*Table 3-1 Optimization result using GCT and hybrid optimization algorithm*

The advantage of hybrid optimization algorithm compared with GA is analyzed as follows. First, the convergent speed of hybrid optimization algorithm is much faster than GA, since two-dimensional random searches for the pump wavelengths and pump path integrals in GA are reduced to only one-dimensional random search for pump path integrals in hybrid optimization algorithm. The pump wavelengths have been chosen depending on GCT, which is high efficient actually.

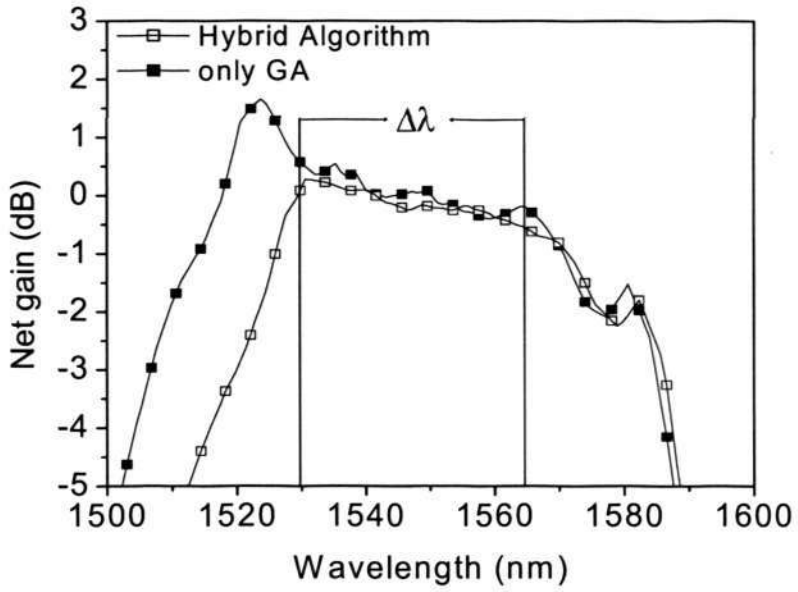


*Figure 3-9 Comparison between hybrid optimization algorithm and GA*

Secondly, since GA is a completely random global search for all possible solutions, any solution satisfying the desired gain requirement, such as gain ripple, bandwidth and pump number, will be selected as a potential pump arrangement for DRA. However, some of these pump arrangements depending on GA are not reasonable or feasible solutions since random search can only guarantee the gain requirement within the desired bandwidth, while ignore the practical gain requirement outside the desired bandwidth. Consequently, optimized pump configuration using GA may waste some pump powers on the gain outside the desired bandwidth and the gain outside the desired bandwidth cannot be ensured to be as low as possible. However, since hybrid optimization algorithm first utilize the geometry characteristics of *Raman* gain profile to select pump wavelengths according to desired gain bandwidth, both the gain spectrum within and outside the desired bandwidth can be optimized simultaneously. In this way, the lowest pump powers can be ensured using the

least number of *Raman* pumps compared with that using GA alone. Optimized gain spectra of DRA using hybrid optimization algorithm and GA are shown in Figure 3-9 respectively. Here for simplicity, SSRI is not considered. When using hybrid optimization algorithm, optimized gain spectrum outside the desired bandwidth ($\Delta\lambda$) decreases rapidly, as shown in Figure 3-9. While GA cannot ensure the optimized gain spectrum outside the desired gain bandwidth to be sufficiently low, which can also be found from Figure 3-9. As a result, the pump power required in GA is much higher than that in hybrid optimization algorithm. The optimization results are compared in Table 3-2. It can be found that total pump power required for GA is 1644mW, while it is only 1380mW for hybrid optimization algorithm.

| Pump wavelength using GA (nm) | 1416 | 1428 | 1467 |
|---|---|---|---|
| Pump power using GA (mW) | 989 | 479 | 176 |
| Pump wavelength using hybrid algorithm (nm) | 1422.5 | 1434 | 1469 |
| Pump power using hybrid algorithm (mW) | 743 | 388 | 249 |

*Table 3-2 Pump powers required in GA and hybrid optimization algorithm*

## 3.4 Conclusions

This chapter proposes several optimization algorithms for multi-wavelength backward pumped DRA and compares their characteristics.

A simple GCT is first proposed to optimize wideband DRA based on the geometric characteristics of the *Raman* gain spectrum. In comparison with traditional solutions using rigorous iterative simulation, such as GA, the suggested method is simpler and more effective. In order to improve the

accuracy of the GCT and increase the convergent speed of GA further, a hybrid optimization algorithm based on GCT and GA is also proposed to optimize the wideband DRA. Compared with the optimization result using GCT alone, hybrid optimization algorithm can achieve much flatter *Raman* gain spectrum. In addition, more reasonable pump arrangement can be obtained using hybrid algorithm than those obtained by using GA alone.

# Chapter 4

# Suppression of Impairments in DRA

## 4.1 Introduction

Implementation of high capacity wavelength division multiplexed (WDM) transmission system requires broadband flat *Raman* gain spectrum over WDM channels. In Chapter 3, two optimization algorithms utilizing multi-wavelength *Raman* pumps are proposed to meet this requirement. Other factors affecting the performance of a *Raman* amplified transmission system are amplified spontaneous emission (ASE), double *Rayleigh* backscattering (DRBS) noise and nonlinear penalty in the amplifier [4]. These impairments will greatly degrade the performance of communication systems. As a result, optimizations of noise and nonlinear performance in distributed *Raman* amplifier (DRA) are also important issues in long haul WDM transmission system design.

Over the past few years, many schemes have been proposed to improve the performance of DRA by minimizing the combined effects of noise and nonlinear impairments. Since optical amplification prior to transmission loss can generally suppress the subsequent ASE noise, DRA combining forward and backward pumping configuration can achieve better noise performance [4, 138]. Another proposed scheme utilizes effective area managed fiber, such as dispersion managed fiber (DMF) within the amplification span to distribute the *Raman* gain more evenly along the span [139, 140] and noise performance can be improved as a result. Other proposed schemes include the use of second or higher order DRA, which can extend the *Raman* gain further into the transmission fiber by higher order *Raman* amplification. In this way, signal power distribution along the span can be made more evenly and hence the noise performance can be improved [92-94].

However, there exist many problems associated with these optimization schemes. The first problem is that in the case of DRA with gain bandwidth exceeding 90nm realized by multi-wavelength *Raman* pumps, although a flat *Raman* gain spectrum over broadband WDM signal channels can be obtained, noise performance is not the same over all the signal channels [85]. Because the system limitations are determined by noise performance in the worst channel [4], it is desirable that both gain and noise spectra over wideband signal channels are flat [81, 82, 84, 137]. The second problem is associated with bi-directional pumped DRA, which has been studied extensively to improve the noise performance in long haul transmission system. However, nonlinear impairments induced by bi-directional pumped DRA are more significant than uni-directional

pumped one. As a result, there is a tradeoff between the improvement in noise and the degradation caused by nonlinear effect. How to obtain the best system performance by balancing the noise improvement and nonlinear degradation is still a practical problem for bi-directional pumped DRA [117]. Compared with common first-order *Raman* amplifications, second-order *Raman* amplifications have been verified as a way to improve the noise performance [4, 92, 141, 142]. However, a relatively low pumping efficiency of the second-order stimulated *Raman* scattering (SRS) and a significant amount of wasted first-order pump power is also a main problem preventing their practical application in transmission systems. It is known that incorporating DMF within the amplification span can make the *Raman* gain distribute more evenly along the span and hence improve the noise performance of transmission system. Again, pump conversion efficiency for effective-area-managed fiber is still not high enough to improve the noise performance effectively. More efficient *Raman* gain mediums are desired to improve the system performance.

This chapter proposes several novel schemes to tackle these problems associated with the existing optimization schemes in order to improve the noise and nonlinear performance in DRA further. They can be classified into active or passive schemes according to the pumping configuration or transmission span. Section 4.2 discusses the improvement of gain and noise performance in a L-band hybrid *Raman*/EDFA, which is obtained by dual-order SRS of a single 1395nm *Raman* fiber laser (RFL) in 75km single mode fiber (SMF) and its corresponding dispersion compensation fiber (DCF) module. The pump conversion efficiency in this scheme is much higher than that uses only the

second order DRA. A passive scheme to improve the system performance is then studied in section 4.3, where the effect of a piece of highly nonlinear photonic crystal fiber (PCF) on the noise characteristics of a backward pumped DRA is studied experimentally. In the last section of this chapter, suppression of polarization dependent gain (PDG) due to signal-to-signal *Raman* interaction (SSRI) is investigated experimentally.

## 4.2 Hybrid *Raman*/EDFA Based on Dual-order SRS

### 4.2.1 Background

Compared with conventional first-order *Raman* amplification, second-order *Raman* amplification, in which the main pump is separated by two *Stokes* orders from signal wave, has been proposed to further improve optical signal to noise ratio (OSNR) in the transmission system, due to its capability in realizing more uniform distribution of signal power along the amplification span. However, relatively low pumping efficiency of the second-order *Raman* scattering and a significant amount of waste of the residual first-order pump power are still issues for their practical application [4, 92, 141, 142]. Effort has been made to address the issue of low pump efficiency of first order *Raman* amplification [104, 105]. The unused residual *Raman* pump power is recycled by using a pump reflector or high *Raman* gain coefficient fiber is employed to reduce the waste of *Raman* pump and consequently to increase overall power conversion efficiency [105]. In [106], the residual pump power after DCF is recycled for secondary signal amplification in a segment of *Erbium* doped fiber (EDF) following the DCF.

However, no attention has been paid to low pumping efficiency and pump recycling issue in second-order *Raman* amplifications. This section discusses a *Raman*/EDFA hybrid amplifier based on dual order SRS of a single pump to realize amplification in L-band. The proposed hybrid amplification scheme inserts a segment of EDF within the span to recycle the residual first order *Raman* pump power. The gain and noise performance of the hybrid amplifier is investigated in terms of location of the EDF within the amplification span. Experimental results show that properly locating the EDF can balance the gain and loss more uniformly along the span and hence improve the system performance in terms of net gain and noise performance.

### 4.2.2 Experimental Setup

Figure 4-1 (a) shows the experimental setup for studying the noise and gain characteristics of a *Raman*/EDFA hybrid amplifier based on dual-order SRS of a single pump. The transmission span includes 75km SMF, a segment of EDF (20m or 4m long) with 1000ppm $Er^{3+}$ and 12.5km DCF module, which can provide both *Raman* amplification and corresponding dispersion compensation simultaneously. The optical signal is provided from WDM laser sources with input power of 0dBm. The *Raman* pump laser is a depolarized RFL with output power of 1W at 1395nm to obtain dual-order SRS. In order to suppress the relative intensity noise (RIN) transferred from pump to signal waves, the pump laser is backward-pumped. Two acousto-optic modulators (AOM1 & AOM2) are used to generate a modulated signal and an optical gating for OSNR measurement. Both switches operate at a modulation frequency of 200kHz, a duty cycle of 50% and have an extinction ratio greater than 90dB. The signal

output power and ASE noise can be measured accurately by controlling the relative phase of both AOMs, as demonstrated in [133]. In order to study the effect of the EDF on the hybrid amplifier, one segment of EDF with 20m (or 4m) length is placed in different positions along the amplification span. After optimizing the length of EDF according to the noise and gain performance in this experiment, 20m long EDF is chosen for L-band amplification and 4m EDF is used for C-band amplification to extend the amplification bandwidth from L-band to the whole C+L band.

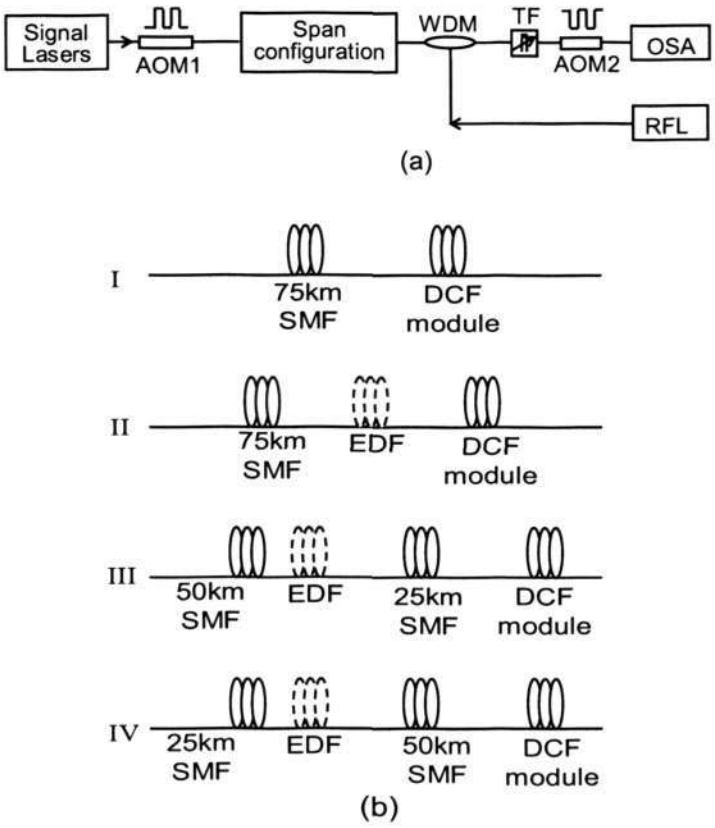


*Figure 4-1 (a) Experimental setup; (b) Span configurations*

Four types of span configurations are considered as shown in Figure 4-1 (b). Configuration I is the conventional amplification span without incorporating

EDF. In configuration II, EDF is placed just before the DCF module. In the third configuration, EDF is placed after 50km SMF from the span input end and in the last configuration, EDF is placed between 25km SMF and 50km SMF plus DCF module.

### 4.2.3 Experimental Results and Discussions

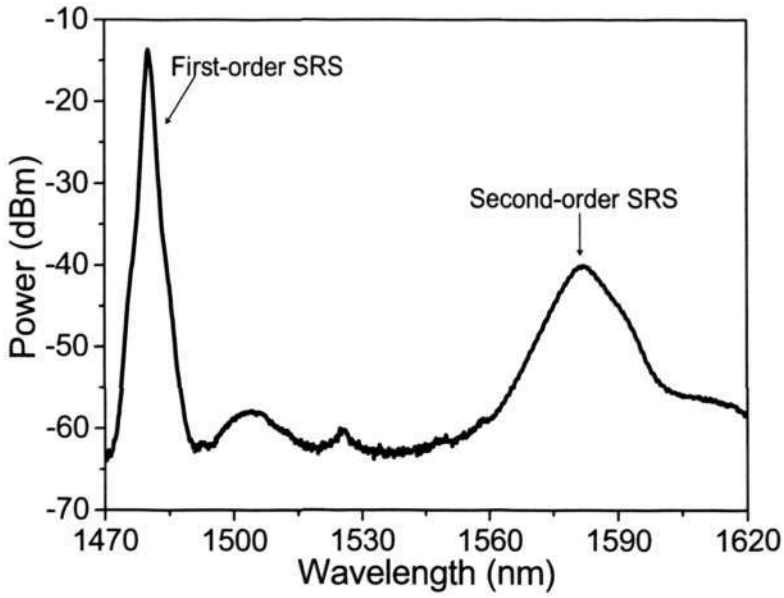


*Figure 4-2 Dual order SRS of 1395nm RFL after 75km SMF+DCF*

Figure 4-2 shows the dual-order SRS of a 1395nm RFL generated in the 75km SMF and DCF module. The first order SRS is at around 1480nm and the second order SRS is located from 1570nm to 1610nm, which provides L-band *Raman* gain. In a pure second order *Raman* amplifier (configuration I), only the second order SRS is used to provide L-band *Raman* gain and the residual first order SRS around 1480nm is wasted. When a segment of EDF is inserted into different locations of the amplification span, the residual first-order SRS around 1480nm as shown in Figure 4-2 can be recycled. In this hybrid amplifier, the

total net gain is contributed from the second-order *Raman* amplification and EDF amplification.

Figure 4-3 shows the net gain plotted against wavelength for four types of span configuration when the EDF length is 20m. The shapes of the net gain curves in four configurations have no obvious difference, but the amounts of the gain exhibit large variations. That is because 20m EDF is long enough to generate gain shift effect and thus provide secondary amplification in L-band from 1570nm to 1610nm by recycling the residual first-order SRS. As shown in Figure 4-3, the improvements of net gain in configuration III and II are more than 4dB and 10dB respectively, compared with that in configuration I. The large increase of net gain in configuration II and III can be explained as follows. In configuration I, only second-order SRS provides L-band amplification and the residual first-order SRS after the SMF+DCF is wasted completely, while it is reused to pump EDF in configuration II and III. In addition, EDF amplification exhibits higher pumping efficiency compared with that of *Raman* amplification. Comparing configurations II, III and IV, the net gain obtained at a given pump power is strongly dependent on the position of the EDF. The net gain of configuration II is the highest and is about 5dB higher than that of configuration III and about 16dB higher than that of configuration IV. Obviously, the closer the EDF is placed to the DCF module, the higher net gain can be obtained. When the EDF is placed closer to the DCF, the residual first-order SRS used to pump the EDF is higher since it suffers less fiber attenuation, leading to higher percentage of gain contributed from the EDF and hence the higher the pump efficiency [143]. On the other hand, the improvement of the

pump efficiency will be decreased by moving the EDF toward the input end of the amplification span due to too large attenuation of the first-order SRS. When the first-order SRS injected into the EDF is too low and not enough to pump the EDF, the EDF becomes an absorption medium rather than a gain medium. As a result, the net gain in configuration IV is even 7dB lower than that in configuration I. Therefore, there is an optimal location of EDF in achieving the maximal net gain.

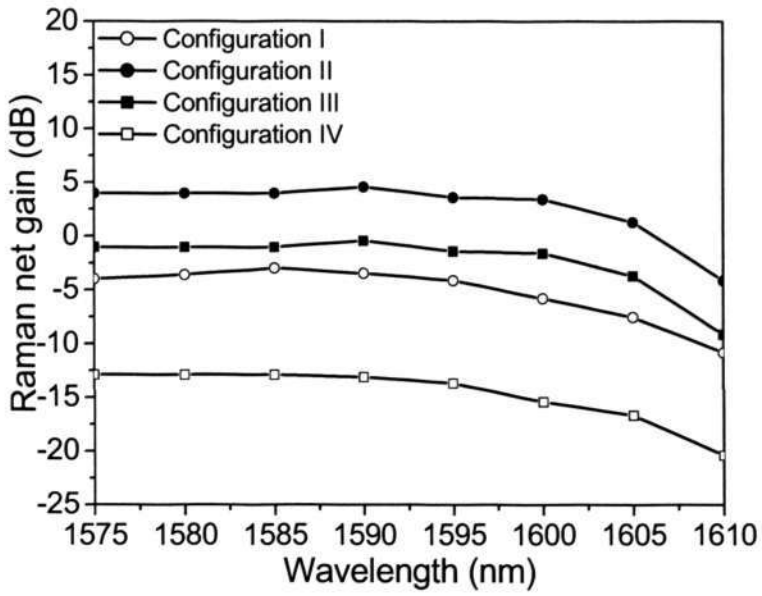


*Figure 4-3 Net gain vs. wavelength for different configurations with 20m EDF*

Figure 4-4 shows the OSNR against wavelength for four types of span configuration when the EDF length is 20m. According to recent studies on minimizing the combined effect of noise and nonlinear, an improved noise performance can be achieved by balancing the gain and loss at every point in the transmission span as analyzed in [144, 145]. It is known that the signal gain near the beginning of the transmission span is the lowest and increases toward the end of span in a pure backward pumped *Raman* amplifier. However, when a

segment of EDF is inserted into the transmission span, the distribution of the signal power along the fiber span will change. The gain of the signal at the position of EDF becomes higher due to the higher pumping efficiency of EDF amplification compared with that of *Raman* amplification. By optimizing the position of EDF, the overall non-uniformity of the signal power distribution along the fiber link can be alleviated and hence the noise performance can be improved.

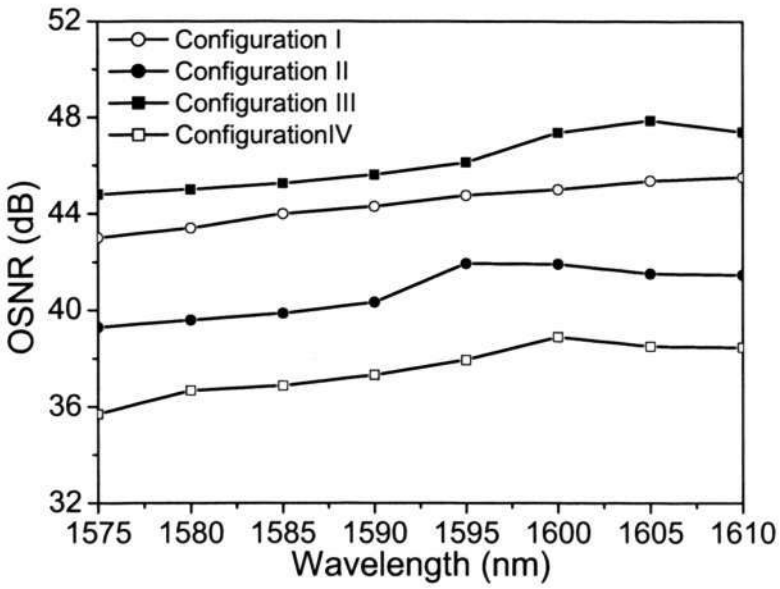


*Figure 4-4 OSNR vs. wavelength for different configurations with 20m EDF*

As shown in Figure 4-4, the best noise performance is obtained in configuration III among the four types of span configuration. Configuration III exhibits about 2dB OSNR improvement compared with that in configuration I where only *Raman* amplification is used, because placing EDF following the 50km SMF in configuration III makes the overall signal power distribution more uniform over the amplification span. Comparing configuration I with II, OSNR in the latter is about 4dB worse than that in the former, although configuration II has the

largest improvement in net gain. This is because configuration II introduces more imbalance of signal power distribution along the span due to larger gain coefficient of the EDF, leading to worse noise performance [144]. Among the four types of span configurations, the worst noise performance is in configuration IV, which is mainly due to too large fiber attenuation to the first-order SRS, leading to too low pump power into the EDF medium. As a result, the imbalance of the signal power distribution along the length of the transmission is aggravated further due to the absorption attenuation from the EDF. It is found that OSNR is also dependent on the position of the EDF. As a result, there is a tradeoff between the gain and noise performance in the hybrid *Raman*/EDFA.

By recycling the residual first-order SRS to pump a short EDF (about 4m), an additional C-band amplification is obtained from the EDF and thus the flat gain bandwidth is extended from L-band to C+L band. Figure 4-5 shows the net gain curves against wavelength for four types of span configuration. 4m EDF is used from configuration II to IV. The gain bandwidth in configuration I is determined by the second-order SRS spectrum of the single-pump source. Since the *Raman* gain spectrum with single pump is not flat over a wideband region, 3dB gain bandwidth in configuration I ranges only from 1570nm to 1610nm, which is the narrowest among the four types of span configuration. However, the extended gain spectrum in configuration II, III and IV ranges from 1520nm to 1610nm and their ripple is less than 5dB. The net gain in L-band obtained in configuration I is the highest among the four configurations since no first-order SRS is used to provide gain in C-band and thus all the gain goes to L-band. For

the other three configurations II, III and IV, the net gain for a given pump power is also strongly dependent on the location of the EDF, as shown in Figure 4-5 and shows a similar trend to that of Figure 4-3. The net gain in configuration II is about 3dB higher than that in configuration III because the residual first-order SRS to pump the EDF in type II is higher than that in configuration III due to less fiber attenuation and absorption attenuation of EDF. For configuration IV, lot of first order SRS power is attenuated by the transmission fiber or absorbed by the EDF. As a result, the net gain in configuration IV is the lowest because the residual first-order SRS injected into the EDF is the lowest and is not enough to pump the EDF. The broadband gain provided in configuration III is between that in configuration I and IV. The absorption attenuation caused by the EDF shows gain degradation not only in C-band EDFA but also in L-band *Raman* amplification.

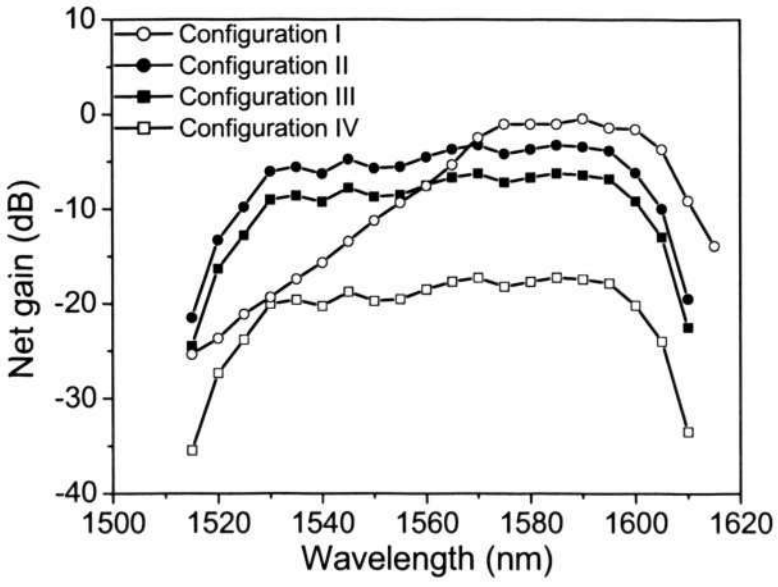


*Figure 4-5 Net gain vs. wavelength for different configuration with 4m EDF*

## 4.3 Effect of Photonic Crystal Fiber on Noise Performance of DRA

### 4.3.1 Background

According to recent studies on minimizing the combined effect of ASE, DRBS noise and nonlinear impairment in DRA [133, 138, 143, 146-148], the key is to balance gain and loss at every point in the fiber, ensuring a flat signal power distribution along the amplification span [139, 144].

In this section, a piece of highly nonlinear PCF [149, 150] with a length of 100m is inserted into a backward pumped DRA. When an optical signal is transmitted along 100m nonlinear PCF and 25km SMF, OSNR of both the ASE and DRBS noise increase. The first reason is that the *Raman* gain is increased at the beginning of the span when the signal passes through the nonlinear PCF. The second is that the PCF with high *Raman* gain coefficient, when placed before the SMF, reduces the signal power excursion and the signal power becomes more flat over the transmission length. However, the OSNR of the DRBS is not improved as much as that of the ASE, due to larger amount of *Rayleigh* scattering in a nonlinear PCF than that in SMF.

### 4.3.2 Properties of Highly Nonlinear Photonic Crystal Fiber

The PCF used in our experiment is the hybrid-core nonlinear dispersion-shifted PCF (zero chromatic dispersion wavelength at 1500nm and dispersion of ~5 ps/nm/km at 1550nm) fabricated by *Crystal Fiber A/S*. The hybrid core region comprising a germanium-doped center element ($n$=1.487) surrounded by three

fluorine-doped regions ($n$=1.440) is embedded in a standard triangular air/silica cladding structure, as shown in Figure 2-3. The diameter of the doped elements equals the pitch ($\Lambda$=1.5μm). The effective area $A_{eff}$ of the fundamental mode is about 3.46$\mu m^2$. The nonlinear coefficient $\gamma$ of the guided mode in this fiber is measured at 1555nm through a direct continuous wave (CW) measurement of the nonlinear phase shift suffered by a beat signal propagating in the fiber. The measurement procedure is fully described in [151]. From the measured nonlinear phase shift versus the launched optical power, the value of $\gamma$ is 11$W^{-1}$ $km^{-1}$, which is about 5 times higher than that of a conventional dispersion shifted fiber.

*Rayleigh* scattering in conventional fibers arises from the light interacting with a material having uneven density. Variations in material density and compositional fluctuations occurring during fiber manufacture process create random inhomogeneities that give rise to refractive index variations. In PCF, in addition to density and compositional fluctuations, *Rayleigh* scattering also arises from structure fluctuations because the geometry of the holes may not be perfectly regular. Here, an optical time domain reflectometer (OTDR) with pulses of 5ns duration is used to measure the *Rayleigh* scattering of the nonlinear PCF. Backscattering parameter $k$ ($k = S \cdot \alpha_s$, where $S$ is the fraction of the light scattered in all directions that is captured by the fiber core and guided back to the OTDR and $\alpha_s$ is a scattering attenuation coefficient per unit length) is about $1.4\times10^{-3}$/km at wavelength of 1560nm. It is up to one order higher than that in a conventional SMF. Because the PCF has different optical characteristics from those of SMF, such as higher *Raman* gain coefficient and

higher *Rayleigh* scattering parameter, DRA obtained by using a PCF can be significantly different from that obtained by using a conventional fiber alone.

### 4.3.3 Effects of Photonic Crystal Fiber on DRA

Figure 4-6 (a) shows the apparatus used to measure the noise characteristics of a backward pumped DRA. The AOM1 generates a modulated signal and the AOM2 provides an optical gating for detection. Both AOMs have an extinction ratio of greater than 90dB operating at a modulation frequency of 200*kHz*. The duty cycles of the modulated AOM and the received AOM are 50%. The input signal power is 0dBm and the wavelength is 1550nm.

As demonstrated in Reference [133], the signal output power is measured when the modulated AOM and the received AOM are working in the same phase. The DRBS and the ASE noise are measured as a sum (the total noise power) with the received AOM sampling window out of phase with the modulated AOM. The DRBS noise appears as a narrow spectral peak on the background of ASE noise observed through an optical spectrum analyzer (OSA). The change of the ASE level can be ignored when the input signal is turned on or off, because only one small signal transmits through the *Raman* amplifier. Here, the ASE power is measured conveniently by turning off the signal. So the DRBS noise is given by subtracting the ASE power from the total noise power. Because the spectral range of the ASE is about 10*THz*, in order to measure the noise in the signal channel band, an optical filter (center wavelength 1550nm and pass-band 1.5nm) is used at the transmission end.

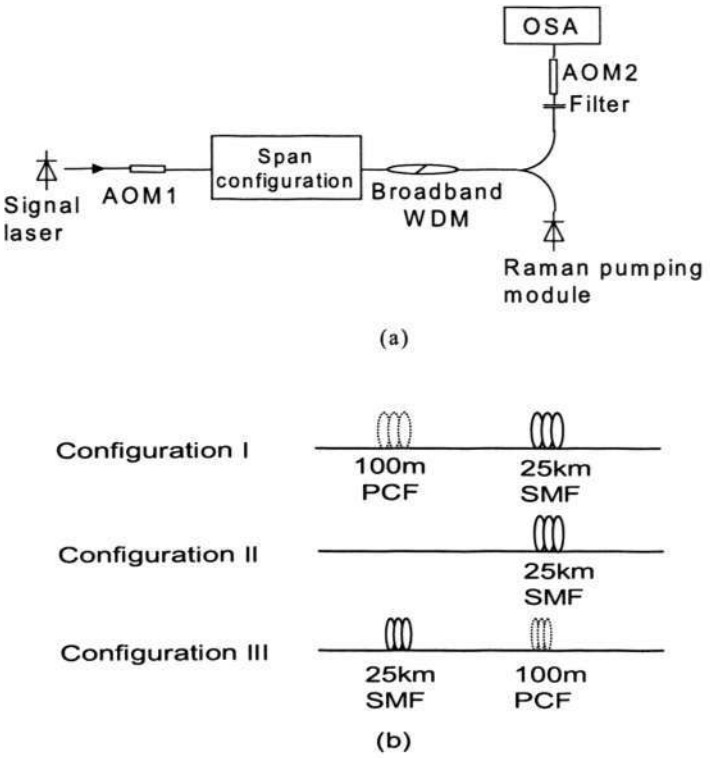


*Figure 4-6 (a) Experiment setup; (b) Span configuration*

A multi-wavelength *Raman* pump module with 250mW output power at 1425nm and 450mW at 1453nm is used to realize a flat *Raman* gain spectrum in C-band, as shown in Figure 4-6 (a). A broadband WDM is used to multiplex the pump and the signal. The *Raman* gain fiber is 25km SMF. In order to observe the effect of the PCF on the *Raman* amplification, a piece of 100m highly nonlinear PCF, whose ends are tapered, is coupled to either the front end (configuration I) or the back end (configuration II) of the SMF. In other words, in configuration I, the PCF is paced before the SMF; in configuration II, only the SMF; in configuration III, the PCF is placed after the SMF. All the three configurations are shown in Figure 4-6 (b) and their gain and noise characteristics have been measured.

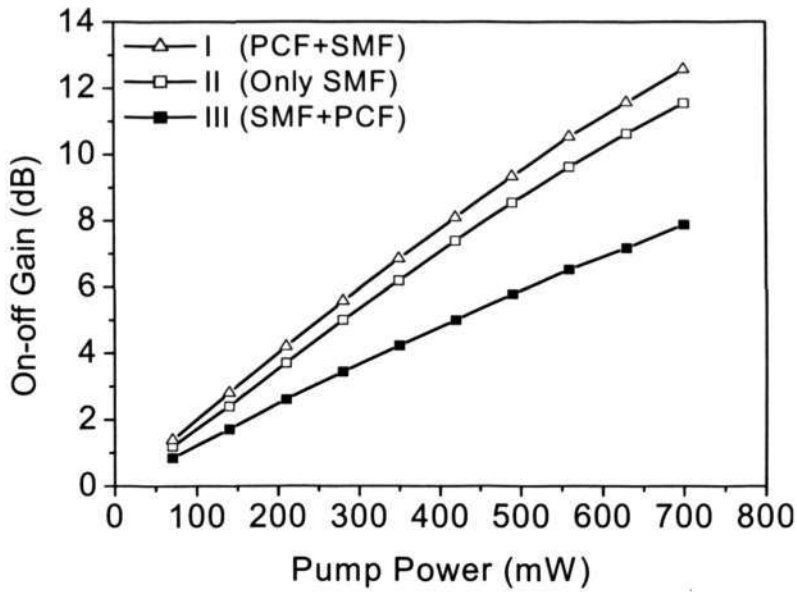


*Figure 4-7 On-off gain as a function of pump power in Raman amplifiers*

Figure 4-7 shows the on-off gain as a function of pump power in DRA for three configurations. On-off gain obtained at a given pump power is strongly dependent on the position arrangement of the PCF. At pump power 70mW (10% of the maximum pump power, total pump power of two *Raman* pumps is 700mW), the on-off gains are 1.4, 1.2 and 0.9*dB* for configuration I, II and III, respectively. With the increase of pump power, the difference of on-off gains for three configurations increases and the slopes of on-off gain versus total pump power have been measured to be 0.125, 0.116 and 0.078 respectively. Thus, at maximum pump power, the on-off gains for three configurations are 12.57, 11.55 and 7.88*dB* respectively. Compared with configuration II, the pumping efficiency for configuration I is improved because the length of transmission medium is increased by inserting the PCF before the SMF and the residual pump power after the SMF is utilized completely. In theory, the closer the highly nonlinear fiber is placed to the span end, the higher the pumping

efficiency due to its large *Raman* gain coefficient of the highly nonlinear fiber [144]. In configuration III, however, the pump efficiency is not improved by moving the PCF to the span end. The largest on-off gain for configuration III is 7.88*dB*, which is about 3.6*dB* smaller than that for Configuration II (only the SMF). That is mainly caused by the large insertion loss (about 1*dB*) of the PCF at the pump laser wavelengths. The pump power after the PCF is reduced dramatically and the pump power injected into the main *Raman* gain medium (the SMF) is lower than that in configuration II. Even though the PCF has large *Raman* gain coefficient, the large insertion loss at the pump wavelength causes impairment.

Figure 4-8 shows the OSNR of the ASE noise ($OSNR_{ASE}$) and the OSNR of the DRBS noise ($OSNR_{DRBS}$) plotted against the on-off gain of the *Raman* amplifier for three configurations. When the PCF is inserted before the SMF (configuration I), both the $OSNR_{ASE}$ and the $OSNR_{DRBS}$ are higher than the OSNR for Configuration II (only the SMF). The $OSNR_{ASE}$ and the $OSNR_{DRBS}$ increases by about 1.4dB and 0.4dB respectively, when the on-off gain is 6.2dB. For a *Raman* amplifier only using SMF, $OSNR_{ASE}$ can be improved to a certain extent by increasing the signal input power or total pump power in a certain range of signal input power and pump power; however, an improvement of the $OSNR_{DRBS}$ cannot be achieved by increasing the signal input power because the ratio between the DRBS noise and signal is independent of the signal input levels [147]. In configuration II (only SMF), the OSNR is the largest while the pump power is the lowest at the beginning of the transmission link. It is known that an ideal signal power distribution is obtained by balancing the gain and the

loss at every point in the amplification link. The most important change which occurs when the highly nonlinear PCF is placed in the fiber link is that of the distribution of optical signal power along the fiber link. In configuration II, only the SMF is used as the *Raman* gain medium. The *Raman* gain of the signal at the beginning of the link is the lowest. When the PCF is placed before the SMF (configuration I), the situation is changed. The *Raman* gain of the signal at the beginning of the link is increased because of the high *Raman* gain coefficient of the PCF. The non-uniformity of the *Raman* gain distribution along the fiber is alleviated. In Figure 4-8 (b), the configuration of configuration (PCF+SMF) is analogous to the negative (-D) and positive (+D) dispersion-managed fiber *Raman* amplifier in [144]: the placing of the PCF before the SMF makes the signal power more constant over the length of the transmission. The larger power variation along the span results in lower OSNR at the output end. As a result, large OSNR in configuration I can be achieved because the signal power excursion is small. The magnitude of DRBS noise over the transmission link increases due to the higher *Rayleigh* scattering coefficient in the PCF, which leads to limited improvement in $OSNR_{DRBS}$ (only 0.4dB), as compared to configuration II.

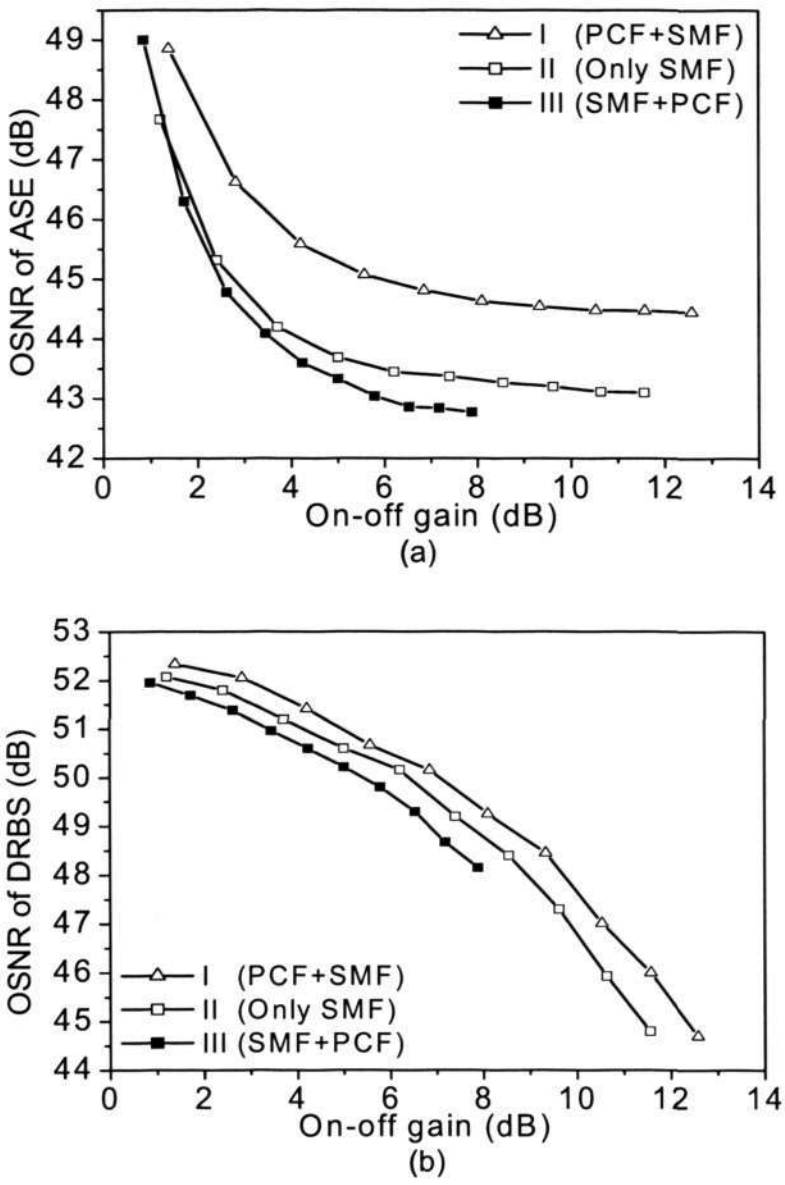


*Figure 4-8 OSNR in Raman amplifier. (a) OSNR of ASE and (b) OSNR of DRBS*

When the PCF is moved to the end of the SMF (configuration III), the $OSNR_{ASE}$ and the $OSNR_{DRBS}$ decrease by about 0.5dB and 0.7dB respectively, as compared to configuration II under an on-off gain of 6.2dB. This can be explained as follows: when a highly nonlinear PCF fiber is inserted at the end of the transmission link of a backward pumped DRA, the pump laser power will

become the highest in the nonlinear fiber. Because of the large *Raman* gain coefficient of the nonlinear fiber, the imbalance of the signal power distribution over the length of the transmission span is aggravated further than that in configuration II. This causes both the $OSNR_{ASE}$ and $OSNR_{DRBS}$ to decrease. As shown in Figure 4-8 (b), the decrease in $OSNR_{DRBS}$ is more significant than that in $OSNR_{ASE}$. The reason is that the DRBS appears at the same spectral region as the signal and the DRBS noise power increases in proportion to the signal power. When the PCF with high *Rayleigh* backscattering is placed at the end of the transmission, the impact of DRBS becomes more significant [144].

In order to give a quantitative analysis about the influence of PCF on the noise performance in DRA, we simulate the power distribution of the signal along the fiber in three span configurations, which is shown in Figure 4-9. It can be found clearly that the lowest signal power along the fiber in configuration I is increased, while the lowest signal power along the fiber in configuration III is decreased compared with that without using PCF in configuration II. As a result, the non-uniformity of the *Raman* gain distribution along the fiber in configuration I is alleviated and the noise performance in this configuration become better, which can be verified by the experimental results above. While the non-uniformity of the *Raman* gain distribution along the fiber in configuration III is degraded and the noise performance in this configuration become worse compared with that without using PCF in configuration II.

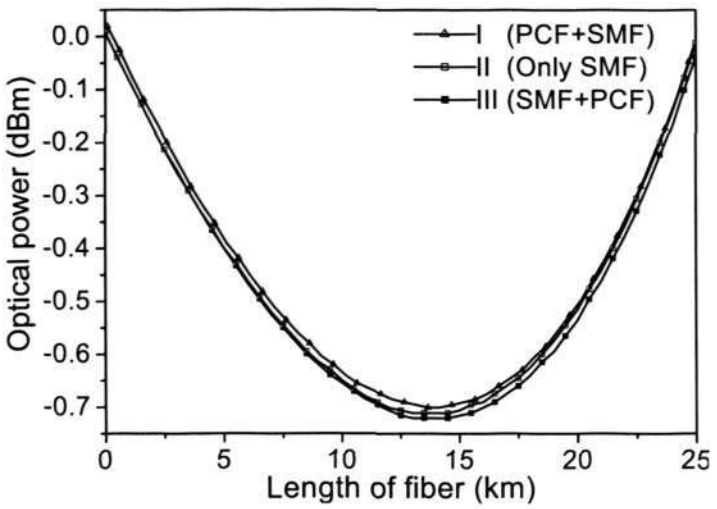


*Figure 4-9 Signal power distribution along the fiber*

## 4.4 Reduction of Polarization Dependent Gain in DRA

### 4.4.1 Introduction

*Raman* amplifiers play a key role in high capacity WDM transmission systems. They offer many advantages compared with other alternative amplification technologies. However, normal *Raman* amplifier implementation suffers from PDG [11]. Studies on the impact of PDG and polarization dependent loss (PDL) in long-haul optical amplified systems have shown that bit error ratio (BER) fluctuations are a strong function of the combined effects of PDG and PDL [13].

It has been found that PDG caused by pump-to-signal *Raman* interaction (PSRI) can be well resolved by depolarizing the *Raman* pump lasers [15]. However, not much research has been done on the mitigation of PDG caused by SSRI. Because *Raman* interaction also exists among WDM signal channels, it is suggested theoretically that PDG is also a function of the relative polarization orientation among WDM signal channels and its magnitude is affected by

polarization mode dispersion (PMD) in the fiber. The implication is that a high PMD in the fiber can reduce the PDG caused by SSRI [11, 14]. However, in practical transmission systems, especially for high-speed transmission, low PMD is desirable for good system performance. Till now, there has been no experimental evaluation on PDG caused by SSRI and no good solution has been proposed to achieve low PDG and PMD simultaneously.

In this section, PDG caused by SSRI is observed experimentally for the first time and the investigation of the influence of PMD and *Raman* gain coefficient of different gain fibers on PDG is carried out. Experimental results show that by using a polarization scrambler (PS), PDG can be reduced effectively whilst keeping the PMD value of the transmission system low.

### 4.4.2 Theoretical Model of Polarization Scrambler

PS can be used to randomize the state of polarization (SOP) of input light in order to reduce the degree of polarization (DOP) effectively on average [9]. In a PS, the electrical field vector of a quasi mono-chromatic light traveling along the z-axis is decomposed into two mutually orthogonal directions, $x$- and $y$-axes. The SOP can be described in terms of amplitude of each electrical field component $E_x$, $E_y$ and their corresponding phase $\varphi_x$, $\varphi_y$, as shown in Equation (4-1). The phase difference between the two polarization directions is given by Equation (4-2). The key purpose of PS is to modulate the phase difference between the two polarizations in such a way as to make the DOP of the input light zero. Because the DOP is a function of modulation amplitude, in order to achieve zero DOP condition, the modulation amplitude would be around 2.405

radians. Dual stage PS is utilized in this experiment. Compared with single-stage PS, the main advantage of multistage scramblers is their ability to depolarize the signal lights independent of their input SOP, thus allowing applications, in which the input SOP is arbitrary [9].

$$E_x = a_x \exp[i\varphi_x(t)]$$
$$E_y = a_y \exp[i\varphi_y(t)] \quad (4\text{-}1)$$

$$\delta(t) = \varphi_x(t) - \varphi_y(t) \quad (4\text{-}2)$$

In a PS, electrodes are used to introduce a modulated e-field. The phase retardation generated in an electrode section of length $L$ is given by Equation (4-3) [9].

$$\delta(t) = \Gamma_y \frac{\pi}{\lambda_0} n_0^3 r_{61} L \frac{V(t)}{G} \quad (4\text{-}3)$$

where $\Gamma_y$ is the spatial overlap of the induced electrical field with the optical fields ($0 \leq \Gamma_y \leq 1$), $\lambda_0$ is the wavelength in free space, $n_0$ is the ordinary index of the refraction, $r_{61}$ represents the property of the $LiNbO_3$, $G$ is the width of the gap between two outer electrodes and $V(t)$ is the electronics voltage applied to two electrodes. Since the induced phase retardation is directly proportional to the wavelength at any given voltage amplitude, hence the DOP varies with wavelength. Besides the obvious $\lambda_0^{-1}$ variation, $\Gamma_y$ is also dependent on wavelength. As a result, the electro-optic PS can introduce different phase retardations for different wavelengths [9]. By using this on WDM signals, the correlation among the SOPs of different wavelength signals can be reduced. This is because the PS using integrated optic device allows high frequency

polarization modulation, leading to very fast changes in the relative orientation among the SOP of the input signals with different wavelength along the fiber length, hence enabling the impact of polarization dependent effects caused by the SSRI to be reduced accordingly.

### 4.4.3 Experimental Setup

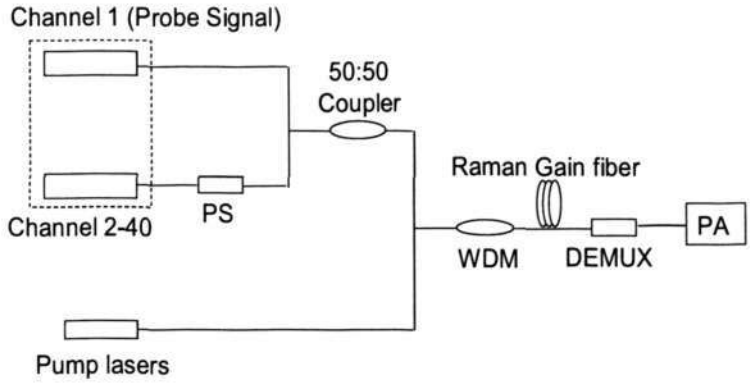


*Figure 4-10 Experimental Setup*

The experimental setup is shown in Figure 4-10. There are a total of 40 CW WDM signal channels (as shown within the dotted frame in Figure 4-10), which are distributed evenly between the wavelengths of 1529.55nm and 1560.61nm. The input power of each channel is 0dBm. In order to investigate the PDG induced only by SSRI, one signal is chosen as a probe signal each time and mixed with the other 39 signal channels through a 50:50 coupler. An electro-optic PS is used in the experimental setup after the 39 channels of WDM signals to investigate the influence of PS on the PDG caused by SSRI. The PS is driven by a sinusoidal signal generator, whose frequency can change from direct current (DC) to 10MHz. The scrambling speed of the scrambler is defined as the driving frequency.

A multi-wavelength pump laser module with 250mW output power at 1425nm and 450mW at 1453nm is used to realize a flat *Raman* gain spectrum in C-band. In order to minimize the PDG caused by PSRI, so as to estimate the PDG primarily due to SSRI, two pump lasers are depolarized using depolarizers. The 40 channel signals and the pump laser signals are coupled into the *Raman* gain fiber through a WDM. In this experiment, two pieces of 15km DCF with 0.36ps and 1ps differential group delays (DGD) respectively are used to investigate the effects of PMD and *Raman* gain coefficients on the PDG. Both fibers have identical technical parameters, except for their PMD values.

A wavelength division de-multiplexer (DEMUX) is used to separate the probe signal from the other 39 WDM signals at the output of the fiber. A polarization analyzer (PA) is used at the output to analyze the PDG and PDL of the system using *Jones* matrix methods. The PA measures the statistical behavior of the PDG of the system. During a short time interval (about 1μs), the input polarization states are scrambled quickly over the *Poincare* sphere and the polarimeter measures the gain for all signal polarization states.

### 4.4.4 Experimental Results and Discussions

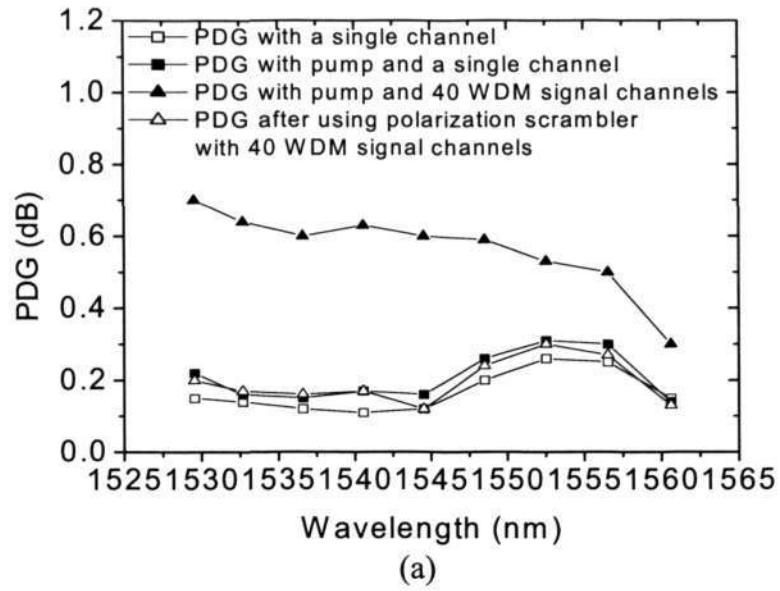


(a)

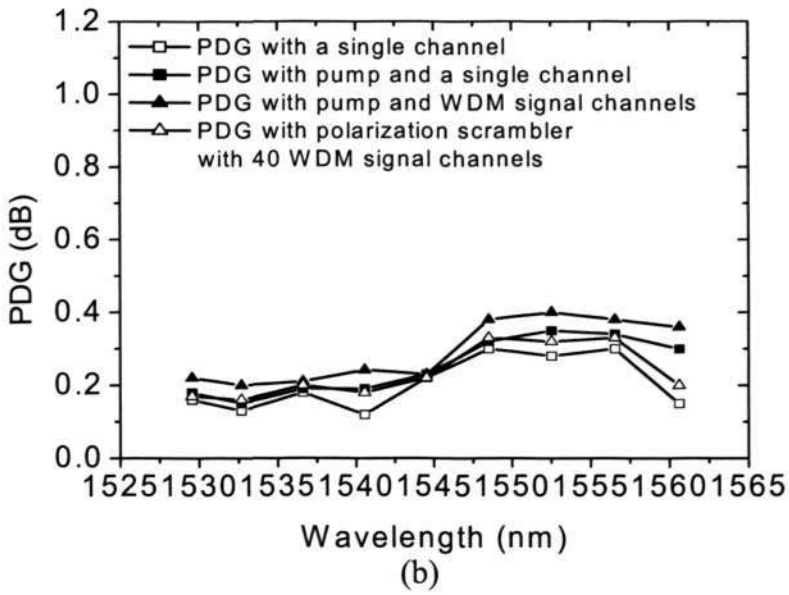


(b)

*Figure 4-11 (a) PDG versus wavelength for DCF with 0.36ps DGD, 12dB on/off gain (b) PDG versus wavelength for DCF with 1ps DGD, 12dB on/off gain*

Figure 4-11 (a) shows the experimental results obtained for a DCF with 0.36ps DGD and 12dB on-off gain. The measured overall PDG is influenced by the PDL caused by all the passive components in the system, the PDG induced by the SSRI, as well as the PDG induced by PSRI. Firstly, the PDG solely due to

the effects of PDL is measured by turning on the probe signal alone, which is about 0.10-0.25dB. It can be found that PDL tends to change considerably with increased channel wavelength in the case without PS, which is caused by the polarization dependent loss characteristics of the components in the experiment setup, such as MUX, DEMUX and etc. When both pump lasers together with the probe signal are turned on, the measured PDG of the probe signal (0.15 – 0.30dB) is slightly higher than that only due to PDL measured previously with only the probe signal. This is because PDG due to PSRI cannot be eliminated completely by the depolarization of the *Raman* pump lasers, therefore it still contributes a small amount to the measured PDG. When all 40 WDM signal channels and the *Raman* pump lasers were turned on, while the PS is disabled, the PDG of the probe signal is about 0.50-0.70dB, which is much larger than that induced by PSRI and the passive components. This is because in ultra-low-PMD fiber, the SOPs of the WDM signals can remain correlated for quite a long transmission distance. Therefore, in this case the PDG caused by SSRI will become very large. When the PS is enabled for the 39 channel signals, the PDG of the probe signal due to SSRI is found to be reduced effectively. This is because the electro-optic PS can introduce different phase retardations for different wavelengths [9]. As a result, the PDG caused by SSRI can be decreased by reducing the correlation between the SOPs among WDM signal channels. In practical implementation, PS can be used to reduce the PDG of WDM channels caused by PDL, PSRI and SSRI simultaneously by using the PS multiplexing all the WDM signals, just before the transmission fiber. However, this is not done here, in order to investigate the SSRI in detail.

Figure 4-11 (b) shows the experimental results obtained for another DCF with 1ps DGD and 12dB on-off gain. The results show that PDG caused by SSRI is strongly dependent on different DGD values of the *Raman* gain fiber. The PDG of the probe signal for a fiber with 0.36ps DGD is clearly found to be higher than that of a fiber with 1ps DGD for all wavelengths. Since both fibers have the same *Raman* gain coefficient and differ only in their PMD values, it is reasonable to assume that PMD can be used to explain the difference in the behaviour of PDG in the *Raman* amplification [11]. For a fiber with a relatively large PMD, the relative orientation among the SOPs of WDM signal channels changes very fast along the fiber length and thus it can reduce the correlation among the SOPs of signal channels [152].

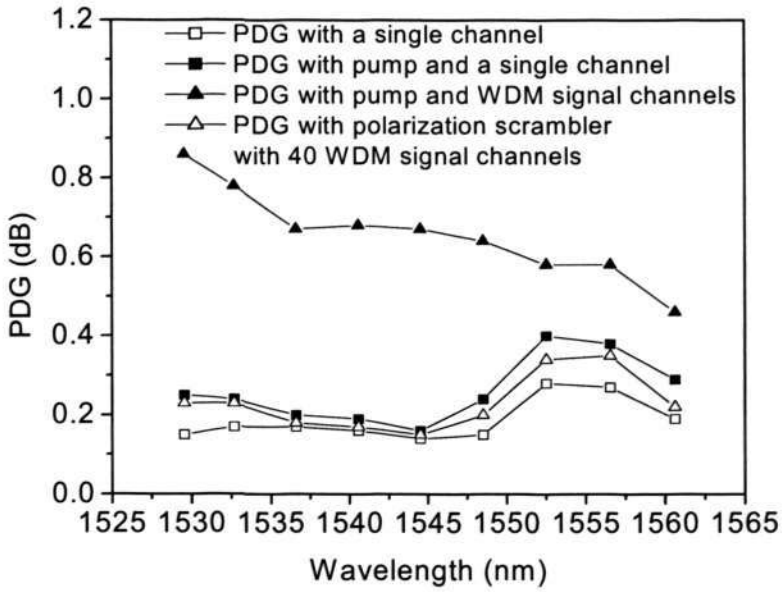


*Figure 4-12 PDG versus wavelength for DCF with 0.36ps DGD, 14dB on/off gain*

To further study the PDG in *Raman* amplifier and the effects of PS on PDG, the influence of different values of on-off gain on the PDG is investigated. Comparing the experimental results in Figure 4-11 (a) and Figure 4-12, it is

found that PDG caused by SSRI in a *Raman* amplifier with 14dB on-off gain is higher than that with 12dB on-off gain. This indicates that the signal power also has quite large influence on SSRI.

Since this experiment focuses on the influence of the PS on the SSRI, only CW signal is studied. As a result, walk-off between the interacting signal channels induced by the dispersion of the transmission fiber does not need to be considered. However, in practical high speed communication system, because the effect of PS on PDG depends strongly on the walk-off between the interacting signal channels [153, 154], extra noise will be introduced if the scrambling rate is not high enough. Further experiments demonstrate that this influence on the 10Gb/s system can be tolerable if the speed of polarization scrambling is high enough.

## 4.5 Conclusions

In the first section of this chapter, the performance of an L-band *Raman*/EDFA hybrid amplifier achieved by incorporating a segment of EDF within the span link is discussed. Experimental results indicate that the position of EDF within the span has a great influence on the performance of the hybrid amplifier. Both gain and noise performance in L-band can be improved with 20m EDF placed in an optimal position. In addition, flat gain bandwidth can be extended from L-band to C+L band by recycling the residual first-order SRS to pump a segment of short (4m) EDF.

The effect of a piece of highly nonlinear PCF on the noise performance of a backward pumped DRA is then investigated. Due to the high *Raman* gain coefficient of the PCF, the *Raman* gain of the signal at the beginning of the link increases even when the pump power is not large. As a result, the power excursion of the signal over the length of the transmission is reduced and better noise performance is achieved by placing the PCF before the SMF. As compared with just having a SMF, the $OSNR_{ASE}$ is improved by about 1.4dB, while the improvement in the $OSNR_{DRBS}$ is about 0.4dB. The improvement in $OSNR_{DRB}$ is limited because the PCF has a large *Rayleigh* scattering coefficient.

In the last section of this chapter, a novel PDG suppression method is proposed and demonstrated by using a PS in the system to improve its performance. By comparing the PDG caused by SSRI among 40 signal channels over different DCF module experimentally, the experimental results show that both DGD and *Raman* gain coefficients influence the value of PDG. By using a PS, PDG due to SSRI can be reduced effectively, whilst ensuring a low PMD value in the transmission system.

# Chapter 5

# New Applications of Fiber *Raman* Amplifier

## 5.1 Introduction

Distributed *Raman* amplifier (DRA) has been used in long-haul or ultra-long-haul fiber transmission systems extensively. The advantages of *Raman* amplification can also be utilized to improve the performance of other systems. For example, *Raman* assisted four wave mixing (FWM) and cross phase modulation (XPM) have been shown to improve the system performance comparing with those without the assistance from *Raman* amplification [23, 29, 30, 33, 35]. In this chapter, some new applications of *Raman* amplification will be proposed and demonstrated.

This chapter is organized as follows. Section 5.2 is devoted to discussing the performance of wavelength division multiplexed (WDM) radio over fiber (RoF) network assisted by DRA. Experimental results indicate that forward pumped

DRA can increase the link optical output power limited by stimulated *Brillouin* scattering (SBS) effect in downstream transmission and backward pumped DRA can improve optical signal to noise ratio (OSNR) in upstream transmission, which is verified by binary phase shift keying (BPSK) transmission experiments. In section 5.3, an all-fiber optical parametric oscillator (OPO) assisted by stimulated *Raman* scattering (SRS) is proposed and demonstrated for the first time. In addition, a depolarized flat broadband spectrum from 1570 to 1640nm based on the combined effects of SRS and parametric effect is obtained simultaneously. In section 5.4, a depolarized high power (200mW) broadband source (1520-1620nm) with high polarization insensitivity is obtained utilizing single pump based on hybrid effects of dual-order *Raman* scattering, parametric process in highly nonlinear dispersion shift fiber (HNDSF) and *Erbium* doped super-fluorescent.

## 5.2 Performance of WDM Radio over Fiber Network Using DRA

### 5.2.1 Background

There has been an increasing amount of focus on the research into fiber-radio networks for the delivery of broadband services [37]. Recently, WDM network is being applied to support large number of base stations (BSs) via fiber-radio feeder network [43]. To allow more remote BSs to share resources, the easiest approach is to increase the launched power of optical signals. Traditionally, boost- *Erbium* doped fiber amplifier (EDFA) and pre-amplification EDFA are chosen for downlink and uplink respectively, to overcome the limited link efficiency in transporting sub-carrier modulated optical signals and to

compensate optical attenuation of WDM components in fiber-radio network. However, in contrast to baseband optical communication links, optical signals in fiber-radio links contain strong carriers with narrow spectral width along with weak modulation sidebands. Consequently, the effect of SBS will significantly limit the maximum achievable optical output power in the downlink of fiber-radio network and thus affect the overall signal to noise ratio (SNR) realizable. While the upstream signal transmission can be supported by EDFA preamplifier to boost the signal power before detection, system performance is often limited by poor SNR due to the low input power into the amplifier. In this section, it is demonstrated that DRA can improve the performance of WDM fiber-radio network without introducing additional impairment from inter-channel crosstalk due to XPM and degradation in spur free dynamic range (SFDR). In downlink, DRA can increase the output optical power limited by SBS effect. Meanwhile, DRA can also improve the OSNR of uplink signal due to its lower effective noise figure (ENF).

### 5.2.2 Network Architecture and Experimental Setup

Figure 5-1 illustrates the experimental setup of a WDM fiber-radio network comprising one central office (CO) and one remote node (RN) connected by a primary ring network. CO performs switching, routing and power control functions, while RN add-drops multiple wavelengths, which can be distributed to remote BSs via a star or ring network. In the downlink, eight channel WDM signals are first multiplexed together using an arrayed-waveguide grating (AWG) and distributed to the RN, where all the channels are dropped before each of them is routed to the designated BS via the short secondary ring

network (or alternatively via a star network) which is not implemented in the experiment. In the uplink, eight WDM channels at the same wavelengths as the dropped channels are added and then routed back to CO. Both link spans consist of 25km single mode fiber (SMF).

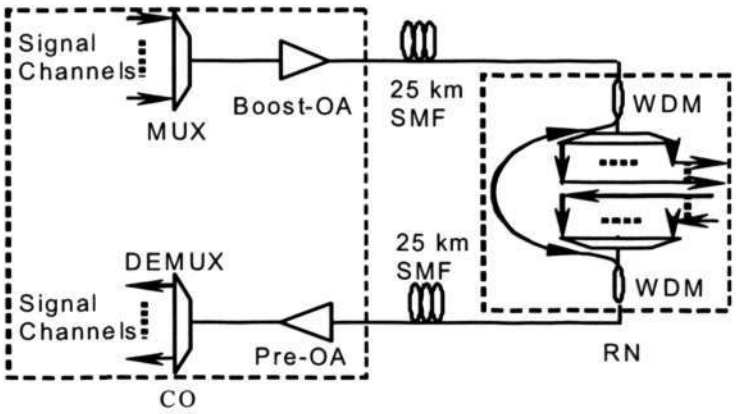


*Figure 5-1 WDM millimeter-wave fiber-radio network*

| | |
|---|---|
| Multiplexer Loss ($L_{MUX}$) | 3dB |
| Small-signal EDFA gain ($G_{EDFA}$) | 30dB |
| EDFA maximum output power ($P_{MAX}$) | 23dBm |
| DRA gain in 25km SMF ($G_{DRA}$) | 15dB |

*Table 5-1 Parameters of optical amplifiers used in the experiment*

To investigate the impact of using different types of amplification schemes, EDFA or DRA are used as optical amplifier (OA) for boosting power in the downlink and for pre-amplification in the uplink. The EDFA has a small-signal gain of 30dB and an output saturation power of 23dBm. A dual-wavelength pump laser module with 250mW output powers at 1425nm and 450mW at 1453nm is used to realize a flat *Raman* gain spectrum in the C-band. The parameters of optical amplifiers used in this experiment are shown in Table 5-1.

The relative intensity noise (RIN) of the *Raman* pumps used in this experiment is about -120dB/Hz. The maximum on-off *Raman* gain in 25km SMF provided by this *Raman* pumping module is more than 15dB. In a practical WDM fiber-radio network, there are many randomly distributed RNs that can block the residual *Raman* pump power. To fully utilize the residual *Raman* pump power, each RN incorporates a by-pass structure composed of two WDMs. In this way, signal and *Raman* pump pass through different paths and then the residual pump power can be reused.

### 5.2.3 Stimulated *Brillouin* Scattering and Noise Limitation

A single channel at 1551.74nm modulated by 37.5GHz RF signal is first studied in downlink using boost-EDFA or forward-pumped DRA. When the launched optical power is amplified to higher than 9dBm by a boost-EDFA, an RF signal at 10.9GHz generated by SBS effect is observed and thus the maximum output optical power is limited due to SBS effect. As a result, even when the launched optical power is as high as 17dBm, the detected link output power (including 3dB de-multiplexer insertion loss) at RN is still less than 6dBm. Therefore, SBS effect limits the achievable maximum link output power in a downlink with boost-EDFA, which is not desirable for long link span and more remote nodes. Since DRA amplifies optical signal along the transmission line with a relatively more flat power distribution along the span, it suffers less accumulated nonlinear effects along the span to achieve the same span output power, leading to larger achievable link output power before SBS effect become significant. In the investigation of this thesis, link output power as high as 6dBm can be

obtained (with -3dBm launched optical power) while still no obvious SBS effect was observed.

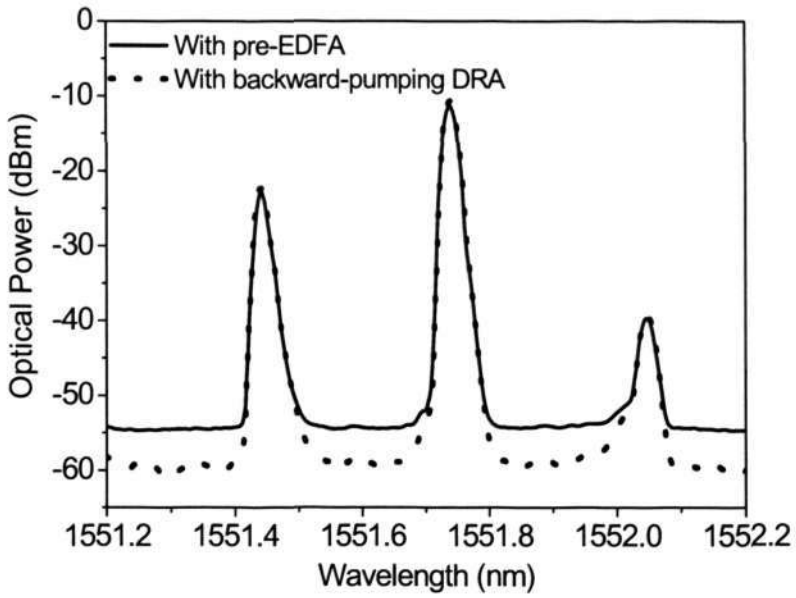


*Figure 5-2 Uplink optical spectra using EDFA or DRA*

The impact of amplification scheme on uplink OSNR is also studied in a fiber radio system [4]. In Figure 5-2, the dotted and solid curves show the uplink signal optical spectra at 1551.74nm using backward pumped DRA and EDFA preamplifier, respectively. Because the ENF of pre-EDFA is higher than that of backward pumped DRA in achieving the same link gain of detected RF signal, the uplink OSNR using backward pumped DRA is 5dB higher than that using pre-EDFA, as shown Figure 5-2.

### 5.2.4 Transmission Experiments

Above discussion shows forward pumped DRA can improve the link output optical power limited by SBS effect which is suffered in downlink when using

boost-EDFA, while backward pumped DRA can improve the OSNR in uplink which is a dominant effect when using pre-EDFA scheme. To further verify these conclusions, 155Mb/s BPSK data is transmitted in both uplink and downlink using different amplification schemes.

#### 5.2.4.1 Experimental Setup

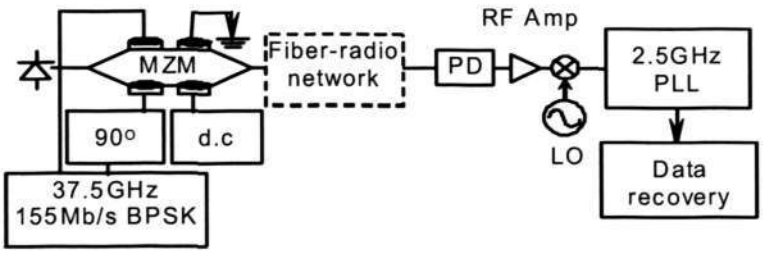


*Figure 5-3 Modulation and detection setup*

Figure 5-3 illustrates the modulation and detection setup of RoF transmission [44]. Eight optical carriers, with wavelengths ranging from 1549.32nm to 1554.98nm with 100GHz channel spacing, are first multiplexed together by a WDM multiplexer (MUX) in CO and then launched into a dual-electrode *Mach-Zehnder* modulator (DE-MZM). A 37.5GHz millimeter-wave signal with BPSK data format is generated by mixing a 37.5GHz local oscillator (LO) signal with a 155Mb/s pseudorandom bit sequence (PRBS) data. The DE-MZM is biased at the transmission quadrature point and the mixed RF signal after drive amplifier is separated to drive the two RF ports of the DE-MZM with a 90° phase shift between the two drive signals. The resultant output of the modulator is the eight optical carriers together with their corresponding optical single sideband (OSSB) modulated signals. The optical signal after transmission and de-multiplexing is detected by a 45GHz photo detector (PD).

The detected electrical signal is amplified using an RF amplifier and then down-converted to an intermediate frequency (IF) of 2.5GHz. Subsequently, the base-band data was recovered using a 2.5GHz electronic phase-locked loop (PLL). The parameters used in RoF transmission experiment are shown in Table 5-2, where the loss of OSSB modulator is about 13dB, the attenuation of transmission fiber is 0.2dB/km and the loss of remote node is mainly caused by de-multiplexer.

| | |
|---|---|
| OSSB modulator loss | 13dB |
| Fiber attenuation | 0.2dB/km |
| Remote node loss ($L_{RN}$) | 13dB |

*Table 5-2 Parameters of components in transmission experiment*

#### 5.2.4.2 Optical Single Sideband Modulation

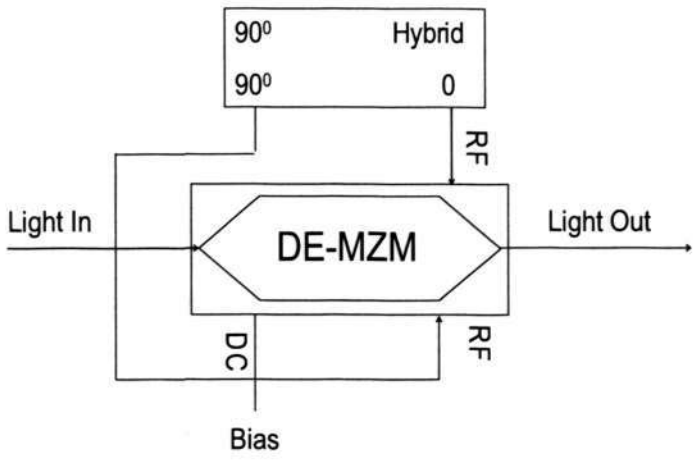


*Figure 5-4 Modulation scheme of SSB*

Because the performance of RoF transmission scheme may be severely limited by fiber chromatic dispersion, which may degrade the received RF power of the radio signals, this effect can be overcome by using OSSB modulation. In this

experiment, OSSB modulation is realized by using a DE-MZM with RF signals applied to both of the two balanced electrodes with $\pm\pi/2$ phase shift between the two arms. A direct current (DC) bias sets the modulator at the quadrature point to obtain OSSB modulation [44]. The modulation scheme is shown in Figure 5-4.

#### 5.2.4.3 Results and Discussions of Transmission Experiment

Figure 5-5 shows the measured BER curves as a function of received optical power for downlink and uplink using EDFA or DRA respectively. All of these experimental results are measured with the same modulation condition. In downlink, the input power into OA is –10dBm for both boost-EDFA and forward pumped DRA, while in uplink, the launched optical power into SMF for both pre-EDFA and backward pumped DRA is -10dBm.

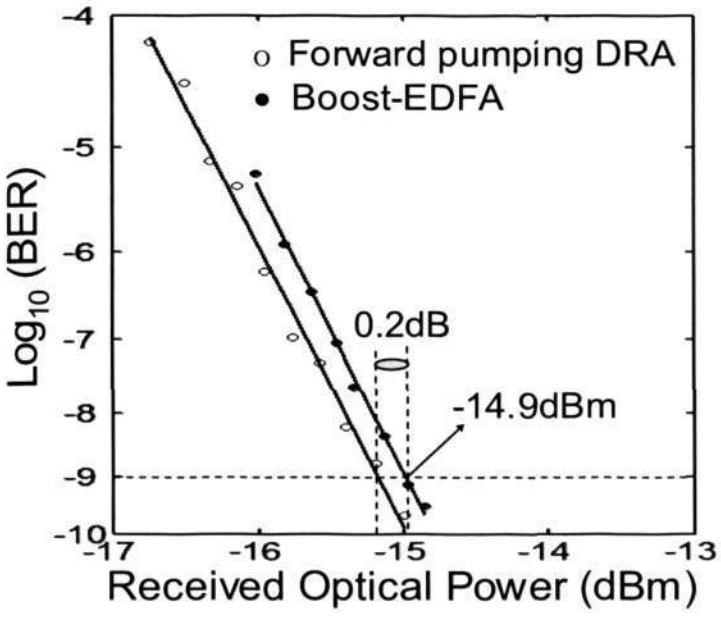


(a)

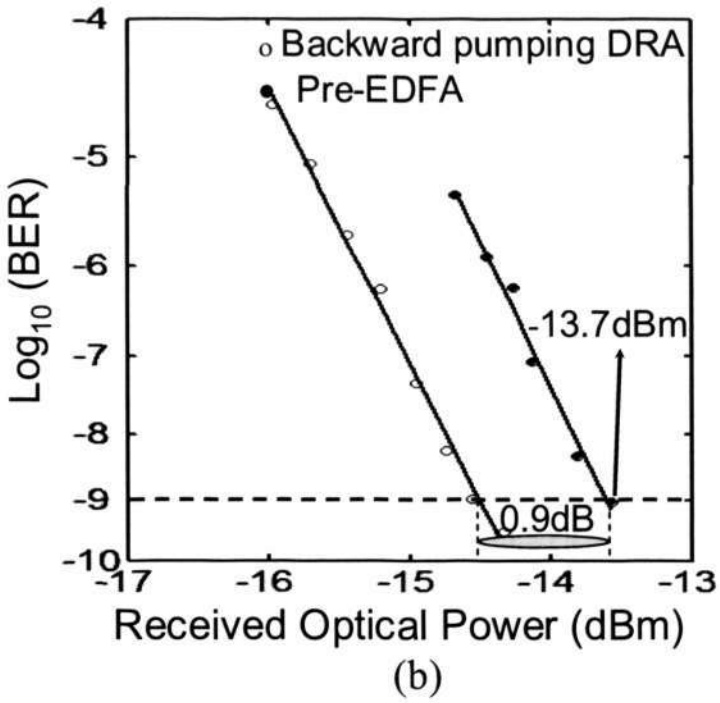


*Figure 5-5 Measured BER curves vs received optical power using different amplification schemes. (a) Downlink; (b) Uplink*

Figure 5-5(a) shows that the receiver sensitivity in downlink using forward pumped DRA is nearly the same as that using boost-EDFA since SBS effect is not significant in both cases with relatively low launched optical power and the ENF of boost-OA has little influence on the system performance. No degradation of the downlink performance due to RIN transfer was observed in this experiment. The sensitivity of uplink using backward pumped DRA is 0.9dB better than that using pre-EDFA because the ENF of DRA is better than that of EDFA, as shown in Figure 5-5(b). Comparing Figure 5-5(a) and Figure 5-5(b), it is found that the sensitivity in downlink is better than that in uplink since the former has better noise performance.

### 5.2.5 Crosstalk and Spur Free Dynamic Range

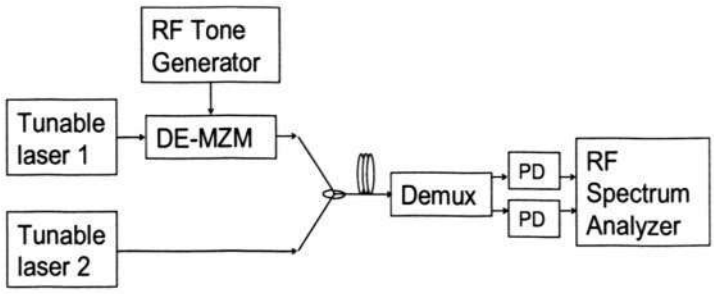


*Figure 5-6 Experimental setup for crosstalk due to XPM*

Crosstalk from adjacent channels in WDM fiber-radio network is an important issue [45]. Previous section shows that DRA can suppress impairment due to downlink SBS effect and improve uplink noise characteristics in WDM fiber-radio network. In this section, the impact of different amplification schemes on the crosstalk impairment from adjacent channels due to XPM in uplink is studied in detail.

The experimental setup used to measure the crosstalk in RoF network system is shown in Figure 5-6. Two tunable laser sources is combined together and then transmitted in 25km SMF. The fiber loss parameter is 0.2dB/km and the fiber dispersion parameter is 17ps/nm.km. The wavelengths of two tunable lasers are 1553.33nm and 1552.52nm respectively. One of the laser outputs is modulated by an RF tone using a DE-MZM, another is CW signal. OSSB modulation can be realized by using a DE-MZM and a $90^0$ hybrid as the modulator is biased at quadrature point. The frequency of the modulated RF tone can be tuned from 1GHz to 18GHz. The power of modulated RF signal is 12dBm. To avoid SBS effect, the power launched into the fiber for both lasers should be kept below

6dBm. The launched optical power for the CW channel is 5.75dBm and that of the channel with SSB modulation is -0.65dBm and. At the output of the 25km span link, the two channels are filtered out by a wavelength de-multiplexer and measured by an RF spectrum analyzer after the photo-detection. Due to XPM, there will be an RF tone present at the CW channel. Since OSSB modulation is used to avoid the power fading due to fiber dispersion, the crosstalk to sub-carrier power ratio (CSR) is defined as the ratio between the RF power arising from crosstalk impairment and optical power of sub-carrier. The adjacent channel isolation of WDM is shown to be greater than 40dB, resulting in a negligible linear crosstalk well below the noise floor.

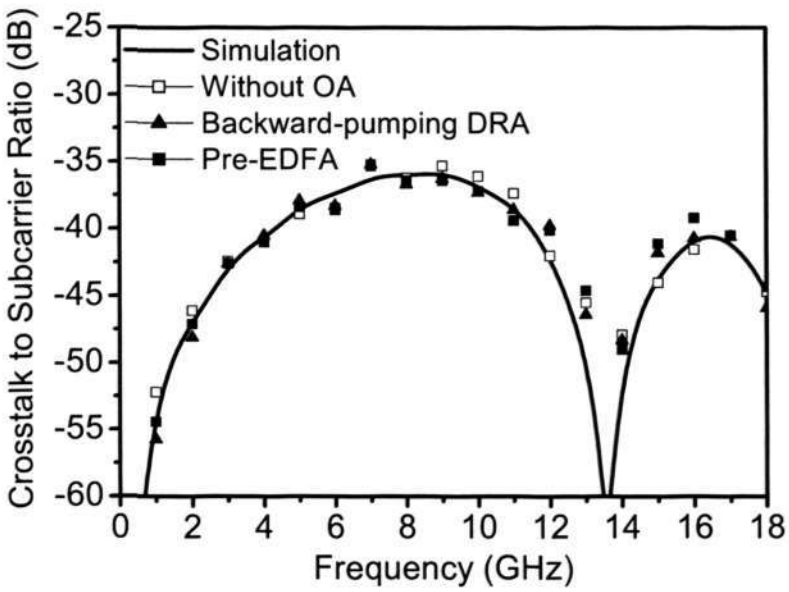


*Figure 5-7 Crosstalk to sub-carrier ratio under different amplification schemes*

Three kinds of amplification schemes investigated here include using pre-EDFA, backward pumped DRA in CO, and without using any optical amplifier at all. As shown in Figure 5-7, the solid line corresponds to the theoretical prediction [46], while the hollow squares, the solid squares and the solid triangles correspond to the original crosstalk ratio without OA, with +7 dB

optical gain from pre-EDFA and backward pumped DRA, respectively. The figure shows that the results of our analytical model very well match the experimental results. Also, the figure confirms that the crosstalk to sub-carrier ratio exhibits a periodic like nature, and for a higher frequency, the maximum possible crosstalk level may not be higher than that at a lower frequency. In addition, Figure 5-7 shows that crosstalk impairment in three amplification schemes are nearly the same [46, 155], which shows that WDM fiber-radio network incorporating DRA does not induce any additional crosstalk impairments imposed from adjacent channels.

Assuming both channels have the same average launched optical power, an approximated expression to estimate the CSR influenced by amplification schemes can be obtained, as shown in Equation (5-1).

$$CSR \approx 16\left[\gamma \overline{P_0} \sin\left(\kappa_m z\right)\right]^2 \left|z_e\right|^2 \rightarrow \frac{16\left[\gamma \overline{P_0} \sin\left(\kappa_m z\right)\right]^2}{\alpha^2 + \left(\omega_m \beta_2 \Delta\omega\right)^2} \tag{5-1}$$

Where $\gamma$ is the fiber nonlinear parameter, $\overline{P_0}$ is the average optical power launched into the fiber, $z$ is the fiber length, $\alpha$ is the fiber loss parameter, $\omega_m$ is the angular frequency of the modulating sub-carrier, $\beta_2$ is the second order dispersion parameter and $\Delta\omega = \omega_0 - \omega_0'$ is the optical channel spacing in angular frequency. $\kappa_m$ and $z_e$ are shown as Equation (5-2) and (5-3) respectively.

$$\kappa_m = \frac{\left(\beta_2 \omega_m^2\right)}{2} \tag{5-2}$$

$$z_e = \left\{1 - \exp\left[-\left(\alpha + j\omega_m \beta_2 \Delta\omega\right) z\right]\right\} / \left(\alpha + j\omega_m \beta_2 \Delta\omega\right) \tag{5-3}$$

It can be found from this equation that to reduce the nonlinear crosstalk level, one can increase the channel spacing or operate the links at higher sub-carrier frequency. The simplest way is just to lower the launched optical power. Lowering 1dB launched optical power can increase 2dB CSR. When one lowers the launched optical power to suppress the nonlinear crosstalk, the received SNR will also be degraded. Optical amplifier may then be used to recover this SNR, which may introduce extra nonlinear crosstalk. However, for a WDM microwave fiber-radio link, $|\omega_m \beta_2 \Delta\omega|$ is a typically much larger than $|\alpha|$ and hence equation shows that $\alpha$ does not have a significant influence on the nonlinear crosstalk level. This is even true for practical systems with fiber amplification. For EDFA, the length of EDF is very short and thus the very small accumulated dispersion in the EDF cannot lead to significant nonlinear crosstalk. For DRA, the equivalent $\alpha$ after taking the *Raman* gain coefficient into account is still much smaller than 0.86 for a practical system. As a result, the optical amplification schemes have little influence on CSR.

In WDM fiber-radio network, the RF signal power uploaded from the CO or BS is inherently dynamic. Therefore, it is important to ensure that the third order inter-modulation products leaked to the adjacent channels will not violate the wireless communications regulations. Traditionally, the SFDR is used to describe both noise and distortion in WDM fiber-radio network. In order to investigate the impact of amplification schemes on the SFDR in fiber-radio network, two RF tones are used to examine the SFDR in the uplink of fiber-radio network, with different amplification schemes, again including using pre-EDFA, backward pumped DRA in CO, and without using OA at all. The RF

receiver bandwidth used in this experiment is 40GHz. Here, only single channel at 1554nm in uplink with -0.1dBm launch power is chosen. Table 5-3 shows that SFDRs in three amplification schemes are nearly the same. Therefore, there is no additional degradation in SFDR induced by using DRA.

| Amplification schemes | Without OA | Pre-EDFA | Backward -DRA |
|---|---|---|---|
| SFDR ($dB.Hz^{2/3}$) | 96.9 | 97.96 | 98.3 |

*Table 5-3 SFDR in different amplification schemes*

## 5.3 Optical Parametric Oscillator Assisted by SRS

### 5.3.1 Background

There has been increasing demand on high power CW fiber sources due to their potential applications in telecommunication, spectroscopy and medicine [47]. OPO is widely recognized as an important component for the development of coherent light sources at wavelengths unavailable for conventional lasers [48]. Generally, OPO is constructed utilizing nonlinear crystals and bulk optics elements, which require careful alignment in order to obtain optimal operation [49]. Optical fiber is a promising medium to generate nonlinear optical effects due to its light confinement and low loss. Indeed, fiber OPO (FOPO) has been reported previously [50, 51]. However, due to the relatively low nonlinear coefficient of optical fibers as compared with the nonlinear crystals, either pulsed pumps or high power CW *Raman* fiber laser (RFL) is required for FOPO. Early theoretical and experimental studies have also revealed that *Raman* assisted FWM typically leads to improved conversion efficiency and parametric gain bandwidth [52]. However, so far there have been no experimental investigations on FOPO assisted by *Raman* effect. In this section, a *Raman*

assisted FOPO is reported for the first time and the influence of SRS on the output characteristics is studied in detail. Furthermore, a depolarized flat broadband light in the range of 1570-1640nm can also be generated in FOPO system, as a result of the combined action of SRS and parametric interaction.

### 5.3.2 Experimental Setup

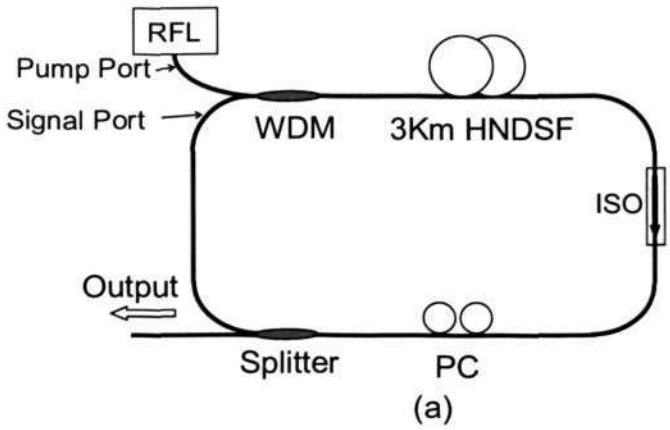


(a)

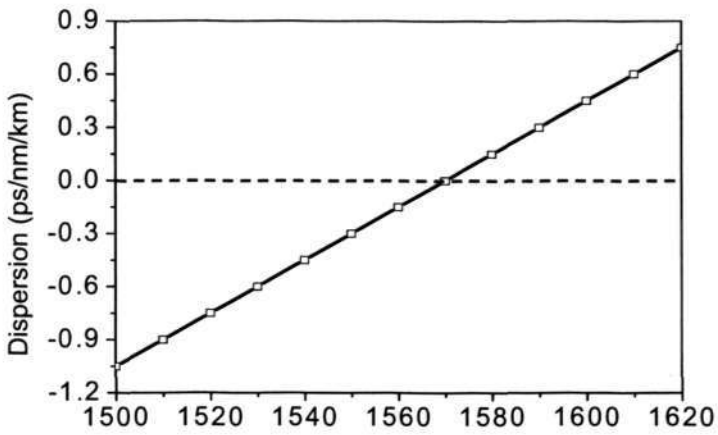


(b)

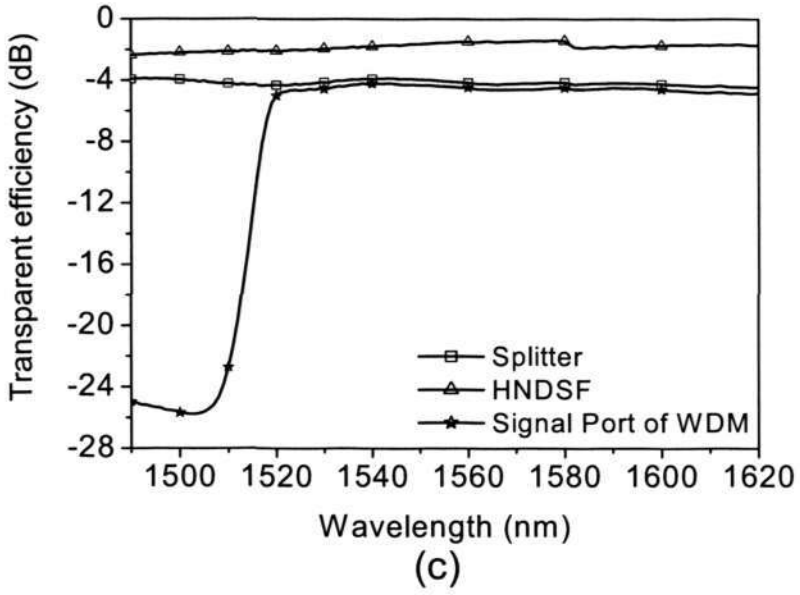


*Figure 5-8 (a) Experimental setup of OPO; (b) Dispersion map of HNDSF; (c) Transmission spectra of components in the cavity*

The SRS assisted FOPO system is schematically shown in Figure 5-8 (a). It is a ring cavity comprising a *Raman* pump source, a broadband WDM, 3km HNDSF, an optical isolator (ISO), a polarization controller (PC) and a fiber power splitter. The *Raman* pump source is a CW RFL with maximum powers of 4W at 1395nm. The pump beam has a degree of polarization less than 5%. The broadband WDM is used to couple the pump into the 3km HNDSF and re-input the SRS generated in the HNDSF back into the ring cavity. The splitter is used to extract approximately 10% of the light from the cavity. The nonlinear coefficient of the HNDSF is $12W^{-1}km^{-1}$ and its zero dispersion wavelength (ZDW) is at 1570nm, with a dispersion slope of $0.015ps/nm^2.km$, as shown in Figure 5-8 (b). The cutoff wavelength of the HNLF is 1180nm. The ISO ensures unidirectional oscillation of the ring cavity and the PC is used to adjust the polarization state of lights in the cavity. The transmission spectra of the components used in the cavity are shown in Figure 5-8 (c). It is seen that the

HNDSF and the splitter have a flat transmission response over the wavelength range of 1490nm to 1620nm; the signal port of the WDM has a high transmission ratio when the wavelength is longer than 1510nm, while the pump port of the WDM has a high transmission ratio when the wavelength is shorter than 1510nm.

### 5.3.3 Results in Parametric Amplifier Process

Since the RFL used is made based on the cascaded SRS, new lasing lines appear due to FWM among different orders of SRS in the laser cavity [47]. Figure 5-9 (a) shows the output spectrum of the RFL. In addition to the main lasing peak at 1395nm, there is a peak at 1445.25nm, which has a peak power about 30dB lower than that of the main peak. Figure 5-9 (a) denotes the 1395nm and 1445.25nm lines as $\lambda_{RFL1}$ and $\lambda_{RFL2}$ respectively.

The one-pass spectrum of the RFL beam through the HNDSF (measured before the ring cavity is formed) is shown in Figure 5-9 (b). Other than the original peaks inherent to the RFL, there appear two new spectral components around the 1486.4nm and 1530.12nm. The spectral component around 1486.4nm is generated due to the first order SRS (FOSRS) of the 1395nm line, and its 20dB down bandwidth is about 7nm, while the one around 1530.12nm is formed through the four-wave parametric process between the $\lambda_{RFL2}$ and the strong 1486.4nm spectral line, its 3dB down bandwidth is about 8nm. The peaks at 1486.4nm and 1530.12nm are denoted as $\lambda_{FOSRS}$ and $\lambda_{FWM}$ respectively.

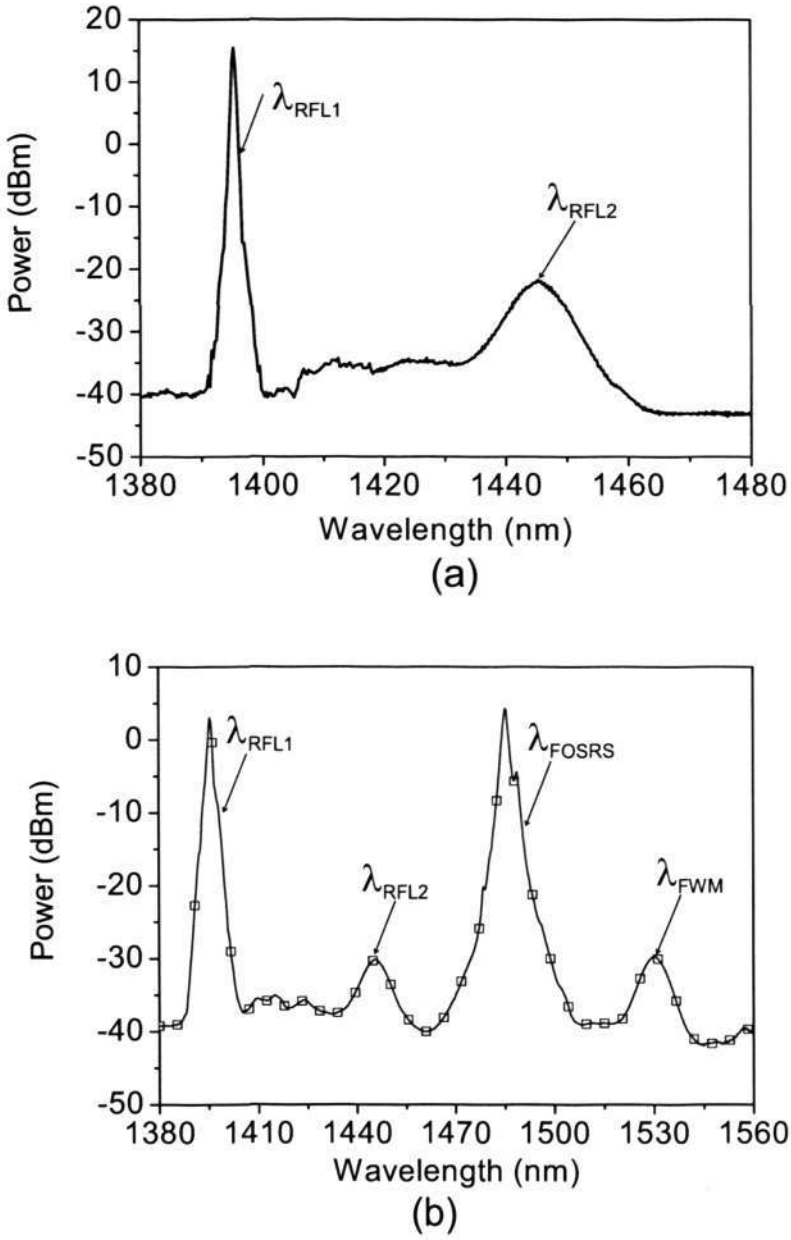


*Figure 5-9 (a) Output spectrum of RFL; (b) Output spectrum after RFL passing HNDSF for single time*

It is found that the peak frequencies of the different spectra agree well with Equation (5-4),

$$2\omega_{FOSRS} = \omega_{RFL\,2} + \omega_{FWM} \quad (5\text{-}4)$$

where $\omega_{FOSRS}$, $\omega_{FRL2}$ and $\omega_{FWM}$ are the angular frequencies of $\lambda_{FOSRS}$, $\lambda_{FRL2}$ and $\lambda_{FWM}$ respectively, which confirms that they are linked with the FWM mechansim.

### 5.3.4 Results in Optical Parametric Oscillator Process

The above parametric process generated a broadband gain around 1530nm. In order to further achieve laser oscillation within this gain bandwidth, a resonant cavity is constructed as shown in Figure 5-8 (a). Because of the transmission feature of the WDM, only the spectral component around 1530.12nm can oscillate in the cavity, the other lights at wavelengths of $\lambda_{FOSRS}$, $\lambda_{RFL1}$ and $\lambda_{RFL2}$ are blocked by the WDM rejection band. It can be found that under strong pumping, laser oscillation at round 1523nm can be obtained. Therefore, a SRS assisted FOPO is firstly demonstrated. For clarity, typical spectra of the FOPO at three different RFL output power levels are shown in Figure 10 (a). It is found that the OPO oscillation wavelength is not exactly at the peak of the gain profile, which is caused by the effective cavity loss and dispersion. The operation of the OPO exhibites the following characteristics: it has a pump threshold of about 1.0W. Above the threshold its output power increases with the RFL power until it reaches a maximal value, it then decreases with the further increase of the RFL pump power.

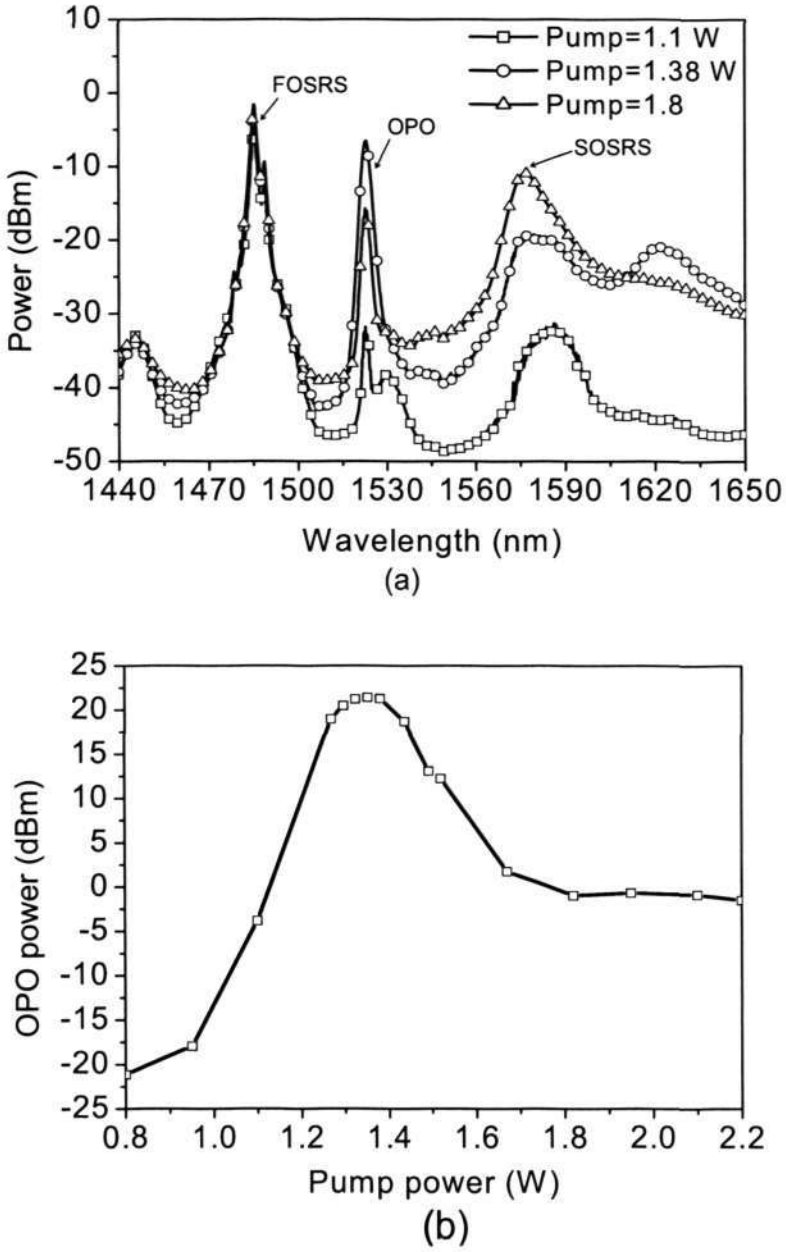


*Figure 5-10 (a) Output spectra of the fiber OPO under different pump powers; (b) Output power of OPO signal versus pump power*

Figure 10 (b) shows the OPO output power measured by selecting the OPO wavelength using an optical bandpass filter. It shows that the maximal OPO output power occurs at the RFL pump power of 1.38W, with a value of about 100mW. The OPO shows clear difference to the conventional one in that the

latter shows output power saturation as the pump power is further increased [48-50]. It is found that the property of the FOPO is caused by the coexistence of higher order SRS with the parameteric process. Apart from involving in the parametric process, the FOSRS light also generates the second order SRS (SOSRS) and transfers energy to it. This process competes with the parametric process. In this system the FOSRS appears when the RFL output power reaches 700mW and its strength increases until the OPO occurs. Further increasing pump power, the energy transfer to the parametric oscillation process then becomes dominant. The OPO output power increases until the RFL power reaches 1.38W, where the *Raman* lasing at the SOSRS starts. Afterwards the energy transfer to the SOSRS becomes dominant and as a result the FOPO strength starts to decrease.

As shown in Figure 5-10 (a), before the *Raman* lasing at the SOSRS wavelength starts, a broad spectrum from 1570 to 1640nm appears. The single peak at 1575nm corresponds to the SOSRS. Its 10dB bandwidth is about 20nm when the pump power is 1.0W. As the RFL power increases, the 10dB bandwidth also increases. In particular, the broadening at the bottom part of the peak is more significant than that at the top. When the OPO appears, a new spectrum component around 1620nm also appears and its strength increases with the OPO strength, which is generated due to the SRS of the OPO signal. The 10dB bandwidth of the broad spectrum can be extended to more than 80nm with ripple less than 5dB when the RFL power is 1.38W. The output power of the broad spectrum filtered out by another WDM at the output port of the splitter is more than 50mW. If the pump increases further, the peak at 1620nm

decreases gradually associated with the decrease of the OPO strength. It is observed that the bandwidth at top of the SOSRS spectrum becomes further narrowed with the increase of RFL since the SOSRS reaches the lasing threshold and starts lasing. The bandwidth at the bottom of the SOSRS spectrum continuously broadens. The broadening of this spectrum from 1570nm to 1650 nm can be attributed to modulation instability plus stimulated Raman effect. Since the zero dispersion wavelength is around 1570 nm and dispersion slope is small, the modulation instability can easily occur for the range of wavelength larger than 1570nm once the SOSRS power is sufficiently high, and significantly broaden the spectrum.

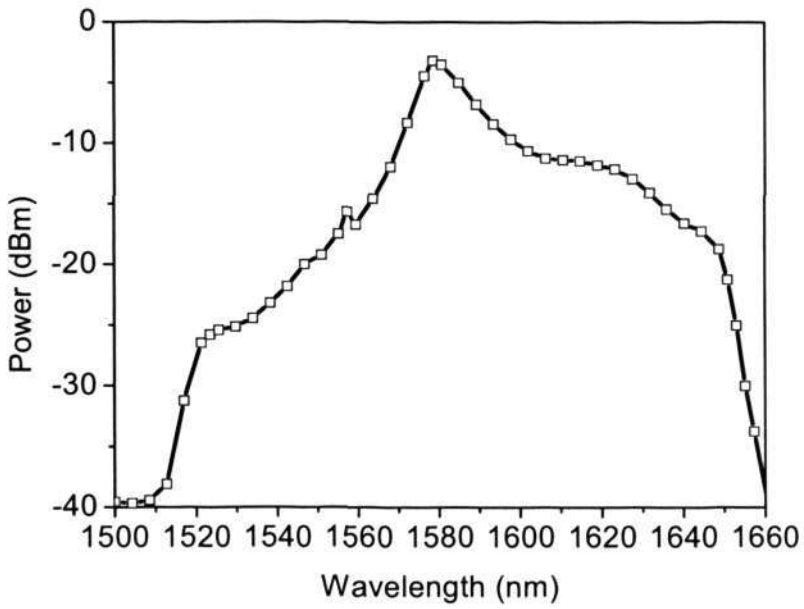


*Figure 5-11 Output broadband sources without oscillation*

The impact of the coupling ratio of the fiber power splitter on the operation of the OPO is also investigated in this chapter. It is found that even up to 50 percent power goes to the output port, the OPO can still occur. While if the

more than 70 percent of splitter power goes to the output port, the residual power at $\lambda_{FOSRS}$ then becomes not strong enough to generate the OPO wave. As a result, there generates a broadband spectrum and no OPO component appears, as shown in Figure 5-11, where 90 percent splitter power goes to output port. The evoluation of the broadband spetcrum can be explained as follows. The SOSRS first appears when the RFL power reaches $700mW$, then with the increase of the RFL power, the bottom of the SOSRS spectrum starts to broaden due to the FWM process between the SOSRS *Stokes* waves and the broadband *Raman* scattering background [52]. As the RFL power increases to the lasing threshold, the top of the SOSRS spectrum becomes narrowed gradually. When the RFL power is increased to 1.4W, a broad spectrum from 1520nm to 1650nm can be obtained with output power about 80mW.

Because OPO signal or broad spectrum is usually used to investigate the spectral characteristics of devices, it is important to avoid the influence of the polarization state on experimental results. Therefore, having a polarization insensitive OPO and broad spectrum light source is important. In this experiment, the polarization state (PS) of the output light is investigated. No variation in either the output power or spectral shape of the OPO signal and broadband light source is observed as the PC is rotated. This polarization insensitivity characteristics of the OPO and broad spectrum can be attributed to the very low degree of polarization of the RFL [52].

## 5.4 Generation of Depolarized Broadband Light Source

### 5.4.1 Introduction

A number of applications in optical communications, spectroscopy and optical sensing require broadband, high power light source. There have been many reports about the generation of broadband source. Rare earth doped super-fluorescent fiber sources have been studied extensively [53]. However, simultaneous achievement of high power and broad bandwidth is still difficult for this technique. Super-continuum generated by nonlinear interactions of ultra-short pulses in optical fiber is also a popular technique. However, the generations of super-continuum have been widely investigated only using pulsed fiber laser that suffer from high cost [54]. The combined effects of SRS and parametric FWM in a ring cavity made by HNDSF can also be used to realize a broadband source, but it requires at least two high power pumps, which increases the cost for broadband source [52].

In this section, in order to reduce the cost and improve the pumping efficiency, a novel technique applying a single 1395nm RFL is proposed to generate a depolarized broadband source with polarization insensitivity. This broadband source is based on the SOSRS, parametric FWM in 3km HNDSF and *Erbium*-doped super-fluorescent by recycling the residual FOSRS to pump 10m EDF. A broadband spectrum from 1520nm to 1620nm with a stable output power more than 200mW is obtained as pump power reaches 1.3W.

### 5.4.2 Experimental Setup

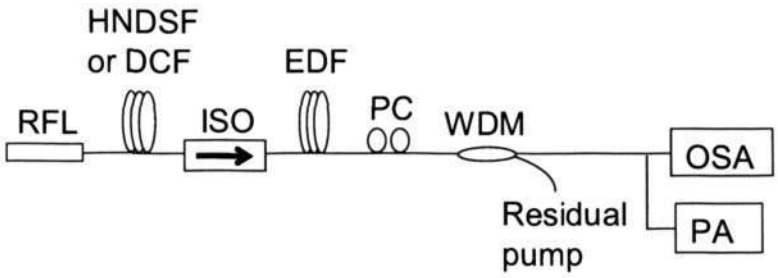


*Figure 5-12 Experimental setup for broadband source generation*

Figure 5-12 shows the apparatus used to generate the broadband source. A 1395nm RFL with maximal output power of 4W is chosen as the pump source to obtain dual-order *Raman stokes* spectrum. The RFL used has a degree of polarization less than 5%. In order to investigate the effect of the ZDW on the SOSRS, 3km HNDSF or 10km dispersion compensation fiber (DCF) is chosen as *Raman* gain medium respectively.

| Parameter at 1570nm | HNDSF | DCF |
|---|---|---|
| Attenuation [dB/km] | 0.74 | 0.55 |
| Dispersion [ps/nm/km] | 0 | -98 |
| Dispersion slope [ps/nm$^2$/km] | 0.015 | 0.3 |
| *Raman* gain coefficient [W$^{-1}$/km] | 8.0 | 5.67 |

*Table 5-4 Fiber parameters of HNDSF and DCF*

The fiber parameters of HNDSF and DCF at 1570nm are listed in Table 5-4. Both fibers have nearly identical technical parameters, except for their dispersion values. 10m EDF with 1000ppm $Er^{3+}$ is spliced after the HNDSF or

DCF. In order to suppress undesirable multi-path interference between the HNDSF or DCF and EDF, an ISO is inserted between the HNDSF or DCF and EDF. A WDM is used to remove the residual pumps power from the output broadband source. An optical spectrum analyzer (OSA) is used to measure output spectra. A polarization analyzer (PA) and a PC are used to study the polarization insensitive characteristics of the broadband source.

### 5.4.3 Experimental Results and Discussions

Figure 5-13 (a) shows the dual-order *Raman stokes* spectrum with 1W power from 1395nm RFL into 3km HNDSF. It is found that FOSRS around the 1486nm first appears as the pump power reaches 500mW and it is enhanced with the increase of pump power. The SOSRS will appear around the 1590nm band when the pump power reaches 700mW and it can be enhanced and broadened continuously as the pump power increases further. In order to study the influence of parametric FWM on the SOSRS, 3km HNDSF is replaced by a 10km DCF.

Figure 5-13 (b) shows the *Raman stokes* spectrum with 1W 1395nm RFL into 10km DCF. SOSRS with the same power and bandwidth as that in HNDSF can not be generated in DCF even increase the pump power to 1.5W. As a result, the high power broadband spectrum around the 1590nm obtained in HNDSF cannot be explained solely via SOSRS, since both of these fibers exhibit a nearly equivalent integrated *Raman* gain. Because the ZDW of HNDSF locates between dual-order *Raman stokes* spectrum, these observations actually result from *Raman*-assisted FWM process. For HNDSF, most of the spectral

components around 1590nm are generated parametrically through the non-degenerate and degenerate FWM that results from the mixing of two photons from the FOSRS with a pump photon, two pump photons and one *stokes* photon and then through subsequent *Raman* amplification. Therefore, the broadening of the SOSRS in HNDSF can be attributed to the high efficiency of FWM effects occurring within *Raman stokes* spectrum due to close around the ZDW [52, 55].

As shown in Figure 5-13 (a), the residual power of the FOSRS after the HNDSF is still high after transferring to the SOSRS. In order to improve the pumping efficiency, the residual power of the FOSRS can be recycled to pump a piece of EDF. When 10m EDF is connected after the HNDSF, C-band super-fluorescent spectrum will be generated. Because the threshold power required generating super-fluorescent spectrum in EDF is lower than that needed to generate the SOSRS, the C-band super-fluorescent spectrum appears prior to the appearance of SOSRS. It is found that the C-band super-fluorescent spectrum increases as the pump power increases until it reaches saturation state. Then, the SOSRS around 1590nm will appear and be enhanced with the further increase of pump power. When the pump power is around 1.3W, the output powers of SOSRS will be as high as C-band super-fluorescent spectrum.

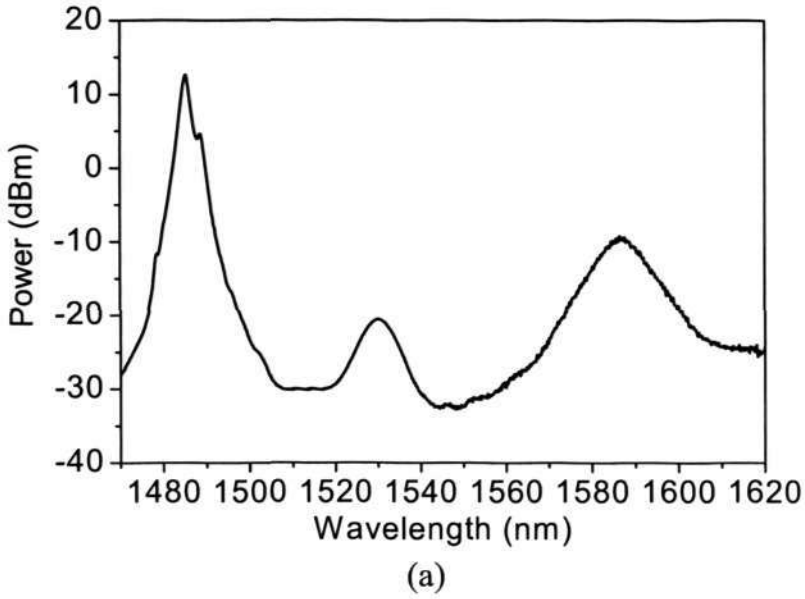


(a)

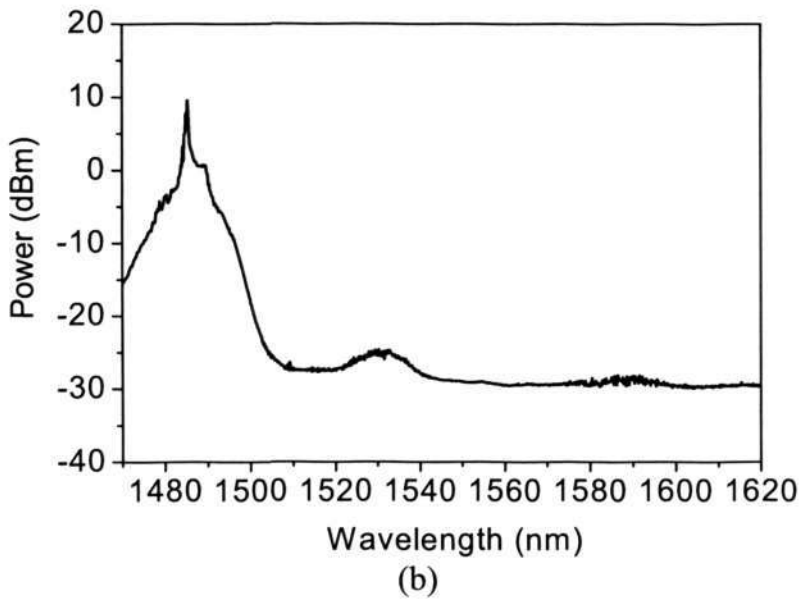


(b)

*Figure 5-13 Output spectrum generated by 1395nm RFL (a) in 3km HNDSF; (b) in 10km DCF*

As shown in Figure 5-14, a broadband source from 1520nm to 1620nm generated by 1395nm RFL in HNDSF and EDF is obtained. The output power of the broadband source is more than 200mW and the ripple of output spectrum from 1530nm to 1590nm is less than 4dB. Both the length of EDF and the

pump power will influence the flatness of broadband source. As the pumping power increases further, the SOSRS becomes higher than C-band super-fluorescent spectrum for a given EDF length, leading to increased non-flatness in spectrum.

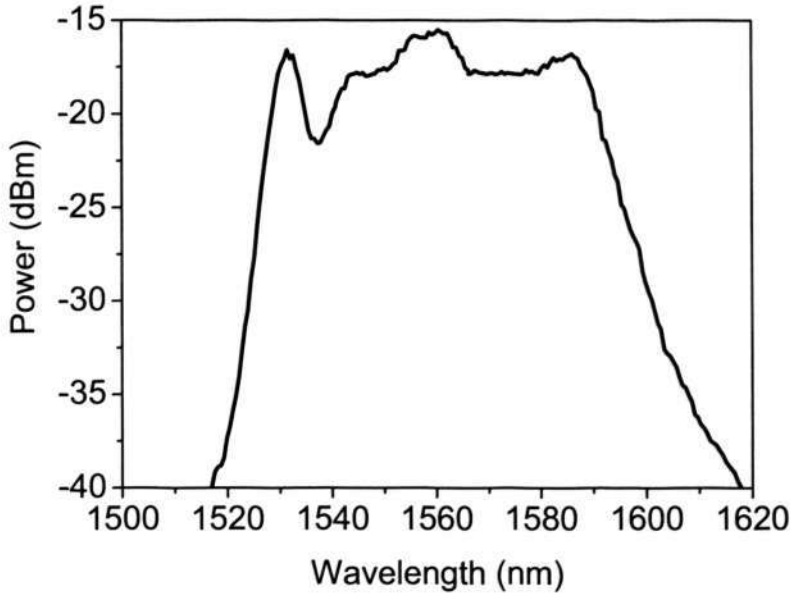


*Figure 5-14 Broadband spectra generated in HNDSF and EDF pumped by 1395nm RFL*

Because a broadband source is usually used to investigate the spectrum characteristics of devices, it is important to avoid the influence of the polarization state on the experimental result. Hence, having a polarization insensitive broadband source is really important [56]. In this experiment, the polarization state of the output spectrum is investigated by using PC and PA. No variation in either the output power or spectral shape of the broadband source was observed as the polarization controller was rotated, due to low degree of polarization of RFL pump.

## 5.5 Conclusions

This chapter first investigates the impact of using different amplification schemes on both uplink and downlink in a WDM fiber-radio system. Experimental results indicate that DRA can suppress impairment induced by SBS effect in downlink transmission and improve noise performance in uplink transmission, compared with its EDFA counterpart. The functionality is verified experimentally with eight channel WDM fiber-radio transmission over 25km SMF downlink and uplink with a channel spacing of 100GHz, each carrying a 37.5GHz RF signal with 155Mb/s BPSK data. Nonlinear impairments such as inter-channel crosstalk and SFDR are also studied under different amplification schemes, experimental results indicate that using DRA does not introduce any additional impairment from crosstalk and degradation in SFDR in fiber over radio network.

Then a SRS assisted polarization insensitive FOPO is proposed and demonstrated for the first time. A depolarized broadband source ranging from 1570nm to 1640nm with high output power and flat spectrum is generated due to the combined action of the SOSRS and parametric process.

In the last section, a stable high-power (200mW) broadband (1520-1620nm) source is obtained based on the combined effects of dual-order *Raman* scattering, parametric process and *Erbium* doped super-fluorescent.

# Chapter 6

# Conclusions and Future Works

## 6.1 Conclusions

We have investigated the characteristics, optimal design and new applications of fiber *Raman* amplifier (FRA) for next generation optical communication systems. In order to improve the system performance and extend the system span, various techniques have been proposed and demonstrated to optimize the FRA, including simple optimization algorithms and novel amplification schemes with better gain, noise and nonlinear performance.

In Chapter 3, a simple geometry compensation technique (GCT) is proposed to optimize the design of wideband *Raman* gain based on the geometric characteristics of stimulated *Raman* scattering (SRS) spectrum. In comparison with traditional solutions using rigorous iterative simulation, the suggested method is simpler and more effective. It is also possible to separate the compensation of gain curve profiles (involving the determination of the pump wavelengths and the pump path integrals) from the calculation of pump power values. The design results have been verified using the complete numerical

model and good agreement has been achieved. However, it is difficult for GCT to reduce the ripple of the broadband *Raman* gain spectrum to be less than 0.8dB and its complexity will be increased greatly as signal-to-signal *Raman* interaction (SSRI) and wavelength dependent loss spectrum of the fiber are considered. In order to solve these problems associated with GCT, a novel hybrid optimization algorithm is also proposed based on the GCT and genetic algorithm (GA). This model optimizes the pump wavelengths using GCT and pump path integrals using GA respectively. Consequently, two dimensional random searches in GA can be reduced to one dimensional random search. In addition, gain ripple of distributed *Raman* amplifier (DRA) can be reduced to be less than 0.2dB using hybrid optimization algorithm.

In Chapter 4, based on dual-order SRS of a single 1395nm *Raman* fiber laser (RFL) in 75km single mode fiber (SMF) and its corresponding dispersion compensation fiber (DCF) module, L-band *Raman/Erbium* doped fiber amplifier (EDFA) hybrid amplifier is realized by incorporating a segment of *Erbium* doped fiber (EDF). Experimental results indicate that the position of EDF within the span has a great influence on the performance of hybrid amplifier. Both gain and noise performance in L-band can be improved with 20m EDF placed in an optimal position. In addition, flat gain bandwidth can be extended from L-band to C+L band by recycling the residual first-order SRS to pump a segment of short (4m) EDF. Due to the same reason, when a piece of highly nonlinear photonic crystal fiber (PCF) is inserted at the beginning of the link, the noise performance of backward pumped DRA will also be improved. Because of the high *Raman* gain efficiency of the PCF, the *Raman* gain of the

signal at the beginning of the span increases even when the pump power is small. As a result, the power excursion of the signal over the length of the transmission is reduced and noise performance is improved by placing the PCF before the SMF. As compared to just having a SMF, the optical signal to noise ratio of amplified spontaneous emission noise ($OSNR_{ASE}$) is improved by about 1.4dB, while the improvement in the optical signal to noise ratio of double *Rayleigh* scattering noise ($OSNR_{DRBS}$) is just about 0.4dB. The improvement in $OSNR_{DRBS}$ is limited because the PCF has a large *Rayleigh* scattering coefficient. In the last section of this chapter, a novel polarization dependent gain (PDG) suppression technique is proposed and demonstrated by using a polarization scrambler (PS) in the system in order to improve its performance. By comparing the PDG caused by SSRI among 40 signal channels over different DCF module experimentally, it is found that both differential group delays (DGD) and *Raman* gain coefficients will influence the value of PDG. By using a PS, PDG due to SSRI can be reduced effectively, whilst ensuring a low polarization mode dispersion (PMD) value in the transmission system simultaneously.

Several new applications of DRA are proposed and demonstrated in Chapter 5. The impact of using different amplification schemes on both uplink and downlink in a wavelength division multiplexer (WDM) fiber-radio system is first investigated. Experimental results indicate that DRA can suppress impairments induced by stimulated *Brillouin* scattering (SBS) effect in downlink transmission and improve noise performance in uplink transmission, compared with its EDFA counterpart. Inter-channel crosstalk and spur free

dynamic range (SFDR) under different amplification schemes are also studied. Experimental results indicate that using DRA does not introduce any additional impairment from crosstalk and degradation in SFDR in radio over fiber network. In the second section of this chapter, a SRS assisted fiber optical parametric oscillator (FOPO), which is insensitive to the polarization states of the two signals involved, is observed for the first time. A depolarized broadband source ranging from 1570nm to 1640nm with high output power and flat spectrum is generated due to the combined action of the second order SRS (SOSRS) and parametric process simultaneously. In the last section of this chapter, a depolarized high power (200mW) broadband source (1520-1620nm) with high polarization insensitivity is obtained using single pump based on hybrid effects of dual-order *Raman* scattering, parametric process in highly nonlinear dispersion shift fiber and *Erbium* doped super-fluorescent.

## 6.2 Future Works

Judged from above analysis in this thesis, it can be found that DRA is a good alternative amplification scheme for future optical communication systems. In addition, there still exist many interesting problems and challenges associated with DRA that are worth studying in future.

### 6.2.1 Automatic Gain Control for Second-order DRA

DRA offers many advantages compared with other alternative amplification technologies [4]. It has been known that second-order *Raman* amplification can provide an improved noise performance compared with first-order *Raman* amplification [156]. However, in modern optical telecommunication systems,

channel add/drop events and accidental cable cuts can cause sudden fluctuations in the overall input signal power to an optical amplifier. Such input signal power fluctuations have been observed to produce gain transients in DRA [109]. Several control schemes have been successfully demonstrated [119, 157]. However, DRA with a long cavity prevents transient gain clamping through an all-optical feedback loop [157], as it will induce signal power oscillations and degrade the system performances before reaching steady-state conditions. In reference [119], transient effect suppression is realized through monitoring the fluctuation of output signal and controlling *Raman* pump lasers accordingly, however, controlling the high power *Raman* pump laser in a transient response is not easy in practical application.

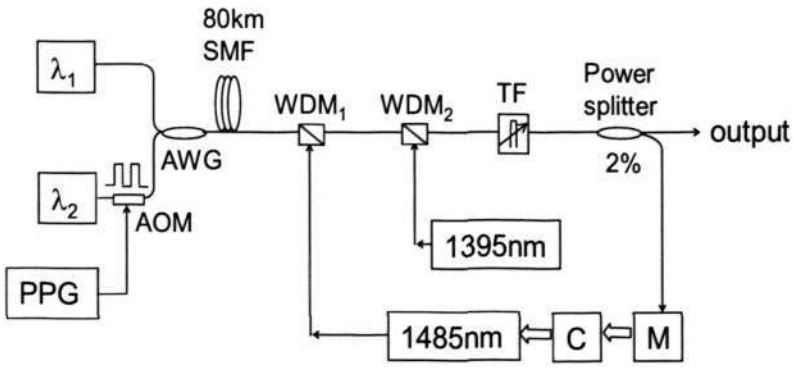


*Figure 6-1 AGC system for second order DRA*

The automatic gain control (AGC) system for second order DRA is composed of two tunable laser sources ($\lambda_1$ and $\lambda_2$), a pulse pattern generator (PPG), a power control system (C), a power monitoring system (M), one acousto-optic modulator (AOM) and a tunable filter (TF). An arrayed waveguide grating (AWG) is used to multiplex the WDM signal channels. The first order *Raman*

pump laser is a low power laser diode (LD) at 1485nm, the second order *Raman* laser is a high power RFL at 1395nm and the dual-order *Raman* pumps are coupled into transmission fiber using $WDM_1$ and $WDM_2$ respectively. Two percent of output signal is extracted for the power monitoring system by a power splitter.

One of future works would like to use this AGC system to suppress transient effect for the second order DRA. The experimental setup is shown in Figure 6-1. The transient gain fluctuation of the second order DRA is expected to be suppressed greatly only through controlling the first order *Raman* pump laser with low power. In this way, the direct controlling of high power *Raman* pumps can be avoided.

### 6.2.2 Reduction of Nonlinear Penalty in DRA System

For next generation dense WDM (DWDM) system employing 40Gbit/s per-channel, intra-channel cross-phase modulation (IXPM) and intra-channel four-wave-mixing (IFWM) will limit the system performance in addition to the inter-channel nonlinear distortions. The IXPM leads to pulse timing jitter, while the IFWM results in the overlapping of the pulses. It has been known that the performance of optical transmission system can be optimized by adjusting the pre-compensation to pre-chirp the pulses since their path-averaged width over the high power, nonlinear sections within the span link is minimized in this way. As a result, overlapping of neighboring pulses and distortion due to intra-channel nonlinear effects can be eliminated by optimizing the per-dispersion compensation [158].

The optimization of the pre-compensation is highly dependent on the signal power distribution along the span link. The effect of pre-compensation in EDFA amplification system has been investigated extensively and the analytical analysis to minimize both the IXPM and IFWM has been derived [158]. However, for a *Raman* amplified transmission system, the signal power distribution is significantly different from that of EDFA amplified transmission system. Especially for DRA, the signal power distributions along the span link are also dependent on different pumping configurations, such as forward pumping, backward pumping and bi-directional pumping schemes. As a result, it is necessary to optimize the pre-compensation for *Raman* amplified transmission system in different pumping schemes in order to minimizing the impact arising from fiber nonlinear effects.

### 6.2.3 Performance of DRA Using Novel Amplification Schemes

We have proposed several novel amplification schemes to improve the noise and nonlinear performance in Chapter 4, such as incorporating a piece of nonlinear PCF in transmission span or utilizing dual-order SRS to pump a piece of remote EDF located down the fiber link to improve the noise and gain performances and also using a PS to reduce PDG effectively while keeping a low PMD value of the transmission system. In future works, these schemes will be verified in practical transmission system to improve the system performance.

### 6.2.4 Theoretical Study of Influence of EDF on Hybrid Amplifier

We have carried out the experimental study on the influence of the distributed

secondary amplification obtained from the EDF along the span on the performance of the hybrid amplifier. Both gain and noise performance of the hybrid amplifier can be improved greatly by optimizing the position of the EDF. However, the theoretical study of this work is also an important issue for the practical design and application of the hybrid amplifier. In future work, we will illustrate the actual computed signal power distribution and give a quantitative analysis of the relation between the noise performance and the secondary amplification obtained from the EDF along the span.

.

# Author's Publications

## Journal Papers:

[1] **Zhaohui Li**, Chao Lu, Jian Chen, Chunliu Zhao, "*Raman* amplifier design using geometry compensation technique," *Optics Express*, vol. **12**, pp.436-441, 2004 (Chapter 3)

[2] **Zhaohui Li**, Zhihong Li, Xiao Hann Li, Chao Lu, Yixin Wang, "Reduction of polarization-dependent gain due to signal-to-signal *Raman* interaction in fiber *Raman* amplifier," *IEEE, Photonics Technology Letters,* vol.**17**, pp.558-560, 2005 (Chapter 4)

[3] **Zhaohui Li,** Chunliu Zhao, Yang Jing Wen, Jian Chen and Chao Lu, "Optimization of a *Raman*/EDFA Hybrid Amplifier based on Dual-order Stimulated *Raman* Scattering of a Single Pump," *Optics Communications,* vol. **265**, pp.655-658, 2005 (Chapter 4)

[4] Chunliu Zhao, **Zhaohui Li**, Xiufeng Yang, Chao Lu, Wei Jin, M. S. Demokan, "Effect of a nonlinear photonic crystal fiber on the noise characterization of a distributed *Raman* amplifier," *IEEE, Photonics Technology Letters*, vol.**17**, pp.561-563, 2005 (Chapter 4)

[5] **Zhaohui Li**, Zhihong Li, Fuyun Lu, Xiufeng Yang, Jian Chen and Chao Lu, "Pump-to-signal FWM of Co-pumped *Raman* Amplifier for Remote Pumps Supervisor," *Optics Communications,* vol. **254**, pp.138-144, 2005

[6] **Zhaohui Li**, Chao Lu and Jian Chen, "Depolarized Broadband Source Generated by Hybrid Effects of *Raman* Scattering, Parametric Process and

*Erbium* Doped Super-fluorescent," *IEE, Electronics Letters*, vol. **41**, pp.1103-1104, 2005 (Chapter 5)

[7] **Zhaohui Li**, Ampalavanapillai Nirmalathas, Masuduzzaman Bakaul, Yang Jing Wen, Linghao Cheng, Jian Chen, Chao Lu and Sheel Aditya, "Performance of WDM Fiber-Radio Network Using Distributed *Raman* Amplifier," *IEEE, Photonics Technology Letters*, vol.**18**, pp.553-555, 2006 (Chapter 5)

[8] **Zhaohui Li**, Yi Dong, Chao Lu, Yang Jing Wen, Yixin Wang, Tee Hiang Cheng and Weisheng Shu, "Comparison of XGM Effects of Manchester-duobinary, RZ-DPSK, NRZ-DPSK, RZ and NRZ Modulation Formats in SOA," *IEEE, Photonics Technology Letters,* vol.**18**, pp. 2680-2682, 2006

[9] Yi Dong, **Zhaohui Li**, Chao Lu, Yixin Wang, Yang Jing Wen, Tee Hiang Cheng and Weisheng Shu, "Improving dispersion tolerance of Manchester coding by incorporating duobinary coding," *IEEE, Photonics Technology Letters,* vol.**18**, pp.1723-1725, 2006

[10] Jian Chen, Xueming Liu, Chao Lu, Yixin Wang and **Zhaohui Li,** "Design of Multi-Stage Gain-Flattened Fiber *Raman* Amplifiers," *IEEE, Journal of Lightwave Technology*, vol.**24**, pp.935-944, 2006

[11] Chun-Liu Zhao, **Zhaohui Li**, M. S. Demokan, Xiufeng Yang, W. Jin and Chao Lu, "Studies on Strain and Temperature Characteristics of a Slanted Multimode Fiber *Bragg* Grating and its Application on Multi-wavelength Fiber *Raman* Ring Laser," *IEEE, Journal of Lightwave Technology*, vol.**24**, pp.2394-2400, 2006

[12] Linghao Cheng, Sheel Aditya, **Zhaohui Li**, Ampalavanapillai Nirmalathas and Chao Lu, "Nonlinear Crosstalk due to XPM in dispersive WDM

Microwave Fiber-Optic Links," *IEEE, Journal of Lightwave Technology*, vol.**24**, pp.2296-2304, 2006

[13] Chun-Liu Zhao, **Zhaohui Li**, M. S. Demokan, Xiufeng Yang, Wei Jin, "Switchable Multi-wavelength SOA-Fiber Ring Laser Based on a Slanted Multimode Fiber *Bragg* Grating," *Optics Communications,* vol. **252**, pp.52-57, 2005

[14] Yi Dong, Jinyun Mo, Zhihong Li, **Zhaohui Li**, Yixin Wang and Chao Lu, "WDM transmission of 16/spl times/10.709 Gb/s over 640-km SSMF using cascaded semiconductor optical amplifiers and DPSK modulation format," *IEEE, Photonics Technology Letters,* vol.**16**, pp.2359-2361, 2004

[15] Linghao Cheng, Sheel Aditya, **Zhaohui Li**, Ampalavanapillai Nirmalathas, A. Alphones, and Ling Chuen One, "Nonlinear Distortion due to Cross-phase Modulation in Microwave Fiber-Optic Links with Optical Single Sideband or Electro-optical Upconversion," Accepted by *IEEE Transactions on Microwave Theory and Techniques*

## Conference Papers:

[16] **Zhaohui Li**, Chao Lu, Jian Chen, "Gain Variation with *Raman* Amplifier Parameters and its Restoration," *The 8th Opto-Electronics and Communications Conference (OECC 2003),* Shang Hai, China (Chapter 3)

[17] **Zhaohui Li** and Chao Lu, "Reduction of Polarization Dependent Gain Due to Signal-to-Signal *Raman* Interaction in Fiber *Raman* Amplifier," *Optical Amplifiers and Their Applications Meeting*, OAA'05, **ME1**. (Chapter 4)

[18] **Zhaohui Li**, Ampalavanapillai Nirmalathas, Linghao Cheng, Chao Lu and Sheel Aditya, "Application of distributed *Raman* amplifier to improve link gain

and noise characteristic of WDM radio over fiber network," *International Topical Meeting on Microwave Photonics, MWP 2005,* **TP-32** (Chapter 5)

[19] Linghao Cheng, Sheel Aditya, **Zhaohui Li**, Arokiaswami Alphones, Michael Ong, "Nonlinear Distortion due to XPM in Dispersive WDM Microwave Fiber-Optic Links With Optical SSB Modulation," *International Topical Meeting on Microwave Photonics, MWP 2005,* **TP-31** (Chapter 5)

[20] **Zhaohui Li**, Ampalavanapillai Nirmalathas, Masuduzzaman Bakaul, Linghao Cheng, Yang Jing Wen and Chao Lu, "Application of Distributed *Raman* Amplifier for the Performance Improvement of WDM Millimeter-Wave Fiber-Radio Network," *18th Annual Lasers and Electro Optics Society Meeting, LEOS'05,* **WO5** (Chapter 5)

[21] **Zhaohui Li**, Fuyun Lu, Zhihong Li, Xiao Hann Lim and Chao Lu, "Pump-to-signal FWM of co-pumped *Raman* amplifier for remote pumps supervisory," *OFC/NFOEC 2005,* CA, USA, **JWA10**

[22] **Zhaohui Li**, Fuyun Lu, Xiao Hann Lim, Xiaoqun Zhou, Yixin Wang and Chao Lu, "Polarization insensitive four-wave mixing assisted by *Raman* amplification: influence of *Raman*-induced *Kerr* effect," *OFC/NFOEC 2005,* CA, USA, **JWA9**

[23] Yi Dong, **Zhaohui Li**, Chao Lu, Yixin Wang, Yang Jing Wen, Tee Hiang Cheng and Weisheng Shu, "Broad-band RF Photonic Phase Modulator Based on a Novel Nonlinear Optical Loop Mirror," *ECOC'06,* **Mo4.4.1**

[24] Linghao Cheng, Aditya Sheel, **Zhaohui Li** and Chao Lu, "Noise due to fiber dispersion in phase dithered microwave fiber optic links," *Advances in Wired and Wireless Communication, 2005 IEEE/Sarnoff Symposium*, pp.106-108, 2005

[25] Jinyu Mo, Yi Dong, Zhihong Li, **Zhaohui Li**, Yixin Wang and Chao Lu, "WDM transmission of 16×10.708Gb/s over 640km SSMF using cascaded SOAs and DPSK modulation format," *ECOC'04*, **We4**

[26] **Zhaohui Li**, Yi Dong, Yang Jing Wen, Yixin Wang, Tee Hiang Cheng, Chao Lu and Weisheng Hu, "Realization of RF Phase Shift on Amplitude Modulated Data for Smart Antenna in Wireless Access Networks," *OFC/NFOEC 2007,* CA, USA, **OWN5**

[27] Yi Dong, **Zhaohui Li**, Changyuan Yu, Yang Jing Wen, Yixin Wang, Chao Lu, Weisheng Hu and Tee Hiang Cheng "Generatioin of Multi-Channel Short-Pulse Sources Using Nonlinear Optical Loop Mirror Based on Photonic Crystal Fiber," *OFC/NFOEC 2007,* CA, USA, **JWA9**

# References

[1] M. N. Islam, "*Raman* Amplifiers for Telecommunications," *IEEE, Journal of Selected Topics in Quantum Electronics*, vol. **8**, pp. 548-559, 2002.

[2] S. Namiki and Y. Emori, "Ultrabroad-Band *Raman* Amplifiers Pumped and Gain-Equalized by Wavelength-Division Multiplexed High-Power Lasers Diodes," *IEEE, Journal of Selected Topics in Quantum Electronics*, vol.**17**, pp. 3-16, 2001.

[3] J. Wang, "Performance Evaluation of DPSK Optical Fiber Communication System," *Univerisity of California, Berkeley*, 2004.

[4] J. Bromage, "*Raman* Amplification for Fiber Communication Systems," *IEEE, Journal of Lightwave Technology*, vol.**22**, pp. 79-93, 2004.

[5] K. Imai, I. Morita, H. Sakata, and N. Edagawa, "A Study on Gain Modulation Dynamics of 80nm-Band High-power *Raman* Amplifier," presented at *Optical Fiber Communication Conference, OFC'98*, TuC3.

[6] C. R. S. Fludger, V. Handerek, and R. J. Mears, "Pump to Signal RIN Transfer in *Raman* Amplifiers," *IEEE, Journal of Lightwave Technology*, vol.**19**, pp. 1140-1148, 2001.

[7] K. Song and S. D. Dods, "Cross Modulation of Pump-Signals in Distributed *Raman* Amplifier, Theory and Experiment," *IEEE, Photonics Technology Letters*, vol.**13**, pp. 1173-1175, 2001.

[8] L. J. Wang, J. T. Lin, and P. Ye, "Analysis of Polarization Dependent Gain in Fiber Amplifiers," *IEEE, Journal of Selected Topics in Quantum Electronics*, vol.**7**, pp. 413-418, 1998.

[9] F. Heismann, "Compact Electro-optic Polarization Scramblers for Optically Amplified Lightwave Systems," *IEEE, Journal of Lightwave Technology*, vol.**14**, pp. 1801-1814, 1996.

[10] Z. Li, Z. Li, X. H. Lim, C. Lu, J. Chen, and Y. Wang, "Reduction of Polarization Dependent Gain due to Signal-to-signal *Raman* Interaction in Fiber *Raman* Amplifier," *IEEE, Photonics Technology Letters*, vol.**17**, pp. 558-560, 2005.

[11] S. Popov, E. Vanin, and G. Jacobsen, "Influence of Polarization Mode Dispersion Value in Dispersion Compensating Fibers on the Polarization Dependence of *Raman* Gain," *Optics Letters*, vol. **27**, pp. 155-157, 2002.

[12] S. Popov, A. Bernson, E. Vanin, G. Jacobsen, and J. Karissson, "Polarization Dependence and Gain Tilt of *Raman* Amplifiers for WDM Systems," presented at *Optical Fiber Communication, OFC'02*, M12-1.

[13] F. Bruyere and O. Audouin, "Penalties in Long-haul Optical Amplifier Systems due to Polarization Dependent Loss and Gain," *IEEE, Photonics Technology Letters*, vol.**6**, pp. 654-657, 1994.

[14] X. Zhou and P. Magill, "Polarization Dependent Gain Due to Signal-signal *Raman* Interaction: can Fiber PMD be to Low?" presented at *Optical Fiber Communication, OFC'04*, WE6.

[15] T. Tokura, T. Kogure, T. Sugihara, K. Shimizu, T. Mizuochi, and K. Motoshima, "Pump Light Depolarization Method for Low PDG *Raman* Amplification," presented at *Optical Fiber Communication, OFC'02*, ThGG24.

[16] S. J. B. Woo, "Wavelength Conversion Technology for WDM Network Applications," *IEEE, Journal of Lightwave Technology*, vol.**14**, pp. 955-966, 1996.

[17] J. M. Wiesenfeld, B. Glance, J. S. Perino, and A. H. Gnauck, "Wavelength Conversion at 10Gbit/s Using a Semiconductor Optical Amplifier," *IEEE, Photonics Technology Letters*, vol.**5**, pp. 1300-1302, 1993.

[18] T. Durhuus, C. Joergensen, B. Mikkelsen, R. J. S. Pederson, and K. E. Stubkjaer, "All Optical Wavelength Conversion by SOAs On a Mach-Zehnder Configuration," *IEEE, Photonics Technology Letters*, vol.**6**, pp. 53-55, 1994.

[19] J. Zohu, N. Park, K. J. Vahala, M. Z. Newkirk, and B. I. Miller, "Four-Wave Mixing Wavelength Conversion Efficiency in Semiconductor Traveling-Wave Amplifiers Measured to 65nm of Wavelength Mixing," *IEEE, Journal of Lightwave Technology*, vol.**6**, pp. 984-986, 1994.

[20] K. Inoue, T. Hasegawa, K. Oda, and H. Toba, "Multi-Channel Frequency Conversion Experiment Using Fiber Four-Wave Mixing," *Electronics Letters*, vol.**29**, pp. 1708-1710, 1993.

[21] T. Morioka, S. Kawanishi, K. Uchiyama, H. Takara, and M. Saruwatari, "Polarization Independent 100 Gbit/s All-optical Demultiplexer Using Four-Wave Mixing in a Polarization Maintaining Fiber Loop," *Electronics Letters*, vol.**30**, pp. 591-592, 1994.

[22] D. A. Chestnut, C. J. S. D. Matos, and J. R. Taylor, "*Raman* Assisted Fiber Optical Parametric Amplifier and Wavelength Converter in Highly Nonlinear Fiber," *Journal of the Optical Society of America B*, vol.**19**, pp. 1901-1904, 2002.

[23] L. Xu, P. K. A. Wai, and H. Y. Tam, "All Optical Shutter Based on *Raman*-assisted Four-Wave Mixing in Dispersion Shifted Fiber," presented at *Optical Fiber Communication, OFC'04*, TuC7.

[24] T. Tanemura and K. Kikuchi, "Polarization-independent Broad-band Wavelength Conversion Using Two-pump Fiber Optical Parametric Amplification Without Idler Spectral Broadening," *IEEE, Photonics Technology Letters*, vol.**15**, pp. 1573-1575, 2003.

[25] T. Sylvestre, H. Maillotte, E. Lantz, and P. T. Dinda, "*Raman* Assisted Parametric Frequency Conversion in a Normally Dispersive Single Mode Fiber," *Optics Letters*, vol.**24**, pp. 1561-1563, 1999.

[26] T. Nakada and F. Kannari, "Dual-Wavelength-Pumped *Raman*-Resonant Four-Wave Mixing," *Journal of the Optical Society of America B*, vol.**10**, pp. 1870-1879, 1993.

[27] A. Uchida, M. Takeoka, T. Nakada, and F. Kannari, "Wide-Range All-Optical Wavelength Conversion Using Dual-Wavelength-Pumped Fiber *Raman* Converter," *IEEE, Journal of Lightwave Technology*, vol.**16**, pp. 92-99, 1998.

[28] M. Tang, Y. D. Gong, and P. Shum, "Wide Range Tunable Wavelength Conversion Using Parametric Effects and *Raman* Amplification in a Double-pass System," presented at *30th European Conference on Optical Communication, ECOC'04*, We4.

[29] M. Tang, Y. D. Gong, and P. Shum, "Broadband Tunable Wavelength Conversion Using *Raman*-assisted Parametric Four-wave Mixing in Highly Nonlinear Fiber with Double-pass Geometry," *IEEE, Photonics Technology Letters*, vol.**17**, pp. 148-150, 2005.

[30] Z. Li, F. Lu, X. H. Lim, X. Zhou, Y. Wang and C. Lu, "Polarization Insensitive Four-Wave Mixing Assisted by *Raman* Amplification: Influence of *Raman*-Induced *Kerr* Effect," Present at *Optical Fiber Communication, OFC'05*, JWA9

[31] W. Wang, H. N. Poulsen, L. Rau, H. F. Chou, J. E. Bowers, and D. J. Blumenthal, "*Raman* Enhanced Regenerative Ultra-fast All-optical Fiber XPM Wavelength Converter," *IEEE, Journal of Lightwave Technology*, vol.**19**, pp. 1105-1115, 2005.

[32] W. Wang, H. N. Poulsen, L. Rau, H. F. Chou, J. E. Bowers, D. J. Blumenthal, and L. G. Nielsen, "Regenerative 80 Gb/s Fiber XPM Wavelength Converter Using a Hybrid *Raman*/EDFA Gain Enhanced Configuration," *IEEE, Journal of Lightwave Technology,* vol.**15**, pp. 1416-1418, 2003.

[33] Y. Nakajima, Y. Shindo, and T. Yoshikawa, "Novel Concept as long Distance Transmission FBG Sensor System Using Distributed *Raman* Amplification," presented at *15th International Conference on Optical Fiber Sensors, OFS'03,* Th1-4.

[34] Y. T. Cho, M. N. Alahbabi, G. Brambilla, and T. P. Newson, "Remote Amplification in Long Range Distributed *Brillouin*-based Temperature Sensors," presented at *17th International Conference on Optical Fiber Sensors, OFS'05,* Tu3-72.

[35] J. H. Lee, Y. G. Han, Y. M. Chang, and S. B. Lee, "*Raman* Amplifier Based Long-distance Remote FBG Strain Sensor with EDF Broadband Source Recycling Residual *Raman* Pump," *Electronics Letters,* vol.**40**, pp. 1106-1107, 2004.

[36] A. J. Seeds, "Microwave Photonics," *IEEE, Transactions on Microwave Theory and Techniques,* vol.**45**, pp. 877-887, 2002.

[37] D. Wake, M. Webster, G. Wimpenny, K. Beacham, and L. Crawford, "Radio over Fiber for Mobile Communications," presented at *International Topical Meeting on Microwave Photonics, MWP'04,* TA-1, 2004.

[38] W. I. Way, "Optical Fiber-based Microcellular Systems: an Overview," *IEICE Transactions on Communications,* vol.**E76-B**, pp. pp.1078-1090, 1993.

[39] G. H. Smith, D. Novak, and C. Lim, "A Millimeter-Wave Full-Duplex Fiber-Radio Star-Tree Architecture Incorporating WDM and SCM," *IEEE, Photonics Technology Letters,* vol.**10**, pp. 1650-1652, 1998.

[40] C. Lim, M. Attygalle, D. Novak and R. Waterhouse, "On the Merging of Millimeter-Wave Fiber Radio Backbone with 25GHz WDM Ring Network," *IEEE, Journal of Lightwave Technology,* vol.**21**, pp. 2203-2210, 2003.

[41] C. Carlsson, H. Martinsson, A. Larsson, and A. Alping, "High Performance Microwave Link Using a Multimode VECSEL and a High Bandwidth Multimode Fiber," presented at *International Topical Meeting on Microwave Photonics, MWP'01,* Tu-3.2.

[42] H. Roussel, R. Helkey, G. Betts, and G. Cox, "Effect of Optical Feed Back on High Dynamic Range *Fabry-Perot* Laser Optical Links," *IEEE, Photonics Technology Letters,* vol.**9**, pp. 106-108, 1997.

[43] C. Lim, A. Nirmalathas, D. Novak, and R. Waterhouse, "Capacity Analysis for WDM Fiber Radio Backbones with Star Tree and Ring Architecture Incorporating Wavelength Interleaving," *IEEE, Journal of Lightwave Technology,* vol.**21**, pp. 3308-3315, 2003.

[44] M. Bakaul, A.Nirmalathas, and C. Lim, "Multi-functional WDM Optical Interface for Millimeter-Wave Fiber-Radio Antenna Base Station," *IEEE, Journal of Lightwave Technology,* vol.**23**, pp. 1210-1218, 2005.

[45] M. R. Phillips and D. M. Ott, "Crosstalk due to Optical Fiber Nonlinearities in WDM CATV Lightwave Systems," *IEEE, Journal of Lightwave Technology,* vol.**17**, pp. 1782-1791, 1999.

[46] L. Cheng, S. Aditya, Z. Li, A. Alphonesand, and M. Ong, "Nonlinear Distortion Due to XPM in Dispersive WDM Microwave Fiber-Optic Links with Optical SSB Modulation," presented at *International Topical Meeting on Microwave Photonics, MWP'05,* TP-31.

[47] C. J. S. D. Matos, D. A. Chestnut, and J. R. Taylor, "Continuous-Wave 1664.7nm Fiber Source Utilizing Four-Wave Mixing and Stimulated *Raman* Scattering," *Applied Physics Letter,* vol.**81**, pp. 1390-1392, 2002.

[48] P. E. Britton, H. L. Offerhaus, D. J. Richardson, P. G. Smith, G. W. Ross, and D. C. Hanna, "Parametric Oscillator Directly Pumped by a 1550nm *Erbium* Fiber Laser," *Optics Letters,* vol.**24**, pp. 975-977, 1999.

[49] C. J. S. Matos and J. R. Taylor, "Continuous-Wave, Totally Fiber Integrated Optical Parametric Oscillator Using Holey Fiber," *Optics Letters,* vol.**29**, pp. 983-985, 2004.

[50] J. E. Sharping, M. Fiorentino, P. Kumar, and R. S. Windeler, "Optical Parametric Oscillator Based on Four-Wave Mixing in Microstructure Fiber," *Optics Letters,* vol.**27**, pp. 1675-1677, 2002.

[51] J. Lasri, P. Devgan, R. Tang, J. E. Sharping, and P. Kumar, "A Microstructure-Fiber-Based 10-GHz Synchronized Tunable Optical Parametric Oscillator in 1550nm Regime," *IEEE, Photonics Technology Letters,* vol.**15**, pp. 1058-1060, 2003.

[52] Y. Wang, W. Zhang, Q. Wang, X. Feng, X. Liu, and J. Peng, "Broadband Source Generated by Stimulated *Raman* Scattering and Four-Wave Mixing in a Highly Nonlinear Optical Fiber Ring Cavity," *Optics Letters,* vol.**29**, pp. 842-844, 2004.

[53] K. Liu, M. Digoneet, G. H. Shaw, B. J. Ainslie, and S. P. Craig, "10mW Superfluorescent Single Mode Fiber Source at 1060nm," *Electronics Letters,* vol.**23**, pp. 1320-1321, 1987.

[54] R. R. Alfano, T*he Supercontinuum Laser Source:* S*pringer-Verlab, New York,* 1989.

[55] F. Vanholsbeeck, S. Coen, P. Emplit, C. Martinelli, and T. Sylvestre, "Cascaded *Raman* Generation in Optical Fibers: Influence of Chromatic Dispersion and *Rayleigh* Backscattering," *Optics Letters,* vol.**29**, pp. 998-1000, 2004.

[56] D. G. Falquier, M. J. F. Digonnet, and H. J. Shaw, "A Depolarized Er-doped Super-Fluorescent Fiber Source With Improved Long-Term Polarization Stability," *IEEE, Photonics Technology Letters*, vol.**13**, pp. 25-27, 2001.

[57] R. H. Stolen and E. P. Ippen, "*Raman* Gain in Glass Optical Waveguides," *Applied Physics Letter,* vol.**22**, pp. 276-278, 1973.

[58] A. Belahlou, S. Bickham, D. Chowdhury, P. Diep, A. Evans, J. M. Grochocinski, P. Han, A. Kobyakov, S. Kumar, G. Luther, J. C. Mauco, Y. Mauro, M. Mlejnek, M. S. K. Muktoyuk, M. T. Murtagh, S. Raghavan, V. Ricci, A. Sevian, N. Taylor, S. Tsuda, M. Vasilyev, and L. Wang, "Fiber Design Considerations for 40Gb/s Systems," *IEEE, Journal of Lightwave Technology,* vol.**20**, pp. 2290-2305, 2002.

[59] C. Brackett, "Dense Wavelength Division Multiplexing Networks: Principle and Applications," *IEEE, Journal of Selected Areas in Communications,* vol.**8**, pp. 948-964, 1990.

[60] S. Namiki, Y. Ikegami, Y. Shirasaka, and I. Oh-ishi, "Highly Coupled High Power Pump Laser Modules," presented at *Optical Amplifiers and Their Applications, OAA'93,* MD5.

[61] T. Kimura, N. Tsukiji, A. Iketani, N. Kimura, H. Murata, and Y. Ikegami, "High Temperature Operation Quarter Watt 1480nm Pump LD Module," presented at *Optical Amplifiers and Their applications, OAA'99,* ThD12.

[62] D. Garbuzov, A. Komissarov, I. Kudryashov, M. Maiorov, R. Roff, and J. Connolly, "High Power *Raman* Pumps Based Ridge Waveguide InGaAsP/InP Diode Lasers," presented at *Optical Fiber Communication, OFC'03,* WO1.

[63] J. Yoshida, N. Tsukiji, A. Nakai, T. Fukushima, and A. Kasukawa, "Highly Reliable High Power 1480nm Pump Lasers for EDFA and *Raman* Amplifiers," presented at *SPIE*, 2001.

[64] S. Koyanagi, A. Mugino, T. Aikiyo, and Y. Ikegami, "The Ultra High Power 1480nm Pump Laser Diode Module with Fiber *Bragg* Grating," presented at *Optical Amplifiers and Their Applications, OAA'98,* MC2.

[65] P. B. Hansen, L. Eskildsen, S. G. Grubb, A. J. Stentz, A. Strasser, J. Judkins, J. J. DeMarco, R. Pedrazzani, and D. J. DiGiovanni, "Capacity Upgrades of Transmission Systems by *Raman* Amplification," *IEEE, Photonics Technology Letters,* vol.**9**, pp. 262-264, 1997.

[66] M. Nissov, C. R. Davidson, K. Rottiwitt, R. Menges, P. C. Corbett, D. Innis, and N. S. Bergano, "100Gb/s (10×10Gb/s) WDM Transmission Over 7200km Using Distributed *Raman* Amplification," presented at 23*th European Conference on Optical Communication, ECOC'97,* pp. 9-12.

[67] Y. Zhu, C. R. S. Fludger, W. S. Lee, P. Lobb, T. Schilhabel, and A. Hadjifotiou, "Experimental Comparison of All-*Raman* and *Raman*/EDFA Hybrid Amplification Using 40Gbit/s Based Transmission Over 400km TW-RS Fiber," *Electronics Letters,* vol.**38**, pp. 893-895, 2002.

[68] Y. Zhu, I. Hardcastle, W. S. Lee, C. R. S. Fludger, A. Hadjufotiou, C. Li, D. Qiao, H. Sun, K. T. Wu, and J. McNicol, "Experimental Comparison of *Raman*-Amplified Dispersion-Managed Fiber Types Using 16×40 Gbit/s Transmission over 500km," *Electronics Letters,* vol.**38**, pp. 895-896, 2002.

[69] J. Bromage, J. C. Bouteiller, H. J. Thiele, K. Brar, L. E. Nelson, S. Stulz, C. Headley, R. Boncek, J. Kim, A. Klein, G. Baynham, L. V. Jorgensen, L. G. Nielsen, R. L. L. Jr., and D. J. DiGiovanni, "WDM Transmission Over Multiple Long Spans With Bidirectional *Raman* Pumping," *IEEE, Journal of Lightwave Technology,* vol.**22**, pp. 225-232, 2004.

[70] M. Morisaki, H. Sugahara, T. Ito, and T. Ono, "2.56Tb/s (64×2.7 Gb/s) WDM Transmission Over 6000km Using All-*Raman* Amplified Inverse Double Hybrid Spans," *IEEE, Photonics Technology Letters,* vol.**15**, pp. 1615-1617, 2003.

[71] T. Mizuochi, K. Kinjo, S. Kajiya, T. Tokura, and K. Motoshima, "Bidirectional Unrepeated 43Gb/s WDM Transmission With C/L Band-Separated *Raman* Amplification," *IEEE, Journal of Lightwave Technology,* vol.**20**, pp. 2079-2085, 2002.

[72] H. Maeda, G. Funatsu, and A. Naka, "Ultra-Long-Span 500km 16×10Gbit/s WDM Un-Repeatered Transmission Using RZ-DPSK Format," *Electronics Letters,* vol.**41**, 2005.

[73] L. Labrunie, F. Boubal, P. L. Roux, and E. Brandon, "500km WDM 12×10 Gbit/s CRZ Repeaterless Transmission Using Second-Order Remote Amplification," *Electronics Letters,* vol.**39**, pp. 1394-1395, 2003.

[74] K. Aida, S. Nishi, Y. Sato, K. Hagimoto, and K. Nakagawa, "1.8Gbit/s 310km Fiber Transmission without Outdoor Repeater Equipment Using a Remotely Pumped in-line Er-doped Fiber Amplifier in An IM=Direct-Direction System," presented at *European Conference on Optical Communication, ECOC'89,* PDA-7.

[75] A. J. Stentz, T. Nielsen, S. G. Grubb, T. A. Strasser, and J. R. Pedrazzani, "*Raman* Ring Amplifier at 1.3$\mu m$ with Analog-Grade Performance and an Output Power of 23dBm," presented at *Optical Fiber Communication Conference, OFC'96.*

[76] P. Gavrilovic, "S-band Discrete *Raman* Amplifiers: Technology and System Performance," presented at *Lasers and Electro-Optics Society, LEOS'2001,* WJ1.

[77] S. S. H. Yam, M. E. Marchic, Y. Akasaka, and L. G. Kazovsky, "Gain Flattened Gain Clamped Discrete *Raman* Amplifier," presented at *Lasers and Electro-Optics, CLEO'04,* pp. 2-3.

[78] H. Kidorf, K. Rottwitt, M. Nissov, M. Ma, and E. Rabarijaona, "Pump Interactions in a 100-nm Bandwidth *Raman* Amplifier," *IEEE, Photonics Technology Letters,* vol.**15**, pp. 392-394, 1999.

[79] X. M. Liu, H. Y. Zhang, and Y. L. Guo, "A Novel Method for *Raman* Amplifier Propagation Equations," *IEEE, Photonics Technology Letters,* vol.**15**, pp. 392-394, 2003.

[80] B. Min, W. J. Lee, and N. Park, "Efficient Formulation of *Raman* Amplifier Propagation Equations with Average Power Analysis," *IEEE, Photonics Technology Letters,* vol.**12**, pp. 1486-1488, 2001.

[81] V. E. Perlin and H. G. Winful, "Optimal Design of Flat-gain Wide-band Fiber *Raman* Amplifiers," IEEE, *Journal of Lightwave Technology,* vol.**20**, pp. 250-254, 2002.

[82] V. E. Perlin and H. G. Winful, "On Distributed *Raman* Amplification for Ultrabroad-band Long-Haul WDM Systems," *IEEE, Journal of Lightwave Technology,* vol.**14**, pp. 176-178, 2002.

[83] Y. Emori and S. Namiki, "100nm Bandwidth Flat Gain *Raman* Amplifiers Pumped and Gain Equalized by 12-wavelength-channel WDM High Power Laser Diodes," presented at *Optical Fiber Communication Conference, OFC'99,* PD19.

[84] S. Kado, Y. Emori, and S. Nmiki, "Gain and Noise Tilt Control in Multi-wavelength Bi-directionally Pumped *Raman* Amplifier," presented at *Optical Fiber Communication Conference, OFC'02,* TuJ4.

[85] C. R. S. Fludger, V. Handerek, and R. J. Mears, "Fundamental Noise Limits in Broadband *Raman* Amplifiers," presented at *Optical Fiber Communication Conference, OFC'01,* MA5.

[86] T. T. Kung, C. T. Chang, J. C. Dung, and S. Chi, "Four-Wave Mixing between Pump and Signal in a Distributed *Raman* Amplifier," *IEEE, Journal of Lightwave Technology,* vol.**21**, pp. 1164-1170, 2003.

[87] M. C. Ho, C. J. Chen, W. S. Wong, and H. K. Lee, "Parametric Interactions Between Pumps and Signals in a Co-Pumped *Raman* Amplifier," presented at *Lasers and Electro-Optics, CLEO'02,* pp.481-482.

[88] J. Bromage, P. J. Winzer, L. E. Nelson, and C. J. McKinstric, "*Raman* Enhanced Pump Signal Four Wave Mixing in Bi-directionally Pumped *Raman* Amplifiers," presented at *Optical Amplifier and Their Application, OAA'02,* OWA5.

[89] J. C. Bouteiller, L. Leng, and C. Headley, "Pump-Pump Four-wave Mixing in Distributed *Raman* Amplified Systems," *IEEE, Journal of Lightwave Technology,* vol.**22**, pp. 723-733.

[90] S. W. William, C. J. Chen, M. C. Mo, and H. K. Lee, "Phase-Matched Four Wave Mixing between Pumps and Signals in a Co-Pumped *Raman* Amplifier," *IEEE, Photonics Technology Letters,* vol.**15**, pp. 209-211, 2003.

[91] F. D. Pasquale and F. Meli, "New *Raman* Pump Module for Reducing Pump-Signal Four-Wave-Mixing Interaction in Co-pumped Distributed *Raman* Amplifier," *IEEE, Journal of Lightwave Technology,* vol.**21**, pp. 1742-1751, 2003.

[92] J. C. Bouteiller, K. Brar, J. Bromage, S. Radic, and C. Headley, "Dual Order *Raman* Pump," *IEEE, Photonics Technology Letters,* vol.**15**, pp. 212-214, 2003.

[93] D. A. Chestnut, C. J. S. d. Matos, P. C. R. Hall, and J. R. Taylor, "Co- and Counter Propagating Second Order Pumped Lumped Fiber *Raman* Amplifiers," presented at *Optical Fiber Communication, OFC'02,* ThB2.

[94] Y. Hadjar, N. J. Traynor, and S. Gray, "Noise Figure Tilt Reduction in Ultrawide-band WDM through Second-order *Raman* Amplification," *IEEE, Photonics Technology Letters,* vol.**16**, pp. 1200-1202, 2004.

[95] S. Faralli and F. D. Pasquale, "Impact of Double *Rayleigh* Scattering Noise in Distributed Higher Order *Raman* Pumping Schemes," *IEEE, Photonics Technology Letters,* vol.**15**, pp. 804-806, 2003.

[96] M. D. Mermelstein, K. Brar, and C. Headley, "RIN Transfer Measurement and Modeling in Dual-order *Raman* Fiber Amplifiers," *IEEE, Journal of Lightwave Technology,* vol.**21**, pp. 1742-1751, 2003.

[97] P. J. Winzer, K. Sherman, and M. Zirngibl, "Time-division Multiplexed *Raman* Pump Experiment Using a Tunable C-band Laser," *IEEE, Photonics Technology Letters,* vol.**14**, pp. 789-791, 2002.

[98] C. R. S. Fludger, V. Handerek, and N. Jolley, "Novel Ultra-Broadband High Performance Distributed *Raman* Amplifier Employing Pump Modulation," presented at *Optical Fiber Communication Conference, OFC'02,* WB4.

[99] C. Martinelli, V. Jolivet, J. L. Moncelet, D. Mongardien, and D. Bayart, "Operating Conditions for Profitable Time Division Multiplexing of the *Raman* Pumps," presented at *European Conference on Optical Communication, ECOC'03,* Tu4.7.5.

[100] G. Bolognini, S. Sugliani, and F. D. pasquale, "Double *Rayleigh* Scattering Noise in *Raman* Amplifier Using Pump Time-Division Multiplexing Schemes," *IEEE, Photonics Technology Letters,* vol.**16**, pp. 1286-1288, 2004.

[101] A. Artamonov, V. Smokovdin, M.Kleshov, S. A. E. Lewis, and S. V. Chernikov, "Enhancement of Double *Rayleigh* Scattering by Pump Intensity Noise in Fiber *Raman* Amplifier," presented at *Optical Fiber Communication, OFC'02,* WB6.

[102] P. J. Winzer, J. Bromage, R. T. Kane, P. A. Sammer, and C. Headley, "Repetition Rate Requirements for Time-Division Multiplexed *Raman* Pumping," *IEEE, Journal of Lightwave Technology,* vol.**22**, pp. 401-408, 2004.

[103] K. Mochizuki, N. Edagawa, and Y. Iwamoto, "Amplified Spontaneous *Raman* Scattering in Fiber *Raman* Amplifiers," *IEEE, Journal of Lightwave Technology,* vol.**4**, pp. 1328-1333, 1986.

[104] J. W. Nicholson, "Dispersion Compensating *Raman* Amplifiers with Pump Reflectors for Increased Efficiency," *IEEE, Journal of Lightwave Technology,* vol.**21**, pp. 1758-1762, 2003.

[105] T. Amano, K. Okamoto, T. Tsuzki, M. Kakui, and M. Shigematsu, "Hybrid Dispersion Compensating *Raman* Amplifier Module Employing Highly Nonlinear Fiber," presented at *Optical Fiber Communication, OFC'03,* WB3.

[106] J. H. Lee, Y. M. Chang, Y. G. Han, S. H. Kim, H. C, and S. B. Lee, "Dispersion-Compensating *Raman*/EDFA hybrid Amplifier Recycling Residual *Raman* Pump for Efficiency Enhancement," *IEEE, Photonics Technology Letters,* vol.**17**, pp. 43-45, 2005.

[107] H. Masuda and S. Kawai, "Wideband and Gain Flattening Hybrid Fiber Amplifier Consisting of an EDFA and a Multi-wavelength Pumped *Raman* Amplifier," *IEEE, Photonics Technology Letters,* vol.**16**, pp. 647-649, 1999.

[108] J. Masum-Thomas, D. Crippa, and A. Maroney, "A 70 nm Wide S-band Amplifier by Cascading TDFA and *Raman* Fiber Amplifier," presented at *Optical Fiber Communication, OFC'01,* WDD9-1.

[109] C. J. Chen and W. S. Wong, "Transient Effects in Saturated *Raman* Amplifiers," *Electronics Letters,* vol.**37**, pp.371-373, 2001.

[110] P. Vorreau, D. C. Kilper, and C. A. White, "Gain Saturation Spectrum of Backward-Pumped Broad-band *Raman* Amplifiers," *IEEE, Photonics Technology Letters,* vol.**17**, pp. 1405-1407, 2005.

[111] S. Kai, R. D. T. Lauder, and M. Premaratne, "Analytical Model Describing Transients Within a Gain Clamped *Erbium*-doped Fiber Amplifier," presented at *Optical Fiber Communication, OFC'99,* pp. 105-109.

[112] A. Bononi and M. Papararo, "Transient Gain Dynamics in Saturated Counter Pumped *Raman* Amplifiers," presented at *Optical Fiber Communication, OFC'02,* ThR1.

[113] A. Bononi and M. Fuochi, "Transient Gain Dynamics in Saturated *Raman* Amplifiers with Multiple Counter-Propagating Pumps," presented at *Optical Fiber Communication Conference, OFC'03,* ThC3.

[114] S. S.-H. Yam, F.-T. An, E. S.-T. Hu, M. E. Marhic, T. Sakamoto, and L. G. Kazovsky, "Gain-Clamped S-band Discrete *Raman* Amplifier," presented at *Optical Fiber Communication Conference, OFC'02,* ThB4.

[115] X. Zhou, H. H. M. Shalaby, C. Lu, P. Shum, and T. H. Cheng, "Theoretical Investigation of Fiber *Raman* Amplifier with Dynamic Gain Control," presented at *Optical Fiber Communication Conference, OFC'01,* WDD17-1.

[116] S. H. Chang, S. K. Kim, H. S. Chung, and M. J. Chu, "Transient Effects and Gain-Control Method in Low Noise Dispersion Compensating Hybrid Fiber Amplifier," *IEEE, Photonics Technology Letters,* vol.**15**, pp. 906-908, 2003.

[117] T. I. Lakoba, "Effect of a *Raman* Co-pump's RIN on the BER for Signal Transmission Using ON-OFF Keying Modulation Format," *IEEE, Journal of Lightwave Technology,* vol.**19**, pp. 382-389, 2001.

[118] S. Chang, S. Kim, H. Chung, M. Chu, and J. Lee, "Transient Effects in Low Noise Dispersion Compensating Hybrid Fiber Amplifier," presented at *Optical Fiber Communication Conference, OFC'03,* ThC2

[119] C. J. Chen, W. S. Wong, Y. W. Lu, M. C. Ho, Y. Cao, M. J. Gassner, J. S. Pease, H. S. Tsai, H. K. Lee, S. Cabot, and Y. Sun, "Control of Transient Effects in Distributed and Lumped *Raman* Amplifiers," *Electronics Letters,* vol.**37**, pp. 1304-1305, 2001.

[120] F. Vanholsbeeck, S. Coen, P. Emplit, M. Haelterman, and T. Sylvestre, "*Raman* Induced Power Tilt in Arbitrarily Large Wavelength Division Multiplexed Systems," *IEEE, Photonics Technology Letters,* vol.**17**, pp. 88-90, 2005.

[121] V. J. Mazurczyk, G. Shaulov, and E. Z. Golovchenko, "Accumulation of Gain Tilt in WDM Amplified Systems Due to *Raman* Crosstalk," *IEEE, Photonics Technology Letters,* vol.**12**, pp. 1573-1575, 2000.

[122] A. Oguri and S. Namiki, "WDM Signal Tilt Behavior in Wideband *Raman* Amplifiers," presented at *European Conference on Optical Communication, ECOC'01.*

[123] R. J. Essiambre, "Effect of *Raman* Noise and Double *Rayleigh* Backscattering on Bi-directionally *Raman* Pumped Systems at Constant Fiber Nonlinearity," presented at *Optical Fiber Communication Conference, OFC'01,* pp. 108-109.

[124] C. Martinelli, L. Lorcy, A. Durecu-legrand, D. Mongardien, S. Borne, and D. Bayart, "RIN Transfer in Co-pumped *Raman* Amplifiers Using Polarization-Combined Diodes," *IEEE, Photonics Technology Letters,* vol.**17**, pp. 1836-1838, 2005.

[125] M. D. Mermelstei, C. Headley, and J. C. Bouteiller, "RIN Transfer Analysis in Pump Depletion Regime for *Raman* Fiber Amplifiers," *Electronics Letters,* vol.**38**, pp. 403-405, 2002.

[126] R. P. Espindola, K. L. Bacher, K. Kojima, N. Chand, S. Srinivasan, G. C. Cho, F. Jin, C. Fuchs, V. Milner, and W. C. Dautremont-Smith, "High Power, Low RIN, Spectrally-Broadened 14××nm DFB Pump for Application in Co-Pumped *Raman* Amplification," presented at *European Conference on Optical Communication, ECOC'01,* pp. 36-37.

[127] R. P. Espindola, K. L. Bacher, K. Kojima, N. Chand, S. Srinivasan, G. C. Cho, F. Jin, C. Fuchs, V. Milner, and W. C. Dautremont-Smith, "Penalty-Free 10 Gbit/s Single-Channel Co-pumped Distributed *Raman* Amplification Using Low RIN 14××nm DFB Pump," *Electronics Letters,* vol.**38**, pp. 113-115, 2002.

[128] M. Mermelstein, K. Rrar, and C. Headley, "RIN Transfer Suppression Technique For 2nd Order *Raman* Pumping Schemes," presented at Optical *Fiber Communication Conference, OFC'03,* ThB5.

[129] G. Sun, "Output Power Clamped *Raman* Fiber Laser with Suppression of Low-Frequency RIN Transfer from Pump Sources," *Electronics Letters,* vol.**41**, pp. 468-469, 2005.

[130] P. Parolari, L. Marazz, L. Bernardini, and M. Martinelli, "Double *Rayleigh* Scattering Noise in Lumped and Distributed *Raman* Amplifiers," *IEEE, Journal of Lightwave Technology,* vol.**19**, pp. 2224-2228, 2003.

[131] C. J. Chen, M. C. Ho, W. S. Wong, T. H. Shang, and L. H. Kyu, "Time Domain Characterization of Transient Effects and Double *Rayleigh* Backscattering Noise in *Raman* Amplifie," presented at *Optical Fiber Communication Conference, OFC'02,* ThGG17.

[132] C. H. Kim, J. Bromage, and R. M. Jopson, "Reflection Induced Penalty in *Raman* Amplified Systems," *IEEE, Photonics Technology Letters,* vol.**14**, pp. 573-575, 2002.

[133] S. A. E. Lewis, S. V. Chernikov, and J. R. Taylor, "Characterization of Double *Rayleigh* Scatter Noise in *Raman* Amplifiers," *IEEE, Photonics Technology Letters,* vol.**12**, pp. 528-530, 2000.

[134] X. Zhou, C. Lu, P. Shum, and T. H. Cheng, "A Simple Model and Optimal Design of a Multi-wavelength Backward-Pumped Fiber *Raman* Amplifier," *IEEE, Photonics Technology Letters,* vol.**13**, pp. 945-947, 2001.

[135] M. Yan, J. Chen, W. Jiang, J. Li, J. Chen, and X. Li, "Automatic Design Scheme for Optical Fiber *Raman* Amplifiers Backward Pumped with Multiple Laser Diode Pumps," *IEEE, Photonics Technology Letters,* vol.**13**, pp. 948-950, 2001.

[136] P. Xiao, Q. Zeng, and J. Huang, "A New Optimal Algorithm for Multi-pump Sources of Distributed Fiber *Raman* Amplifier," *IEEE, Photonics Technology Letters,* vol.**15**, pp. 206-208, 2003.

[137] Z. Li, C. Lu, J. Chen, and C. Zhao, "*Raman* Amplifier Design Using Geometry Compensation Technique," *Optics Express,* vol.**12**, pp. 436-441, 2003.

[138] R. J. Essiambre, P. Winzer, J. Bromage, and C. H. Kim, "Design of Bidirectionally Pumped Fiber Amplifiers Generating Double *Rayleigh* Backscattering," *IEEE, Photonics Technology Letters,* vol.**14**, pp. 914-916, 2002.

[139] M. Vasilyev, "*Raman* Assisted Transmission: Toward Ideal Distributed Amplification," presented at *Optical Fiber Communication Conference, OFC'03,* WB1.

[140] A. Kobyakov, M. Vasilyev, and A. Evans, "Performance Analysis of *Raman* Amplifiers Based on Dispersion-Managed Fibers," presented at *Optical Fiber Communication Conference, OFC'03,* WB2.

[141] K. Rottwitt, A. J. Stentz, T. N. Nielsen, P. B. Hnsen, K. Feder, and K. Walker, "80-km Bi-Directionally Pumped Distributed *Raman* Amplifier Using Second Order Pumping," presented at *European Conference on Optical Communication, ECOC'99.*

[142] L. Labrunie, F. Boubal, E. Brandon, L. Pirou, A. Tran, and J. P. Blondel, "1.6Terabits/s (160×0.66 Gbit/s) Unrepeatered Transmission over 321km Using Second Order Pumping Distributed *Raman* Amplification," presented at *Optical Amplifier and Their Application, OAA'01.*

[143] *A.* Kobyakov, M. Vasilyev, S. Tsuda, G. Giudice, and S. Ten, "Analytical Model for *Raman* Noise Figure in Dispersion-Managed Fibers," *IEEE, Photonics Technology Letters,* vol.**15**, pp. 30-32, 2003.

[144] R. Hainberger, T. Hoshida, T. Terahara, and H. Onaka, "Comparision of Span Configurations of *Raman* Amplified Dispersion Managed Fibers," *IEEE, Photonics Technology Letters,* vol.**14**, pp. 471-473, 2002.

[145] C. L. Zhao, Z. Li, X. Yang, and C. Lu, "Effect of a Nonlinear Photonic Crystal Fiber on the Noise Characterization of a Distributed *Raman* Amplifier," *IEEE, Photonics Technology Letters,* vol.**17**, pp. 561-563, 2005.

[146] B. Hansen, L. Eskildsen, A. J. Stentz, T. A. Strasser, J. Judkins, J. J. DeMarco, R. Pedrazzani, and D. J. DiGivanni, "*Rayleigh* Scattering Limitations

in Distributed *Raman* Pre-amplifiers," *IEEE, Photonics Technology Letters,* vol.**10**, pp. 159-161, 1998.

[147] S. H. Chang, S. K. Kim, M. J. Chua, and J. H. Lee, "Limitations in Fiber *Raman* Amplifiers Imposed by *Rayleigh* Scattering of Signals," *Electronics Letters,* vol.**38**, pp. 865-867, 2002.

[148] M. Vasilyev, B. Szalabofka, S. Tsuda, J. M. Grochocinski, and A. F. Evans, "Reduction of *Raman* MPI and Noise Figure in Dispersion Managed Fiber," *Electronics Letters,* vol.**38**, pp. 271-272, 2002.

[149] C. J. S. d. Matos, K. P. Hansen, and J. R. Taylor, "Experimental Characterization of *Raman* Gain Efficiency of Holey Fiber," *Electronics Letters,* vol.**39**, pp. 424-425, 2003.

[150] Z. Yusoff, J. H. Lee, W. Belardi, T. M. Monro, P. C. The, and D. J. Richardson, "*Raman* Effects in a Highly Nonlinear Holey Fiber: Amplification and Modulation," *Optics Letters,* vol.**27**, pp. 424-426, 2002.

[151] Boskovic, S. V. Chernikov, J. R. Taylor, L. Gruner-Nielsen, and O. A. Levring, "Direct Continuous-Wave Measurement of $n_2$ in Various Types of Telecommunication Fiber at 1.55μm," *Optics Letters,* vol.**21**, pp. 1966-1968, 1996.

[152] Q. Lin and G. Agrawal, "PMD Effects in Fiber-based *Raman* Amplifiers," presented at *Optical Fiber Communication Conference, OFC'03,* TuC4.

[153] Q. Lin and G. Agrawal, "Vector Theory of Stimulated *Raman* Scattering and its Application to Fiber-Based *Raman* Amplifiers," *Journal of the Optical Society of America B,* vol.**20**, pp. 1616-1631, 2003.

[154] X. Liu, C. R. Giles, X. Wei, Y. H. Kao, C. Xie, L. Moller, L. Kang, and A. J. V. Wijingaarden, "Experimental Demonstration of Broadband PMD Mitigation through Distributed Fast Polarization Scrambling and FEC," presented at *European Conference on Optical Communication, ECOC'04,* Th4.1.4.

[155] L. Cheng, S. Aditya, Z. Li, and A. Nirmalathas, "Nonlinear Crosstalk due to XPM in dispersive WDM Microwave Fiber-Optic Links," *IEEE, Journal of Lightwave Technology,* vol.**24**, pp.2296-2304, 2006

[156] J. C. Bouteiller, K. Brar, J. Bromage, S. Radic, and C. Headley, "Dual-order *Raman* Pump Providing Improved Noise Figure and Large Gain Bandwidth," presented at *Optical Fiber Communication Conference, OFC'02,* FB3.

[157] G. Bolognini and F. D. Pasquale, "Transient Effects in Gain Clamped Discrete *Raman* Amplifier Cascades," *IEEE, Photonics Technology Letters,* vol.**16**, pp. 66-68, 2004.

[158] R. I. Killey, H. J. Thiele, V. Mikhailov, and P. Bayvel, "Reduction of Intra-Channel Nonlinear Distortion in 40Gb/s Based WDM Transmission Over Standard Fiber," *IEEE, Photonics Technology Letters,* vol.**16**, pp. 66-68, 2004.